Nuclear Magnetic Resonance and Relaxation Studies of Simple Cobalt Complexes

by

Christopher William Kirby

A thesis

presented to the University of Waterloo

in fulfilment of the

thesis requirement for the degree of

Master of Science

in

Chemistry

Waterloo, Ontario, Canada, 1996

©Christopher William Kirby 1996

National Library of Canada
Acquisitions and Bibliographic Services
395 Wellington Street
Ottawa ON K1A 0N4
Canada

Bibliothèque nationale du Canada
Acquisitions et services bibliographiques
395, rue Wellington
Ottawa ON K1A 0N4
Canada

Your file Votre référence

Our file Notre référence

The author has granted a non-exclusive licence allowing the National Library of Canada to reproduce, loan, distribute or sell copies of his/her thesis by any means and in any form or format, making this thesis available to interested persons.

The author retains ownership of the copyright in his/her thesis. Neither the thesis nor substantial extracts from it may be printed or otherwise reproduced with the author's permission.

L'auteur a accordé une licence non exclusive permettant à la Bibliothèque nationale du Canada de reproduire, prêter, distribuer ou vendre des copies de sa thèse de quelque manière et sous quelque forme que ce soit pour mettre des exemplaires de cette thèse à la disposition des personnes intéressées.

L'auteur conserve la propriété du droit d'auteur qui protège sa thèse. Ni la thèse ni des extraits substantiels de celle-ci ne doivent être imprimés ou autrement reproduits sans son autorisation.

0-612-21536-9

Canada

The University of Waterloo requires the signatures of all persons using or photocopying this thesis. Please sign below, and give address and date.

Abstract

Nuclear magnetic resonance (NMR) studies have been performed on a series of diamagnetic cobalt(III) complexes in both solution and the solid state. Variable-temperature solution cobalt-59 nuclear magnetic relaxation studies revealed that the dominant relaxation mechanism of these complexes in solution was the quadrupolar mechanism at room temperature. At higher temperatures, three of the complexes studied were observed to experience non-linear relaxation as temperature increased indicating that the spin-rotation relaxation mechanism was a contributor to relaxation at these temperatures. Spin-rotation constants were determined for these three complexes allowing the first determination of the absolute chemical shielding scale for cobalt. For solid samples, the chemical shift and electric field gradient (efg) tensors of eleven complexes were elucidated *via* simulation of solid-state ^{59}Co NMR spectra. Symmetry arguments, Gaussian 94 calculations, or residual quadrupolar effects on the dipolar coupling with an adjacent spin-$\frac{1}{2}$ nuclei allowed for the determination of the orientation of the efg tensor in the molecular frame. The relative orientation of the chemical shift tensor was known with respect to the efg tensor from the simulation of the solid-state ^{59}Co spectra, allowing the assignment of specific ligand planes responsible for observed values of chemical shift principal components. The possibility of using cobalt-59 NMR as a site-specific probe of molecular structure is proposed.

Acknowledgements

First and foremost, I must thank my supervisor, Professor Bill Power. Bill has continually been a source of knowledge, training, encouragement, and patience over the time I have been working in his lab. He has spent time training me in the art of acquiring solid-state NMR spectra and has taught me scientific ethics including that you must be proud of your work. It has truly been a pleasure to work in his lab for the past two years.

Thanks must be given to those who have given me technical support for this research. Jan Venne and Dr. Sandra Mooibroek gave me the basic high resolution training on the NMR spectrometers at the University of Waterloo, Valerie Robinson helped in the acquisition of the solid-state ^{59}Co spectra acquired at the University of Guelph, and Greg Clarke provided constant computer support.

Not being an apt synthetic chemist, I am grateful to those who have donated, synthesized, or aided in the synthesis of the compounds I studied. In this regard I would like to thank Dr. A. J. Carty for donation of $[Co(NH_3)_5NO_2]Cl_2$, Connie Puranda for the synthesis of *cis* and *trans*-$[Co(NH_3)_4(NO_2)_2]NO_3$ as well as *cis*-$[Co(NH_3)_4CO_3]NO_3$, and Dr. Bryon Koene from Dr. Linda Nazar's group for supplying a bomb and aiding in the synthesis of *fac*-$Co(CN)_3(NH_3)_3$. I also have to thank Amanda Doherty-Kirby for helping me acquire pH measurements for the Na[Co(edta)] variable concentration study and Dr. Gilles Lajoie for allowing me to use his pH meter.

My lab group has made my time at Waterloo interesting. I thank Mike, Gillian, and Hasan for many discussions, advice, and for making my time in the lab more enjoyable.

Financial support from the University of Waterloo, including a University of Waterloo Graduate Scholarship and a travel award, is gratefully acknowledged.

I wish to acknowledge the support my family has given me especially that of my mother. She has always encouraged me to not settle for second best throughout my academic career.

Finally I must thank Amanda again for putting up with me for the last 19 months. She has been my biggest encouragement, has read this thesis, and has listened to all of my results - even though not always interested in them. I'm glad that she chose Waterloo for grad school - otherwise the drive home every night would have been a killer!

List of Abbreviations

α, β, γ	Euler angles relating the CS tensor in the PAS of the efg tensor
B_o	magnetic field strength
CS	chemical shielding
CSA	chemical shielding anisotropy
χ	quadrupolar coupling constant
DD	direct dipolar
δ_{ii}	principal component of a chemical shift tensor
δ_{iso}	isotropic chemical shift
ΔJ	anisotropy of the indirect spin-spin coupling tensor
$\Delta\nu_{1/2}$	linewidth at half maximum
$\Delta\sigma^s$	anisotropy of the symmetric part of the chemical shielding tensor
efg	electric field gradient
$\hat{\mathcal{H}}$	Hamiltonian operator
η_Q	asymmetry of the efg (quadrupolar) tensor
η_{CS}	asymmetry of the chemical shielding tensor
I, S	nuclear spin quantum numbers
J_{iso}	isotropic spin-spin coupling constant
m_I	z-component of a nuclear spin quantum number
nOe	nuclear Overhauser effect
ν_0	Larmor frequency

PAS	principal axis system
Q	quadrupolar
θ, ϕ	angles defining the orientation of B_o in the PAS of the efg tensor
ϑ, φ	angles defining the orientation of B_o in the PAS of the chemical shielding tensor
R_{DD}	dipolar coupling constant
RF	radiofrequency
SR	spin-rotation
σ	chemical shielding
σ_a	antisymmetric part of the chemical shielding tensor
σ_d	diamagnetic chemical shielding
σ_p	paramagnetic chemical shielding
σ_{ii}	principal component of a chemical shielding tensor
T_1	spin-lattice (longitudinal) relaxation time
T_2	natural spin-spin (transverse) relaxation time
T_2^*	effective spin-spin (transverse) relaxation time
τ_c	rotational correlation time
τ_l	general rotational correlation time where l = 0, 1, or 2 depending on the tensor being averaged
ω_o	angular Larmor frequency
Ω	span of the chemical shift (or shielding) tensor

Contents

1 Introductory Comments 1

2 NMR Interactions 4

2.1 The Zeeman Interaction 5

2.2 The Radiofrequency Interaction 5

2.3 The Chemical Shielding Interaction 6

2.4 The Direct Dipolar Interaction 13

2.5 The Indirect Spin-Spin Interaction 15

2.6 The Quadrupolar Interaction 16

2.7 The Spin-Rotation Interaction 18

3 Solution NMR Studies of Cobalt Complexes 20

3.1 General Information about Cobalt-59 20

3.2 Previous Cobalt-59 Relaxation Studies 21

3.3 Relaxation Theory 25

3.3.1 General Relaxation Theory 25

3.3.2 Relaxation Mechanisms 27

3.3.3 Methods of Measuring T_1 and T_2 32
3.4 Experimental 37
3.5 Results 39
3.5.1 Variable Temperature 39
3.5.2 Variable Concentration 51
3.6 Discussion 59
3.7 Conclusions 67

4 Solid-State Cobalt-59 NMR **68**
4.1 Introduction 68
4.1.1 Previous Solid-State Cobalt-59 NMR Studies 68
4.1.2 NMR Lineshapes 70
4.2 Theory 71
4.3 Experimental 77
4.4 Results 78
4.5 Discussion 84
4.6 Conclusions 93

5 Concluding Remarks **94**

A Solid-State ^{59}Co NMR Spectra **98**

Bibliography **110**

List of Tables

3.1 Summary of the ^{59}Co NMR data acquired at 294 K (ambient temperature) and 11.7 T. 38

3.2 Rotational activation energies and quadrupolar coupling constants determined from analysis of ^{59}Co relaxation data. 44

3.3 Isotropic ^{59}Co chemical shifts, moments of inertia, and spin-rotation constants (derived from analyses of relaxation data) for three cobalt complexes displaying spin-rotation relaxation. 50

3.4 pH measurements of Na[Co(edta)] solutions 54

4.1 Summary of the solid-state ^{59}Co NMR data. 79

4.2 Comparison of solution and solid-state ^{59}Co NMR results. 84

4.3 T_{1CSA} from solid-state ^{59}Co NMR data. 92

List of Figures

2.1 The orientation of B_o in the PAS of the chemical shielding tensor. . 9

2.2 NMR spectra showing sites of a) cubic, b) axial, and c) less than axial symmetry. 11

3.1 a: Nuclear spin in the absence of a magnetic field b: Nuclear spins in the presence of a magnetic field, B_o, after waiting the relaxation times T_1 and T_2. 26

3.2 Plots of $\ln(T_1)$ vs. 1000/T for Q, CSA, and SR relaxation 29

3.3 The inversion-recovery pulse sequence. 33

3.4 Cobalt-59 NMR spectra of *cis*-$[Co(NH_3)_4CO_3]NO_3$ acquired using the inversion recovery pulse sequence. The T_1 obtained from these spectra is 242 $\pm$ 2 μs. 35

3.5 Cobalt-59 NMR spectrum of *cis*-$[Co(NH_3)_4CO_3]NO_3$ (solid line) and Lorentzian fit (dashed line). The linewidth obtained from the fit is 1300 Hz which corresponds to a T_2^* of 245 $\pm$ 12 μs. 36

3.6 Plots of $\ln(T_1)$ *vs.* 1000/T for the 6 octahedral cobalt(III) complexes with longer room temperature T_1's studied at 4.7 and 11.7 T. . . . 41

3.7 Plots of $\ln(T_1)$ *vs.* 1000/T for the 6 octahedral cobalt(III) complexes with the shorter room temperature T_1's studied at 4.7 and 11.7 T. . 42

3.8 Plots of $\ln(T_2^*)$ *vs.* 1000/T for the twelve complexes studied at 11.7 T. 49

3.9 Plot of T_1^{-1} (^{59}Co) *vs.* concentration for Na[Co(edta)]. 52

3.10 Plot of T_1^{-1} (^{23}Na) *vs.* concentration for Na[Co(edta)]. 53

3.11 Pictorial representation of Na[Co(edta)]. 55

3.12 Plots of the $^{13}C\{^1H\}$ and ^1H spectra of Na[Co(edta)] in the p^2H range of 5.98 - 6.12 at 11.7 T. 56

3.13 Plots of the $^{13}C\{^1H\}$ and ^1H spectra of Na[Co(edta)] in the p^2H range of 6.50 - 6.55 at 11.7 T. 57

3.14 Plots of the $^{13}C\{^1H\}$ and ^1H spectra of Na[Co(edta)] in the p^2H range of 6.85 - 7.16 at 11.7 T. 58

3.15 T_1 curves show the competition between Q and SR mechanisms of relaxation for (a) efficient *vs.* Q relaxation and (b) two different moments of inertia for SR relaxation. 61

3.16 Plot of spin-rotation constant (*c*) *vs.* chemical shift (δ_{iso}) for the three complexes. The line intercepts the x-axis at -3578 ppm. . . . 65

3.17 The chemical shift and absolute chemical shielding scales for cobalt. The chemical shift for the bare cobalt nucleus is determined to be -1412 (non-relativistic). 66

4.1 Plots of E/h of nuclear spin energy level *vs.* ^{59}Co Larmor frequency using a constant quadrupolar coupling constant of 33 MHz. 72

4.2 a) The magnetic field vector, B_o, is oriented in PAS of the chemical shielding tensor by (ϑ, φ) and in the PAS of the efg tensor by (θ, ϕ). b) The Euler angles (α, β, γ) orient the chemical shielding tensor in the PAS of the efg tensor. 76

4.3 Simulations of $[Co(en)_3]Cl_3$ at 11.7 T if a) only chemical shift anisotropy is present, b) only the quadrupolar interaction is present, c) both tensors are present. d) The experimental spectrum. 81

4.4 Cobalt-59 spectra of $[Co(NH_3)_5Cl]Cl_2$ after phasing using a) a single pulse experiment b) a single pulse experiment and baseline correcting c) a spin-echo experiment. 83

4.5 Chemical shift/shielding tensors for the complexes in this study. . . 86

4.6 ^{13}C MAS spectrum of $[Co(NH_3)_5CH_3](NO_3)_2$ acquired at 4.7 T. The simulation was done using the following parameters: χ = 33 MHz, η_Q = 0, R_{DD} = 925 Hz, J_{iso} = 110 Hz, ΔJ = -4275 Hz, α_{DD} = 0°, and β_{DD} (the orientation of the eq_{33} with respect to the Co-C bond) = 90°. 89

Chapter 1

Introductory Comments

This thesis is concerned with the study of nuclear magnetic resonance (NMR) spectroscopy with particular interest in cobalt-59. This interest in cobalt complexes stems from several sources. Cobalt is a metal involved in biological processes, especially famous for its role in pernicious anemia (vitamin B_{12} deficiency). Protein bound co-enzyme B_{12} is thought to be crucial for B_{12}-catalyzed enzymatic radical reactions.[1] Hydrolysis of amino acid esters, amides, and peptides, as well as peptide synthesis have been observed to be promoted by cobalt(III).[2] Cobalt complexes have been observed to selectively bind DNA,[3] have been extensively studied in photochemistry,[4] and have been observed to bind poly(vinylpyridine) and can be used as a cross linker in these polymers.[5] We wish to gain a better understanding of simple cobalt(III) complexes in both solution and the solid-state with the long term goal of using cobalt NMR as a site-specific probe of molecular structure in more complicated systems. Cobalt(III) is an excellent choice for studying these systems because it forms diamagnetic complexes when adopting an

octahedral geometry. In this conformation it is substitutionally inert. Cobalt-59 is also the only naturally occurring isotope of cobalt and therefore, sensitivity in NMR spectroscopy would not present a problem as is sometimes observed for less abundant isotopes.

Chapter 2 contains theory which will be used in the remainder of this thesis. This includes a description of NMR interactions which are relevant to NMR spectroscopy of diamagnetic compounds in both solution and the solid state. All of the interactions are described briefly with the exception of the chemical shielding interaction for which a full theoretical and mathematical description is presented.

Chapter 3 contains the results of variable-temperature ^{59}Co nuclear magnetic relaxation studies on a series of octahedral cobalt(III) complexes and a variable-concentration multinuclear NMR study on Na[Co(edta)]. Variation of the magnetic field and temperature was performed to determine unambiguously the dominant ^{59}Co relaxation mechanism(s) for these complexes in aqueous media. It had been suggested previously that the chemical shielding anisotropy relaxation mechanism contributed to the relaxation of such complexes. If this suggestion was correct, we would have a way to measure the chemical shielding anisotropy from solution NMR spectra (the first time for a quadrupolar nucleus) making the analysis of solid-state NMR spectra unnecessary. The dominant relaxation mechanism was found to be the quadrupolar mechanism for all of the complexes in the study at room temperature. At higher temperatures, spin-rotation was also observed to contribute to complexes with high symmetry or a large moment of inertia. An absolute chemical shielding scale is proposed by using spin-rotation constants obtained from a fitting of the T_1

curves in conjunction with previously calculated diamagnetic shielding constants.

A solid-state ^{59}Co NMR study is contained in Chapter 4. Within this chapter, the chemical shift and electric field gradient tensors of eleven cobalt(III) complexes are presented. The orientations of the electric field gradient tensors were determined in the molecular frame *via* symmetry arguments, Gaussian 94 calculations, or residual quadrupolar effects on the dipolar coupling with an adjacent spin-$\frac{1}{2}$ nucleus. This allowed the elucidation of the orientation of the chemical shift tensors using the Euler angles determined in the simulations. Specific ligand planes were determined to be responsible for observed values of the chemical shift principal components. From the experimentally determined chemical shift tensors, room-temperature spin-lattice relaxation times were calculated considering only the chemical shielding anisotropy relaxation mechanism to be present. These calculations further proved that the chemical shielding anisotropy relaxation mechanism does not contribute to cobalt relaxation in these complexes. A comparison between solution and solid-state isotropic chemical shifts and quadrupolar coupling constants is also presented.

The final chapter in this thesis briefly reviews the conclusions drawn in Chapters 3 and 4 as well as proposing future work that builds on the results of this project. A proposed direction in which this research is leading is given along with possible situations where cobalt-59 NMR can be used as a site-specific probe of structure.

Chapter 2

NMR Interactions

In any state of matter the full nuclear spin Hamiltonian of a diamagnetic compound is given as[6]

$$\hat{\mathcal{H}}_T = \hat{\mathcal{H}}_Z + \hat{\mathcal{H}}_{RF} + \hat{\mathcal{H}}_{CS} + \hat{\mathcal{H}}_{DD} + \hat{\mathcal{H}}_J + \hat{\mathcal{H}}_Q + \hat{\mathcal{H}}_{SR} \tag{2.1}$$

where the total Hamiltonian (T) is the sum of the Zeeman (Z), radiofrequency (RF), chemical shielding (CS), direct dipolar (DD), indirect spin-spin (J), quadrupolar (Q), and spin rotation (SR) Hamiltonians. The Zeeman interaction is the basic NMR interaction and all of the other interactions are perturbations of this interaction. Many monographs and reviews describe, in detail, the origin of the effects of the different interactions;[6, 7, 8] a brief discussion of each is provided here as background for the remainder of this thesis.

2.1 The Zeeman Interaction

If a nucleus possessing spin (*i.e*, I > 0) is placed in a magnetic field, B_o, 2I + 1 nuclear spin energy levels are created. The energy spacing between the energy levels (*i.e.*, the differences in energy) is dependent on the magnetic moment of a nucleus, μ, and B_o,

$$\hat{\mathcal{H}}_Z = -\mu \cdot \vec{B}_o = -\gamma_I \hbar \vec{B}_o \cdot \hat{I} \tag{2.2}$$

where γ_I is the magnetogyric ratio for nuclear isotope I and $\hat{I}$ is the nuclear spin angular momentum vector of isotope I. By convention, B_o is chosen to be along the laboratory z-axis. Units of frequency are preferred to energy in NMR. The frequency at which a pure Zeeman transition occurs is given by the Larmor frequency, ν_o, of a given nuclear isotope,

$$\nu_o = \frac{\gamma_I B_o}{2\pi} \tag{2.3}$$

where ν_o is in Hz. All of the interactions to follow are perturbations of this basic interaction.

2.2 The Radiofrequency Interaction

Without the radiofrequency (RF) interaction, NMR would not be possible. In a pulse Fourier Transform NMR (FTNMR) experiment, a time-dependent radio frequency field, B_{RF}, along the x-axis induces a transition between nuclear spin energy levels,

$$\hat{\mathcal{H}}_{RF} = -\gamma_I \hbar \vec{B_{RF}} \cdot \hat{I} \tag{2.4}$$

where

$$B_{RF}(t) = (B_1 \cos \omega t, 0, 0) \tag{2.5}$$

and B_1 is the amplitude of the RF field with a carrier frequency of $\omega/2\pi$. The time-dependent fields of the RF Hamiltonian can be used for all FTNMR experiments to allow observation (and suppression if desired) of the effects of the following Hamiltonians.

2.3 The Chemical Shielding Interaction

When a magnetic field is imposed on an atom or molecule, the electrons surrounding the nucleus (or nuclei) are induced into currents. As the electrons circulate about the nucleus, they shield (either positively or negatively) the nucleus from the magnetic field. This phenomenon is known as chemical shielding. Since this shielding is induced by the magnetic field, it is proportional to the magnetic field strength,

$$\hat{\mathcal{H}}_{CS} = -\gamma_I \hbar \hat{I} \cdot \overline{\sigma} \cdot \vec{B}_o \tag{2.6}$$

where $\overline{\sigma}$ is the chemical shielding tensor. The chemical shielding tensor describes the effect of the electrons as they modify the magnetic field experienced by the nuclear spin, I.

The chemical shielding Hamiltonian can be expanded as

$$\hat{\mathcal{H}}_{CS} = \gamma_I \hbar \left\{ \begin{pmatrix} I_x & I_y & I_z \end{pmatrix} \begin{pmatrix} \sigma_{xx} & \sigma_{xy} & \sigma_{xz} \\ \sigma_{yx} & \sigma_{yy} & \sigma_{yz} \\ \sigma_{zx} & \sigma_{zy} & \sigma_{zz} \end{pmatrix} \begin{pmatrix} B_x \\ B_y \\ B_z \end{pmatrix} \right\}. \tag{2.7}$$

This equation can be simplified if B_o is taken to be along the z-axis (in the usual convention). I_x and I_y do not commute with $\hat{\mathcal{H}}_{CS}$ if B_o is along z, therefore only one term survives: $I_z \sigma_{zz}^{Lab} B_o$. This lab frame chemical shielding tensor can be expressed as

$$\sigma_{zz}^{Lab} = \tilde{\sigma} = \begin{pmatrix} \sigma_{11} & \sigma_{12} & \sigma_{13} \\ \sigma_{21} & \sigma_{22} & \sigma_{23} \\ \sigma_{31} & \sigma_{32} & \sigma_{33} \end{pmatrix} \tag{2.8}$$

where $\tilde{\sigma}$ can be further broken down into symmetric ($\tilde{\sigma}^s$) and antisymmetric ($\tilde{\sigma}^a$) terms using the transform ($\tilde{\sigma}^T$) of the tensor in equation 2.8. These two terms are

$$\tilde{\sigma}^s = \frac{1}{2}(\tilde{\sigma} + \tilde{\sigma}^T) \tag{2.9}$$

and

$$\tilde{\sigma}^a = \frac{1}{2}(\tilde{\sigma} - \tilde{\sigma}^T). \tag{2.10}$$

In an NMR experiment, one can only directly observe the symmetric part of a chemical shielding tensor and this tensor is usually described in its principal axis

system (PAS) as

$$\sigma^s = R_{PAS}^{-1}\tilde{\sigma}^s R_{PAS} = \begin{pmatrix} \sigma_{11} & 0 & 0 \\ 0 & \sigma_{22} & 0 \\ 0 & 0 & \sigma_{33} \end{pmatrix} \tag{2.11}$$

where R_{PAS} and R_{PAS}^{-1} are rotational transformations[9] from the lab frame to the PAS. The three diagonal elements above are known as the three principal components of the chemical shielding tensor where σ_{11} is the least shielded, σ_{33} is the most shielded, and σ_{22} is between, or equal to one of, the two extremes. The difference between the least shielded and most shielded component of the tensor is known as the span (Ω). Two other measures commonly used in describing the anisotropic behavior of the chemical shielding tensor are the asymmetry of the chemical shielding tensor (η_{CS}) and the anisotropy of the chemical shielding tensor ($\Delta\sigma^s$). If $|(\sigma_{11} - \sigma_{iso})| \leq |(\sigma_{33} - \sigma_{iso})|$ then

$$\eta_{CS} = \frac{\sigma_{22} - \sigma_{11}}{\sigma_{33} - \sigma_{iso}} \quad and \quad \Delta\sigma^s = \sigma_{33} - \frac{\sigma_{22} + \sigma_{11}}{2}. \tag{2.12}$$

In the opposite case where $|(\sigma_{11} - \sigma_{iso})| \geq |(\sigma_{33} - \sigma_{iso})|$ then

$$\eta_{CS} = \frac{\sigma_{22} - \sigma_{33}}{\sigma_{11} - \sigma_{iso}} \quad and \quad \Delta\sigma^s = \sigma_{11} - \frac{\sigma_{22} + \sigma_{33}}{2}. \tag{2.13}$$

Both Ω and $\Delta\sigma^s$ are measures of the orientation dependence of the chemical shielding tensor.[10]

The anisotropic chemical shielding interaction can be represented in its PAS as seen in Figure 2.1 where ϑ and φ are the polar and azimuthal angles describing the

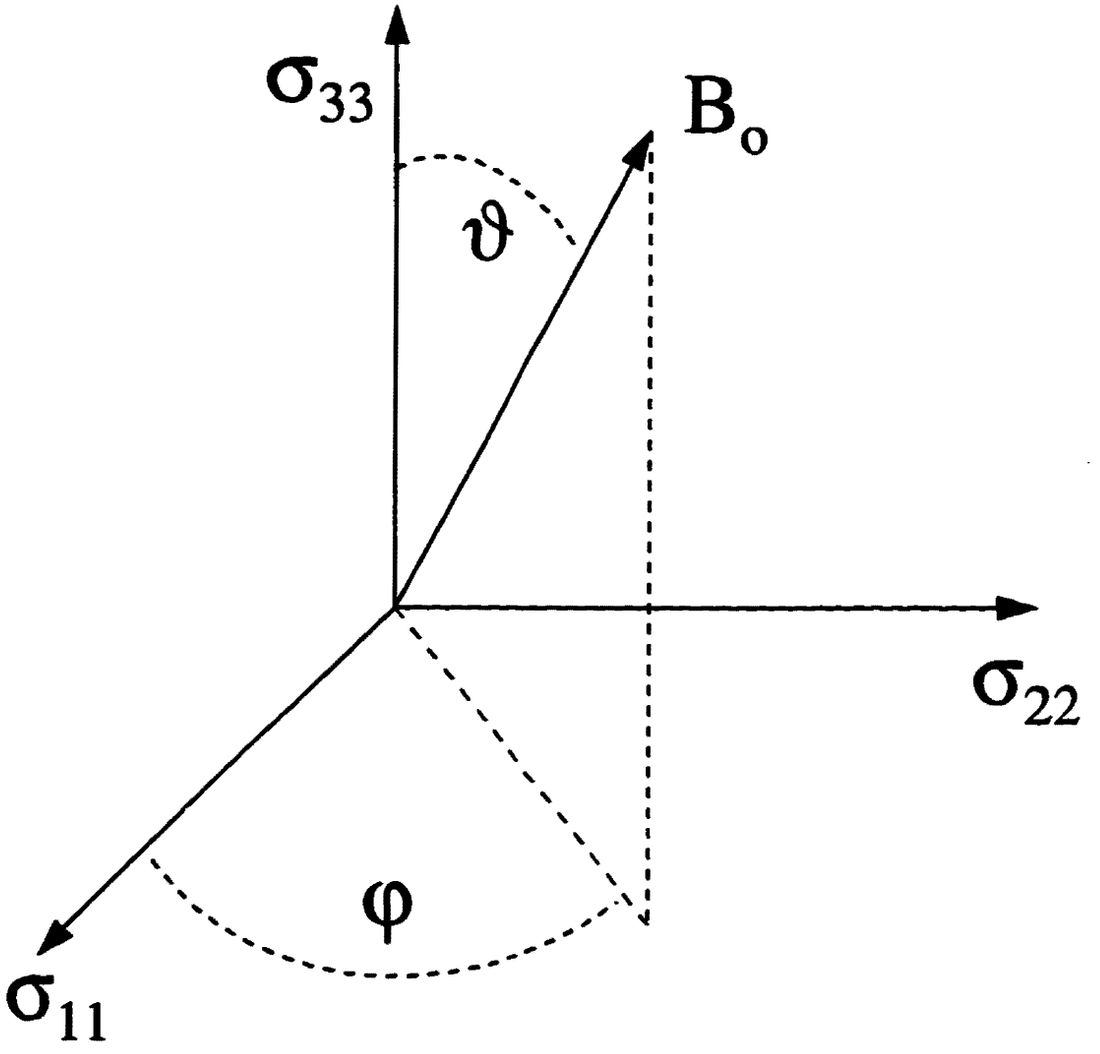


Figure 2.1: The orientation of B_o in the PAS of the chemical shielding tensor.

orientation of B_o in the PAS. These two angles and the three principal components of the chemical shielding tensor underlie the anisotropic lineshapes observed in many solid-state NMR experiments. The lineshape (ν_σ) of a nucleus in a powder sample dominated by chemical shielding can be described as

$$\nu_\sigma = \nu_o[1 - (\sigma_{11}\sin^2\vartheta\cos^2\varphi + \sigma_{22}\sin^2\vartheta\sin^2\varphi + \sigma_{33}\cos^2\vartheta)]. \tag{2.14}$$

Examples of the effects of chemical shielding anisotropy can be seen in Figure 2.2. In this figure, sites of cubic, axial, and less than axial symmetry are displayed. Cubic symmetry is observed for nuclei in sites with tetrahedral or higher point symmetry. In these cases all components are equal ($\sigma_{11} = \sigma_{22} = \sigma_{33}$). Axial symmetry is observed in sites with 3-fold or higher point symmetry. In such cases, either $\sigma_{11} = \sigma_{22} \neq \sigma_{33}$ or $\sigma_{11} \neq \sigma_{22} = \sigma_{33}$. In sites with less than 3-fold point symmetry, $\sigma_{11} \neq \sigma_{22} \neq \sigma_{33}$ and one observes a non-axially symmetric powder pattern.

The above breakdown of a tensor was purely mathematical. Chemists, however, want to be able to interpret chemical shielding tensors through a theoretical model of molecular structure or bonding. Ramsey[11] was the first to propose that chemical shielding could be broken down into two terms; diamagnetic and paramagnetic. These two terms are given as follows.[12]

$$\sigma = \sigma_d + \sigma_p \tag{2.15}$$

$$\sigma_d = \frac{e^2}{2m}\frac{\mu_o}{4\pi}\left\langle 0 \left| \sum_k r_{kN}^{-3}(r_k \cdot r_{kN}\mathbf{1} - r_k r_{kN}) \right| 0 \right\rangle \tag{2.16}$$

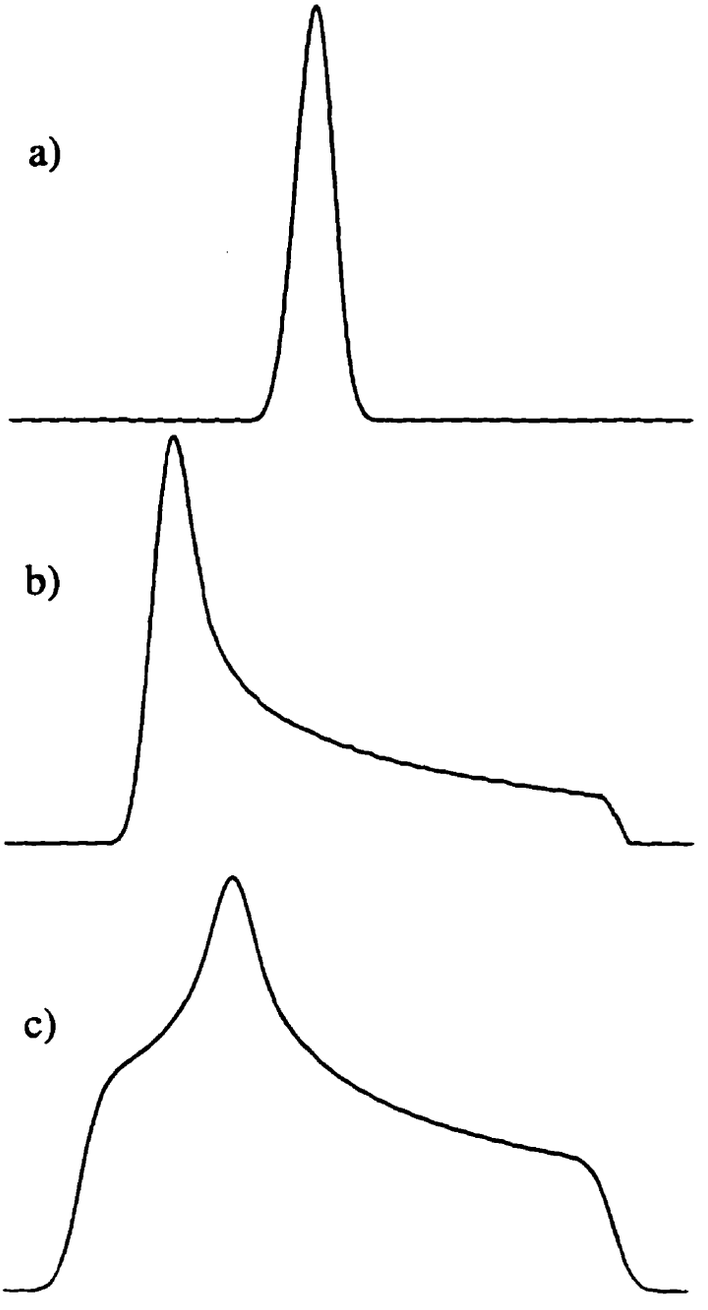


Figure 2.2: NMR spectra showing sites of a) cubic, b) axial, and c) less than axial symmetry.

$$\sigma_p = -\frac{e^2}{2m}\frac{\mu_o}{4\pi}\sum_{n\neq 0}\frac{\left\langle 0\left|\sum_k r_{kN}^{-3} l_{kN}\right|n\right\rangle\langle n|\sum_k l_k|0\rangle + \langle 0|\sum_k l_k|n\rangle\left\langle n\left|\sum_k r_{kN}^{-3} l_{kN}\right|0\right\rangle}{{}^1E_n - E_o} \tag{2.17}$$

where r is the position vector for an electron and l is the angular momentum operator, both of which are with respect to either a chosen origin (k) or to the observed nucleus (kN). The diamagnetic term (equation 2.16) is only dependent on the ground state wave functions and is almost invariant for a given nucleus. The paramagnetic term, which is dependent on both ground and excited state wave functions, causes the variation in chemical shielding from compound to compound for most nuclear isotopes. The two exceptions are hydrogen and lithium because the valence shell for these nuclei are s-orbitals. Therefore, the excited states are much higher in energy than the ground state making σ_p small and allowing the small variations in σ_d to become important. Both σ_d and σ_p also include a radial density (r^{-3}) term. Cobalt has one of the largest r^{-3} terms resulting in large sensitivity in its shielding. In calculated chemical shielding tensors, the diamagnetic term is more readily calculated (since it is only dependent on the ground state wave functions) and such calculations have been performed for many atoms.[13, 14] Calculated NMR chemical shieldings are defined on a scale with respect to the bare nucleus at 0 ppm. This scale is known as the absolute chemical shielding scale.

NMR spectra, however, are normally recorded in terms of the chemical shift, δ, rather than shielding, σ. Chemical shifts provide positions of signals with respect to a reference compound (*e.g.*, TMS for ^{1}H and ^{13}C), in field-independent units of ppm (parts per million). Chemical shielding is also referenced to a standard, the bare nucleus, and also uses a field-independent scale of ppm. To convert between these

two scales, the value of the chemical shift of the bare nucleus is necessary. From this, the absolute shielding of the reference compound (σ_{ref}) can be determined. The following equation then provides absolute chemical shieldings:

$$\sigma_{ii} = \sigma_{ref} - \delta_{ii} \tag{2.18}$$

Therefore, NMR spectra can be obtained, analyzed to determine the chemical shift tensor, and these results can be converted to the chemical shielding scale using equation 2.18. This process, however, is impossible for nuclei for which there is no known absolute chemical shielding scale, making direct comparison with calculated values impossible.

2.4 The Direct Dipolar Interaction

Two nuclear spins, I and S, can interact through space in a manner similar to two bar magnets. This interaction is known as the direct dipolar (to be referred to as only dipolar henceforth) interaction and can be expressed as

$$\hat{\mathcal{H}}_{DD} = h\hat{I} \cdot \tilde{D} \cdot \hat{S} \tag{2.19}$$

where I and S can be like or unlike spins, and $\tilde{D}$ is the dipolar tensor. Equation 2.19 can be expanded in much the same way as the chemical shielding interaction and also simplified in a similar manner. The dipolar tensor is both axially symmetric

and traceless as seen in equation 2.20,

$$\tilde{D} = R_{DD} \begin{pmatrix} 1 & 0 & 0 \\ 0 & 1 & 0 \\ 0 & 0 & -2 \end{pmatrix} \Rightarrow R_{DD}(3cos^2\psi - 1) \tag{2.20}$$

where ψ is the angle between B_o and the internuclear vector, and R_{DD} is the dipolar coupling constant. Therefore, one need only know R_{DD} to completely characterize the dipolar interaction,

$$R_{DD} = \frac{\mu_o}{4\pi} \frac{\gamma_I \gamma_S}{r_{IS}^3} \frac{\hbar}{2\pi} \tag{2.21}$$

where r_{IS} is the internuclear distance and R_{DD} is given in Hz.

The dipolar interaction has different effects in solution and the solid state. As seen in equation 2.21, dipolar coupling is stronger for shorter internuclear distances and for large magnetogyric ratios. In the solid state, such dipolar couplings are observed to broaden lines. An example of large dipolar coupling is ^1H coupling to heteronuclei in an organic compound. Dipolar coupling can also contribute to the relaxation in all phases and is observed to be dominant in spin-1/2 nuclei bonded to protons in solution (*vide infra*). The dipolar interaction can be used to increase the sensitivity of heteronuclei in solution. This effect is known as the nuclear Overhauser effect (nOe).[15]

2.5 The Indirect Spin-Spin Interaction

In contrast to the direct interaction between two nuclei in the dipolar interaction, nuclei can also communicate through the electrons between nuclei. This is known as the indirect spin-spin interaction and is given as

$$\hat{\mathcal{H}}_J = \hat{I} \cdot \tilde{J} \cdot \hat{S} \tag{2.22}$$

where $\tilde{J}$ is the indirect spin-spin coupling tensor. Equation 2.22 can be expanded similarly to $\tilde{\sigma}$ to obtain a general tensor with both symmetric and antisymmetric terms. The indirect spin-spin interaction is usually assumed to be axially symmetric with an isotropic average that can be measured in solution as J_{iso}. Assuming axial symmetry, the tensor $\tilde{J}$ can be written as

$$\tilde{J} = \begin{pmatrix} J_\perp & 0 & 0 \\ 0 & J_\perp & 0 \\ 0 & 0 & J_\parallel \end{pmatrix} = J_{iso}\mathbf{1} + \begin{pmatrix} -\Delta J/3 & 0 & 0 \\ 0 & -\Delta J/3 & 0 \\ 0 & 0 & 2\Delta J/3 \end{pmatrix} \tag{2.23}$$

where

$$\Delta J = J_\parallel - J_\perp. \tag{2.24}$$

$J_\perp$ and $J_\parallel$ are the perpendicular and parallel components of $\tilde{J}$ with respect to the internuclear vector and 1 is the unit tensor. As shown in equation 2.23, $\tilde{J}$ can be broken down into isotropic and anisotropic terms. The anisotropic term is averaged to zero in solution NMR due to rapid molecular tumbling. However, ΔJ can be observed in solid-state NMR but only in combination with the direct dipolar

interaction due to their identical spin operators. Therefore, if ΔJ is non-zero, one observes an effective dipolar coupling constant,

$$R_{eff} = R_{DD} - \frac{\Delta J}{3}. \tag{2.25}$$

If a bond length is available from a different technique (*e.g.*, X-ray or neutron diffraction), R_{DD} can be calculated using equation 2.21. Using solid-state NMR one can then measure R_{eff} and therefore obtain a value of ΔJ.[16, 17]

2.6 The Quadrupolar Interaction

In this research the quadrupolar interaction is important because ^{59}Co is a quadrupolar nucleus (I = 7/2). The quadrupolar interaction, in general, is large in comparison to the effects of the dipolar and indirect spin-spin Hamiltonians (*i.e.*, the dipolar and indirect spin-spin interactions normally will not be important when dealing with quadrupolar nuclei).

There are two quantities to consider when dealing with quadrupolar nuclei, the nuclear quadrupole moment (eQ) and the electric field gradient (efg). The nuclear quadrupole moment is due to the asymmetric charge distribution within a nucleus and the efg is the Laplacian of the potential of the electrons surrounding a nucleus. These two phenomena combine to give the quadrupolar interaction,

$$\hat{\mathcal{H}}_Q = \frac{eQ}{2I(2I-1)} \hat{I} \cdot e\tilde{q} \cdot \hat{I} \tag{2.26}$$

where $e\tilde{q}$ is the efg (or quadrupolar) tensor. The efg tensor can be represented in the same fashion as the chemical shielding tensors except ϑ and φ are replaced by θ and ϕ and the σ_{ii} are replace by eq_{ii} (where eq_{11}, eq_{22}, and eq_{33} are the three principal components of the efg tensor, and θ and ϕ define the orientation of B_o in the PAS of the efg tensor). The angles θ and ϕ are not necessarily equal to ϑ and φ because the chemical shielding and quadrupolar interactions arise from different interactions with the local electronic environment. Chemical shielding, as previously described, arises from currents about the nuclei while the quadrupolar interaction is dependent on the distribution of electronic charge around the nuclei. Therefore, theses independent interactions will have different orientations with respect to B_o. The efg tensor, like the dipolar tensor, is traceless and therefore cannot be observed directly in solution; however, it can be non-axially symmetric. In the solid-state, one can determine the quadrupolar coupling constant, χ (this is a measure of the strength of the quadrupolar interaction) and the asymmetry parameter, η_Q, to completely describe the efg tensor.

$$\chi = \frac{e^2 q_{33} Q}{h} \tag{2.27}$$

$$\eta_Q = \frac{eq_{22} - eq_{11}}{eq_{33}} \tag{2.28}$$

This interaction will be important throughout this thesis and it and the chemical shielding interaction will be the focus of Chapter 4 where solid-state ^{59}Co NMR spectra are reported, analyzed, and discussed in detail.

2.7 The Spin-Rotation Interaction

The rotational angular momentum of a molecule, $\mathcal{J}$, is found to be large if the moment of inertia of that molecule, $\mathcal{I}$, is large,

$$\mathcal{J} = \omega\mathcal{I} \tag{2.29}$$

where ω is the angular velocity of the molecule. In such systems the spin-rotation interaction can be a relevant contributor to the total NMR Hamiltonian,

$$\hat{\mathcal{H}}_{SR} = \hat{I} \cdot \tilde{c} \cdot \mathcal{J} \tag{2.30}$$

where $\tilde{c}$ is the spin-rotation tensor relating $\hat{I}$ and $\mathcal{J}$. Thus the SR interaction is a coupling of a molecule's rotational angular momentum to the nuclear spin of nuclei within the molecule. As a molecule rotates, magnetic fields are produced by the circulating electrons; these fields may couple with the nuclear spins. As the rate of molecular rotation changes, the fields fluctuate due to changes in the rotation rate and cause relaxation of the nuclei. One can obtain SR constants indirectly from NMR measurements if nuclei relax through this SR mechanism (*vide infra*) and the moment of inertia of the molecule is known. Characterization of SR constants allows for the estimation of the degree of paramagnetic shielding a complex exhibits.[11, 18, 19] This relationship arises because both SR and σ_p are produced by circulating electron currents due to unquenching of orbital angular momentum. Extrapolation to an SR constant of zero from a plot of SR constants *vs.* isotropic chemical shifts yields σ_d (*i.e.*, at SR constants of zero, σ_p is zero).

Using a calculated value of σ_d, a value of the chemical shift of a bare nucleus is obtained, thereby producing an absolute chemical shielding scale for that nucleus.

Chapter 3

Solution NMR Studies of Cobalt Complexes

3.1 General Information about Cobalt-59

Cobalt-59 has been a nucleus of interest from the early days of NMR.[20] Its high magnetogyric ratio ($\gamma = 6.317 \times 10^7$ rad $T^{-1}s^{-1}$ which is close to that of ^{13}C)[21] and its high natural abundance (100%) make it a sensitive nucleus for NMR studies (27.7% as receptive as the most sensitive nucleus to study by NMR - ^1H). Even with its high receptivity, ^{59}Co NMR spectroscopy is difficult to study due to the large chemical shift range (over 18 000 ppm)[22] and the inherent wide lines of this nucleus in both solution and the solid-state. The large chemical shift range, for which no absolute shielding reference exists, results from a variety of factors, the most significant of which is the large value of $<r^{-3}>_{3d}$ for cobalt.[23] The wide lines arise from efficient relaxation of cobalt nuclei. One would expect this efficient

relaxation to be through the quadrupolar mechanism of relaxation as ^{59}Co is a quadrupolar nucleus with nuclear spin quantum number (I) of 7/2.

3.2 Previous Cobalt-59 Relaxation Studies

The relaxation mechanisms of cobalt nuclei have been the topic of several ^{59}Co NMR studies. Ader and Loewenstein[24] studied the spin-lattice relaxation time (T_1's) of aqueous $Co(CN)_6^{3-}$, $Co(NH_3)_6^{3+}$, and $Co(en)_3^{3+}$ with variation of the counterion, the temperature, the concentration, the solvent, and the field. The dominant relaxation mechanism of the cobalt center in these complexes was stated to be through the quadrupolar mechanism. The electric field gradient (efg) that is needed for quadrupolar relaxation to occur was proposed to be produced by ionic association of the cobalt ion with the counterion (there is no static efg for $Co(CN)_6^{3-}$ or $Co(NH_3)_6^{3+}$ because they possess octahedral symmetry). A linear relationship between $\ln(T_1)$ and 1000/T was observed over a broad temperature range for $Co(en)_3^{3+}$ and this linear relationship was observed to hold below 323 K for $Co(CN)_6^{3-}$ and $Co(NH_3)_6^{3+}$. At temperatures above 323 K, a "tailing off" was observed; *i.e.*, the T_1's did not continue to increase linearly but were less than one would expect from the lower temperature measurements. Suggestions made for the non-ideal high-temperature behavior were (1) the correlation times for the quadrupolar interaction may not be an exponential function of temperature, (2) the quadrupolar coupling might vary with temperature, or (3) spin-rotation relaxation may be contributing to the total relaxation at higher temperatures. A subsequent multinuclear NMR study by Jordan[25] of the cobalt hexaamine cation

in dimethylsulfoxide provided evidence for the participation of the spin-rotation mechanism at higher temperature as the correct interpretation.

Other investigations of the nature of cobalt relaxation abound in the literature. Doddrell and co-workers[26] completed a room-temperature ^{59}Co T_1 study of a series of cobalt complexes with local octahedral symmetry (*e.g.*, $Co(acac)_3$ has six oxygen atoms around the cobalt center, therefore local O_h symmetry, but the whole molecule does not have O_h symmetry). Valiev's vibrationally-induced nuclear spin relaxation model[27] was suggested to be the origin of the unexpectedly-efficient ^{59}Co relaxation in symmetric cobalt(III) complexes, where shorter ^{59}Co relaxation times were measured in larger complexes (*e.g.*, $Co(tropolonato)_3$) than in smaller complexes (*e.g.*, $Co(acac)_3$) with the "same" local symmetry (*i.e.*, both of these complexes have six oxygen atoms around the cobalt centre). Valiev's model was treated with a full theoretical approach for a series of quadrupolar nuclei by Brown and Colpa,[28] who pointed out that the vibrational excitation was not necessary to create transient efg's at the cobalt nuclei since static efg's exist in both of the above complexes. Osten and Jameson[29] calculated relaxation rates for a series of quadrupolar nuclei using the vibrationally-induced nuclear spin relaxation model and obtained estimates of relaxation rates which were orders of magnitude too small compared to experimentally observed relaxation rates. The alternative models of collision-deformation by van der Waals interactions (an "intermolecular" effect) and octopole-induced efg's were investigated and these predicted relaxation rates of the correct order of magnitude.

Bryant and his co-workers[30, 31, 32, 33, 34] have also published a series of pa-

pers dealing with relaxation in highly symmetric cobalt complexes. They found that perturbations in the first coordination sphere caused large changes in relaxation rates of the central cobalt nucleus,[33] presumably due to changes in the cobalt quadrupolar coupling constant, while changes in the second coordination sphere made little to no contribution to the strength of the quadrupolar interaction.[30] Subsequent studies indicated that second sphere coordination induced time-dependent changes in the efg at the central atom, which were used as a measure of "ion-pairing" in the ionic solutions.[34] This ion-pairing effect is similar to the ideas presented by Ader and Loewenstein[24] and has been reported most recently in the cobalt relaxation of Δ-$[Co(R,R\text{-chxn})_3]^{3+}$ (chxn = *trans*-(1R,2R)-1,2-diaminocyclohexane).[35] Bryant also concluded that scalar relaxation of the second kind[36] from ^{59}Co coupled to ^{14}N in high-symmetry N-bonded cobalt complexes contributes to the spin-spin relaxation (T_2) in these complexes.[31, 32]

In 1983, Eaton and co-workers published a series of ^{59}Co NMR T_2 (*via* linewidth measurements)[37, 38, 39] and T_1 studies[40] of cobalt complexes that varied from high symmetry (*e.g.*, $Co(CN)_6^{3-}$ with O_h symmetry) to low symmetry (*e.g.*, *cis*-$Co(NH_3)_4CO_3^+$ with C_{2v} symmetry). Complexes with less than O_h symmetry were found to have ^{59}Co relaxation times that decreased with increasing field strength, which they took to be evidence that chemical shielding anisotropy was contributing to the relaxation of the "low-symmetry" complexes. According to their interpretation, the antisymmetric part of the chemical shielding tensor (σ^a) dominated the relaxation of these complexes because T_1 values were found to be less than corresponding T_2 values. These studies have been brought into question recently in

a review of the chemical shielding tensor.[41] According to Anet and O'Leary, a molecule with D_{4h} symmetry (*e.g.*, trans-CoX_4Y_2) must possess a σ^a of zero while the symmetric part of the tensor must be large. Therefore, if relaxation was through the chemical shielding anisotropy mechanism of relaxation, one would expect T_1 to be greater than T_2 (*vide infra*). Eaton and co-workers argued that hydrogen bonding solvents break the symmetry through second-sphere complexation and therefore σ^a could contribute to the overall relaxation, but Anet and O'Leary state that an enormous value for σ^a would be required to explain Eaton's data. No alternate explanation for the T_1/T_2 ratios has been given other than an unknown systematic error may be influencing the observations.

One possible source of error in several of the earlier studies may have been the use of saturated solutions. A recent study of ^{59}Co T_1's of $Co(acac)_3$ in acetonitrile was conducted as a function of both temperature and concentration.[42] The importance of a variable-concentration study can be understood by considering the Debye expression,

$$\tau_c = \frac{V\eta}{kT}, \tag{3.1}$$

where η is viscosity, k is the Boltzmann constant, T is temperature, V is the volume of a complex, and τ_c is the rotational correlation time (the time it takes for a molecule to tumble $\sim$ 1 radian). If the concentration of a solution is increased, η (hence τ_c) increases. In extreme narrowing (*vide infra*) $\tau_c \propto T_1^{-1}$. Therefore, a plot of T_1^{-1} *vs.* concentration should be linear if the extreme narrowing condition holds. This relationship holds for the $Co(acac)_3$-acetonitrile system at concentrations below 80 mM but deviates from ideality at concentrations greater than 80 mM. Hence,

the importance of using dilute solutions for T_1 studies was demonstrated.

3.3 Relaxation Theory

3.3.1 General Relaxation Theory

Nuclear spins have a random orientation in the absence of a magnetic field. When a magnetic field (B_o) is placed along an axis (by convention the z-axis), net magnetization (M_o) will result along this axis at a rate characterized by the first order time constants T_1 and T_2. T_1 and T_2 are relaxation time constants given by the following differential equations:

$$\frac{dM_z}{dt} = -\frac{M_z - M_o}{T_1} = \frac{M_o - M_z}{T_1} \tag{3.2}$$

$$\frac{dM_x}{dt} = -\frac{M_x}{T_2} \qquad \frac{dM_y}{dt} = -\frac{M_y}{T_2} \tag{3.3}$$

where $M_{x,y,z}$ describes magnetization along the x, y, and z-axes respectively and M_o is the equilibrium magnetization. A pictorial description of the effect of applying a magnetic field to a collection of nuclear spins is seen in Figure 3.1. The spin-lattice or longitudinal relaxation time, T_1, is the time constant describing the approach to equilibrium of magnetization along the z-axis. The spin-spin or transverse relaxation time, T_2, is the time constant describing the approach to equilibrium of magnetization in the x-y plane. These same equations describe the recovery towards equilibrium by a nuclear spin system after a perturbation occurs (*e.g.*, a radiofrequency pulse).

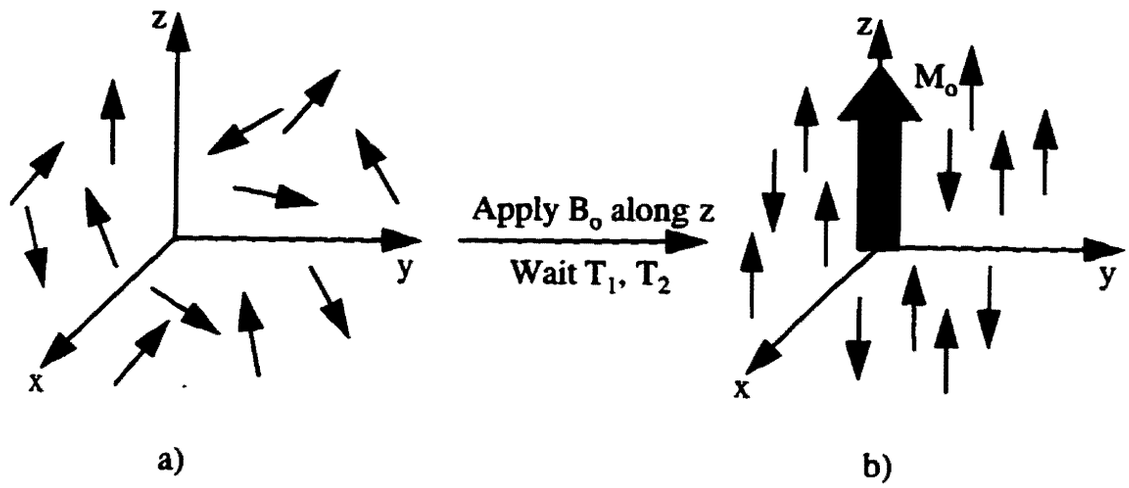


Figure 3.1: a: Nuclear spin in the absence of a magnetic field b: Nuclear spins in the presence of a magnetic field, B_o, after waiting the relaxation times T_1 and T_2.

For relaxation to occur, a local magnetic field must be present fluctuating at the Larmor frequency, ν_o. These fluctuations are described in terms of the spectral density, $J(\omega_o)$,[43]

$$J(\omega_o) = \frac{2\tau_l}{1+\omega_o^2\tau_l^2} \tag{3.4}$$

where ω_o is the angular Larmor frequency (*i.e.*, $\omega_o = 2\pi\nu_o = \gamma B_o$) and τ_l is a general rotational correlation time. In general, the longitudinal relaxation rate for the quadrupolar mechanism, T_{1Q}^{-1}, can be expressed as,

$$T_{1Q}^{-1} = \frac{3}{200}\left(\frac{e^2qQ}{\hbar}\right)^2\left(1+\frac{\eta_Q^2}{3}\right)\frac{2I+3}{I^2(2I-1)}[J(\omega_o)+4J(2\omega_o)] \tag{3.5}$$

while the transverse quadrupolar relaxation rate, T_{2Q}^{-1}, is given by

$$T_{2Q}^{-1} = \frac{3}{400}\left(\frac{e^2qQ}{\hbar}\right)^2\left(1+\frac{\eta_Q^2}{3}\right)\frac{2I+3}{I^2(2I-1)}[3J(0)+5J(\omega_o)+2J(2\omega_o)] \tag{3.6}$$

The other interactions have similar relaxation expressions. The temperature dependence of nuclear spin relaxation is normally defined completely by the spectral density terms, through the dependence of the correlation time, given generally as τ_l, on temperature. However, this does not preclude an additional temperature dependence of the fluctuating local field.

3.3.2 Relaxation Mechanisms

There are five different mechanisms of relaxation possible for diamagnetic compounds. These mechanisms are quadrupolar (Q), dipolar (D), scalar (J), chemical

shielding anisotropy (CSA), and spin rotation (SR). Plots of $\ln(T_1)$ *vs.* 1000/T are given in Figure 3.2 for Q, CSA, and SR (the plots for D and J are similar to that of Q). Studying the Q curve of Figure 3.2, three distinct regions are observed. At the lowest point of the curve $\omega_o^2\tau_l^2 = 1$; this is known as the T_1 minimum. To the left of the minimum, nuclei are in the extreme narrowing region of the T_1 curve. In this region $\omega_o^2\tau_l^2 \ll 1$. To the right of the minimum, $\omega_o^2\tau_l^2 > 1$ and nuclei are in the slow tumbling region of the T_1 curve.

To discover which region of a T_1 curve is relevant to the nuclei under study (for all T_1 curves except SR because SR only occurs when the extreme narrowing condition holds), a variable temperature experiment must be performed. Temperature increases to the left in the T_1 curves. Looking at either Q or CSA, one observes that, if the temperature is increased and the T_1 increases, the nuclei are in the extreme narrowing region of the curve; likewise, if the temperature is increased and the T_1 decreases, the nuclei are in the slow tumbling region of the curve (or SR is dominating); if the T_1 varies little with temperature, the nuclei are near the T_1 minimum (or SR and a second relaxation mechanism are competing).

If the nuclei are in the extreme narrowing region of the T_1 curve, the relaxation rates for Q, D, J, CSA, and SR can be described as[6]

$$T_{1Q}^{-1} = \frac{3\pi^2}{10}\chi^2\left(1+\frac{\eta_Q^2}{3}\right)\left(\frac{2I+3}{I^2(2I-1)}\right)\tau_2 \tag{3.7}$$

$$T_{1D_{IS}}^{-1} = \frac{16\pi^2}{3}R_{DD}^2 S(S+1)\tau_2 \tag{3.8}$$

$$T_{1D_{II}}^{-1} = 8\pi^2 R_{DD}^2 I(I+1)\tau_2 \tag{3.9}$$

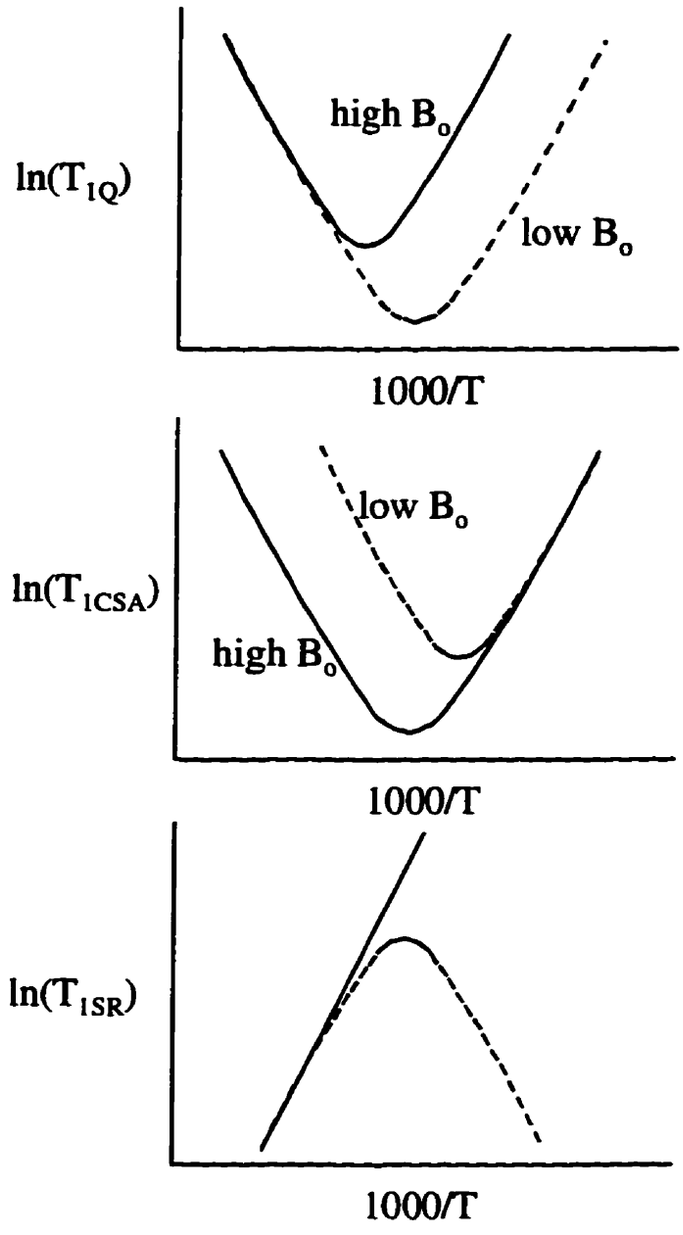


Figure 3.2: Plots of $\ln(T_1)$ vs. 1000/T for Q, CSA, and SR relaxation

$$T_{1J}^{-1} = \frac{8\pi^2}{9} S(S+1) \left(3J_{iso}^2 \tau_o + 2(J^a)^2 \tau_1 + \frac{2}{3}(\Delta J^s)^2 \left(1 + \frac{\eta_J^2}{3} \right) \tau_2 \right) \tag{3.10}$$

$$T_{1CSA}^{-1} = \gamma^2 B_o^2 \left(\frac{2}{3}(\sigma^a)^2 \tau_1 + \frac{2}{15}(\Delta\sigma^s)^2 \left(1 + \frac{\eta_{CS}^2}{3} \right) \tau_2 \right) \tag{3.11}$$

$$T_{1SR}^{-1} = \frac{2}{3} \frac{kT}{\hbar^2} \sum_{i,j=x,y,z} \mathcal{I} c_{ij}^2 \tau_{Jj} \tag{3.12}$$

$$\tau_J \tau_l = \frac{\mathcal{I}}{l(l+1)kT} \tag{3.13}$$

$$T_{1Total}^{-1} = \sum_{\lambda} T_{1\lambda}^{-1} \tag{3.14}$$

where τ_l is the time over which fluctuations of zero, first, or second (l = 0, 1, or 2) rank tensors occur (commonly referred to as the correlation time), χ is the quadrupolar coupling constant, η is the asymmetry of a given tensor, I and S are nuclear spin quantum numbers, J_{iso}, J^a, and ΔJ^s are the isotropic, antisymmetric, and symmetric anisotropy terms of the indirect spin-spin tensor, σ^a and $\Delta\sigma^s$ are the antisymmetric and symmetric anisotropy terms of the chemical shielding tensor, $\mathcal{I}$ is the moment of inertia ($\mathcal{I} = \Sigma_i m_i r_i^2$ where m_i and r_i are the mass and distance of atom i from the axis defining $\mathcal{I}$ through the centre of gravity)[44], c_{ij} are the direction cosines of the SR tensor in the PAS of $\mathcal{I}$, τ_J is the angular momentum correlation time, and λ denotes the different relaxation mechanisms.

If the T_1 curves for Q and CSA are compared, different behavior with respect to B_o on either side of the T_1 minimum is apparent. This difference in behavior can be understood readily by the presence of the B_o^2 term in the relaxation rate equation for CSA. From the above equations (when the extreme narrowing condition applies), it is evident that there is no field dependence for any relaxation mechanism except

CSA, and the field dependence for CSA is such that at a given temperature the T_1 at a higher field will be less than the T_1 at a lower field. In slow tumbling, a field dependence is introduced into Q, D, and J (SR only occurs in extreme narrowing) and a loss of field dependence is observed for CSA. This field dependence arises from the reduction of equation 3.4 to $J(\omega_o) = 2\omega_o^{-2}\tau_l^{-1}$ in the slow tumbling regime. Since $\omega_o = \gamma B_o$, a field dependence is introduced into Q, D, and J and is lost from CSA when the new spectral density is substituted for the old one (*i.e.*, replace τ_l with $2\omega_o^{-2}\tau_l^{-1}$).

For the SR curve in Figure 3.2, a solid line and a dashed curve are given. The dashed curve is observed if, at lower temperatures, a relaxation mechanism other than SR is dominant and SR becomes a greater contributor as temperature increases. That is to say, at lower temperatures, more efficient relaxation occurs *via* another mechanism (right hand side of dashed line). At higher temperatures, SR starts to contribute more and relaxation no longer decreases in efficiency monotonically (centre where the dashed and solid lines start to meet). When very high temperatures are reached, SR becomes the dominant mechanism of relaxation and relaxation now increases in efficiency with increasing temperature (solid line left of the maximum of the dashed line). If SR were the dominant mechanism of relaxation for a molecule, relaxation data would be obtained where relaxation would decrease in efficiency as the temperature was lowered (the solid line).

The expressions for T_2 are similar to those for T_1 with the addition of a zero-frequency spectral density term (see equation 3.6) for all mechanisms except SR.[6] T_1 and T_2 are equal for most mechanisms of relaxation in extreme narrowing.

The two exceptions are 1) when a relaxation mechanism, such as scalar relaxation of the second kind, contributes to T_2 with little to no influence on T_1, and 2) when CSA relaxation is significant. Since T_2 relaxation is sensitive to fluctuations on a much slower time scale due to the J(0) term and scalar relaxation depends on spectral densities at the difference in Larmor frequencies of the two nuclei, this relaxation mechanism is often observed to contribute solely to T_2. For CSA relaxation, $T_1/T_2 = 7/6$ if $\Delta\sigma^s$ is the sole contributor, whereas, if σ^a exclusively contributes, $T_1/T_2 = 1/2$.[41] If T_1 and T_2 are equal, CSA relaxation may still be contributing, but it requires a perfect balance of $\Delta\sigma^s$ and σ^a. In light of these relationships among the different relaxation mechanisms, it is clear that one must perform both variable-temperature and variable-field experiments to determine the mechanisms contributing to the overall relaxation.

3.3.3 Methods of Measuring T_1 and T_2

To obtain a simple, pulse FT NMR 1-D spectrum, one applies a RF pulse, collects a time-domain signal in the form of a free induction decay (FID) and then performs a Fourier transformation of this time-domain signal to transform it into the frequency domain. A slightly more complicated pulse sequence, most commonly the inversion recovery pulse sequence, is used to obtain values of T_1. This pulse sequence is seen in Figure 3.3. The π (or 180°) pulse rotates the net magnetization from the equilibrium position, M_o, to -M_o. One then waits a variable delay time, t_D, after which a $\pi/2$ (or 90°) pulse is applied rotating the magnetization into the x-y plane where it can be recorded in the form of an FID. One would first obtain negative signals at short t_D.

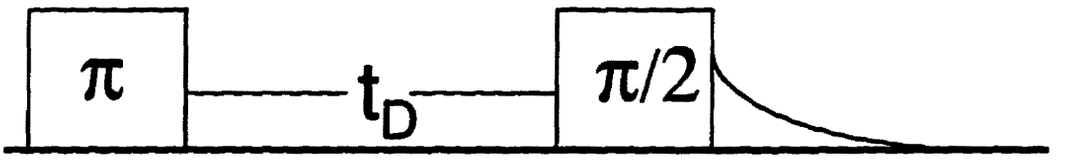


Figure 3.3: The inversion-recovery pulse sequence.

As t_D increases, the signals will become less negative, then positive, and continue to become more positive until the maximum signal is obtained when nuclei have sufficient time to return to equilibrium before the second pulse. The spectra from a series of inversion recovery experiments for *cis*-$[Co(NH_3)_4CO_3]NO_3$ are shown in Figure 3.4. Integrating equation 3.2 from $-M_o$ (the initial magnetization after the π pulse) to $+M_o$ (the final magnetization at equilibrium) results in the following expression;

$$M_o - M(t_D) = 2M_o e^{\frac{-t_d}{T_1}}. \tag{3.15}$$

Using the intensity of the recorded signals as a function of delay time, a curve can be fit in the form of equation 3.15 from which a value of T_1 can be obtained. As an example, the T_1 for *cis*-$[Co(NH_3)_4CO_3]NO_3$ is 242 $\pm$ 2 μs at ambient temperature.

A common method to obtain T_2's is to measure the linewidth at half-height, $\Delta\nu_{1/2}$. This is actually a measure of T_2^* and is given by

$$T_2^* = \frac{1}{\pi\Delta\nu_{1/2}}. \tag{3.16}$$

In the absence of field inhomogeneities, $T_2^* = T_2$. Figure 3.5 shows the 1-D ^{59}Co spectrum (solid line) of *cis*-$[Co(NH_3)_4CO_3]NO_3$ and a Lorentzian line fit (dashed line) of the experimental spectrum. From the fit, a $\Delta\nu_{1/2}$ of 1300 Hz is obtained. This corresponds to a T_2^* of 245 $\pm$ 12 μs.

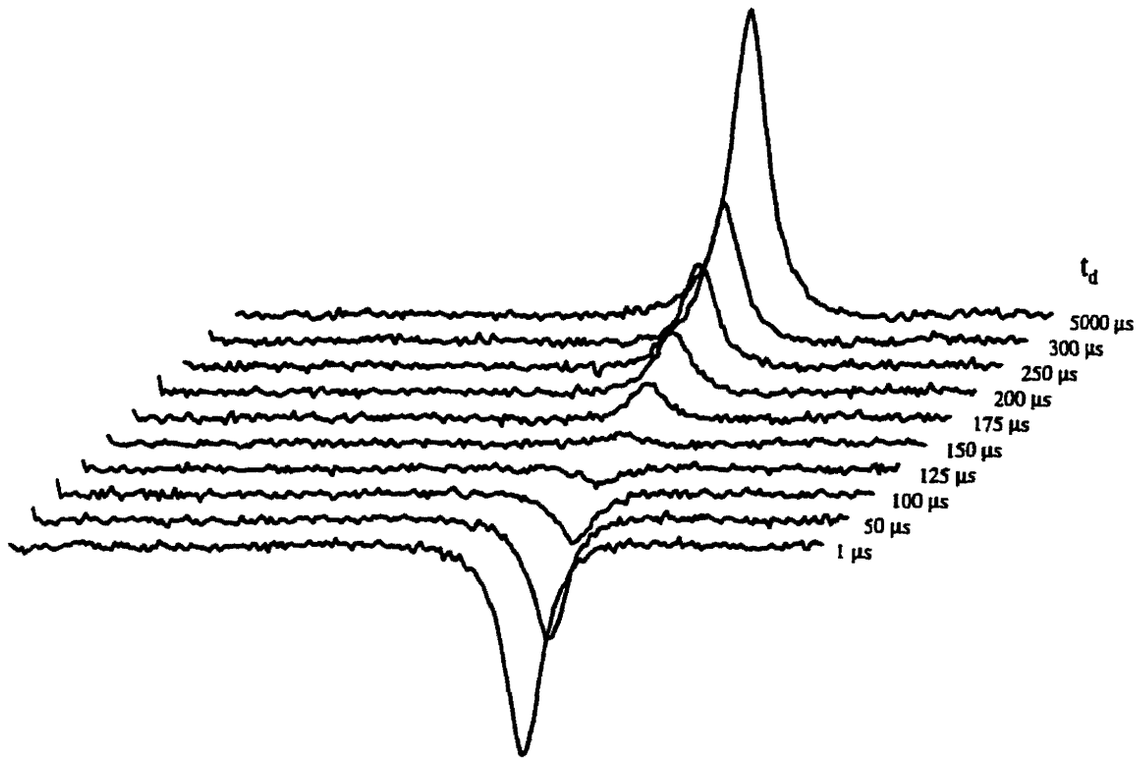


Figure 3.4: Cobalt-59 NMR spectra of *cis*-$[Co(NH_3)_4CO_3]NO_3$ acquired using the inversion recovery pulse sequence. The T_1 obtained from these spectra is 242 ± 2 µs.

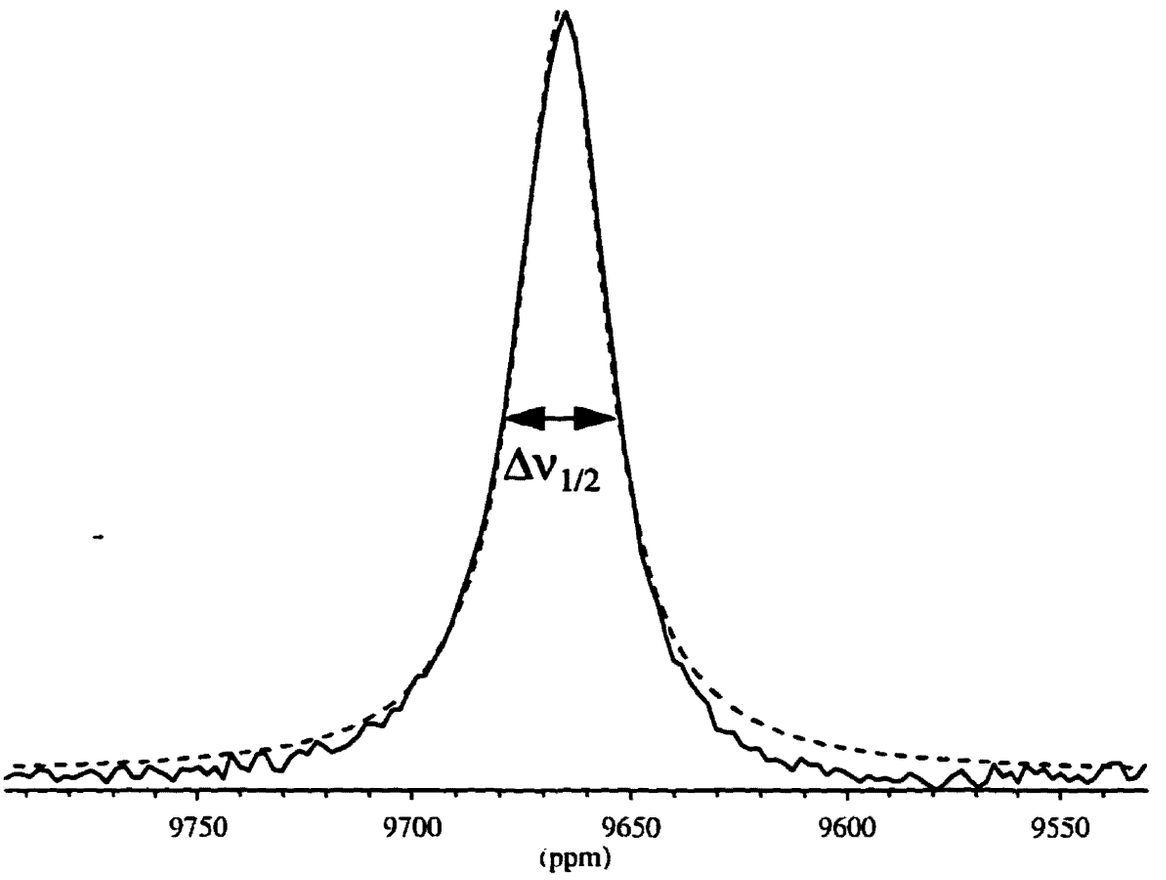


Figure 3.5: Cobalt-59 NMR spectrum of *cis*-$[Co(NH_3)_4CO_3]NO_3$ (solid line) and Lorentzian fit (dashed line). The linewidth obtained from the fit is 1300 Hz which corresponds to a T_2^* of 245 $\pm$ 12 μs.

3.4 Experimental

Cobalt(III) octahedral complexes were made by standard literature procedures or were available commercially (see Table 3.1 for references). For the ^{59}Co NMR studies, commercially available 99.9% $^{2}H_2O$ was used without further purification. Solutions were prepared by dissolving approximately 20 mg of a cobalt complex in 2.0 mL of $^{2}H_2O$ (the exact concentrations are shown in Table 3.1).

Cobalt-59 NMR spectra were recorded on Bruker AC-200 (B_o = 4.7 T) and AMX-500 (B_o = 11.7 T) spectrometers which have resonance frequencies for ^{59}Co at 47.48 MHz and 118.1 MHz respectively. All cobalt-59 spectra were referenced to 1.0 M aqueous $K_3[Co(CN)_6]$. Spin-lattice relaxation times were measured using the inversion recovery pulse sequence. The π and $\pi/2$ pulses were calibrated on each sample. A $\pi/2$ pulse of 11 μs was most common on the AC-200 and on the AMX-500 a 14.5 μs pulse was the average $\pi/2$ pulse. The linewidths at half height ($\Delta\nu_{1/2}$) were obtained by fitting Lorentzian lines to the experimental spectra. All ^{59}Co spectra were obtained on resonance with a ^{2}H field-frequency lock for optimal field stability.

A multinuclear variable-concentration study was performed on Na[Co(edta)]. Solutions were prepared through dilution of a 200 mM stock solution in $^{2}H_2O$. Solutions were degassed through a freeze/pump/thaw cycle to remove paramagnetic oxygen and sealed in 5 mm NMR tubes. All spectra were obtained at ambient temperature on a Bruker AMX-500 spectrometer with a ^{2}H field-frequency lock for field stability. A standard inversion-recovery pulse sequence was used for the ^{23}Na and ^{59}Co spin-lattice relaxation measurements. Simple 1-D spectra were obtained

Table 3.1: Summary of the ^{59}Co NMR data acquired at 294 K (ambient temperature) and 11.7 T.

Compound	δ_{iso}	Concentration	Synthesis	$\Delta\nu_{1/2}$	T_2^*	T_1
$K_3[Co(CN)_6]$	-1 ppm	32.5 mM	a	6.5 ± 1 Hz	49.0 ± 8.0 ms	120 ± 0.2 ms
$[Co(NH_3)_6]Cl_3$	8076 ppm	42.6 mM	b	126 ± 4 Hz	2.53 ± 0.08 ms	42.2 ± 0.2 ms
$[Co(NH_3)_5(NO_2)]Cl_2$	7565 ppm	43.7 mM	c	166 ± 4 Hz	1.92 ± 0.04 ms	4.23 ± 0.02 ms
$Co(acac)_3$	12570 ppm	< 14.3 mM	d	190 ± 6 Hz	1.68 ± 0.03 ms	1.78 ± 0.03 ms
[Co(sepulchrate)]Cl_3	6931 ppm	23.9 mM	d	244 ± 6 Hz	1.30 ± 0.04 ms	1.44 ± 0.04 ms
trans-$[Co(NH_3)_4(NO_2)_2]NO_3$	7157 ppm	< 17.8 mM	e	440 ± 15 Hz	723 ± 26 μs	921 ± 16 μs
cis-$[Co(NH_3)_4(NO_2)_2]NO_3$	7227 ppm	35.6 mM	e	434 ± 15 Hz	733 ± 23 μs	879 ± 9 μs
fac-$Co(CN)_3(NH_3)_3$	3289 ppm	< 15.6 mM	f	417 ± 15 Hz	763 ± 29 μs	774 ± 20 μs
$[Co(NH_3)_5(CO_3)]NO_3 \cdot \frac{1}{2}H_2O$	9053 ppm	42.9 mM	d	1265 ± 60 Hz	252 ± 12 μs	258 ± 3 μs
cis-$[Co(NH_3)_4(CO_3)]NO_3$	9662 ppm	41.8 mM	g	1300 ± 60 Hz	245 ± 12 μs	242 ± 2 μs
$[Co(NH_3)_5Cl]Cl_2$	8793 ppm	14.9 mM	d	2021 ± 75 Hz	158 ± 6 μs	154 ± 2 μs
Na[Co(edta)]	10237 ppm	40.0 mM	h	2641 ± 90 Hz	121 ± 5 μs	119 ± 2 μs

All spectra were acquired in ^2H_2O and referenced to aqueous 1.0 M $K_3[Co(CN)_6]$. (a) Obtained from BDH.

(b) See ref. [45]. (c) Generously donated by A. J. Carty (University of Waterloo). (d) Obtained from Aldrich.

(e) See ref. [46]. (f) See ref. [47]. (g) See ref. [48]. (h) See ref. [49].

with a one-pulse experiment for ^{1}H, ^{23}Na, and ^{59}Co while inverse-gated and power-gated decoupling were used to obtain the ^{13}C spectra to determine the nOe. A single ^{13}C T_1 experiment was acquired on the 40 mM solution to determine a correlation time at room temperature for this concentration (this experiment was also performed on the Co(sepulchrate)$^{3+}$ ion). Proton and carbon spectra were referenced to TMS, cobalt spectra were referenced to 1.0 M $K_3[Co(CN)_6]$ (aq), and sodium spectra were referenced to an infinitely dilute solution of aqueous NaCl (*i.e.*, solutions of 1.0 M, 0.1 M, and 0.01 M were measured and extrapolated to infinite dilution).

A Pascal program developed in our laboratory was used to generate the non-linear least-square fits of the $\ln(T_1)$ *vs.* 1000/T plots. Moments of inertia were calculated using Microsoft Excel (atomic coordinates into $\mathcal{I} = \Sigma_i\, m_i r_i^2$) and *Hyperchem 4.5* from Hypercube, Inc., Waterloo, ON, Canada.

3.5 Results

3.5.1 Variable Temperature

The ambient temperature δ_{iso}'s, T_1's, and $\Delta\nu_{1/2}$'s recorded at 11.7 T for the compounds studied here are shown in Table 3.1. The compounds are arranged in order of decreasing T_1. As shown in Table 3.1, these compounds span a large chemical shift range (over 12 000 ppm), a large range of T_1's (10^3 difference between the shortest and longest), and the linewidths vary from narrow (on the order of Hz) to very wide (on the order of kHz). The dependence of the longitudinal relaxation

times on temperature for the compounds in Table 3.1 are seen in Figures 3.6 and 3.7 where the complexes with the longer room temperature T_1's are seen in Figure 3.6 and the others are in Figure 3.7. The two sets of data for each compound correspond to the two fields (4.7 T and 11.7 T) at which spectra were acquired in this study. The resonance frequencies vary from compound to compound due to large chemical shift differences; spectra were acquired on-resonance for each compound. In all cases, the data clearly fall under extreme narrowing conditions, $\omega_o^2\tau_2^2 \ll 1$. at room temperature; the longitudinal relaxation times increase as temperature is increased. Due to the temperature limitations imposed by the aqueous solvent, the minima of the temperature dependence of longitudinal relaxation times could not be reached.

Analysis of the temperature-dependence of the ^{59}Co longitudinal relaxation *via* T_1 *vs.* inverse temperature plots readily provides values for the activation energies of molecular tumbling from the slopes of the curves. Determination of interaction constants relevant to the mechanism(s) of relaxation require knowledge of the rotational correlation times. Values of the correlation times are available *via* characterization of the T_1 minimum. Low-temperature limitations of the aqueous solvent used in this study precluded definition of this region of the ^{59}Co relaxation curve, which would have provided the best description of the correlation times for each complex. As an alternative, approximate values of the correlation time, τ_2, have been determined *via* ^{13}C longitudinal relaxation measurements. In situations where the heteronuclear ^{13}C-^{1}H dipolar relaxation mechanism dominates ^{13}C longitudinal relaxation, the $T_1(^{13}C)$ values of methine and methylene carbons can be

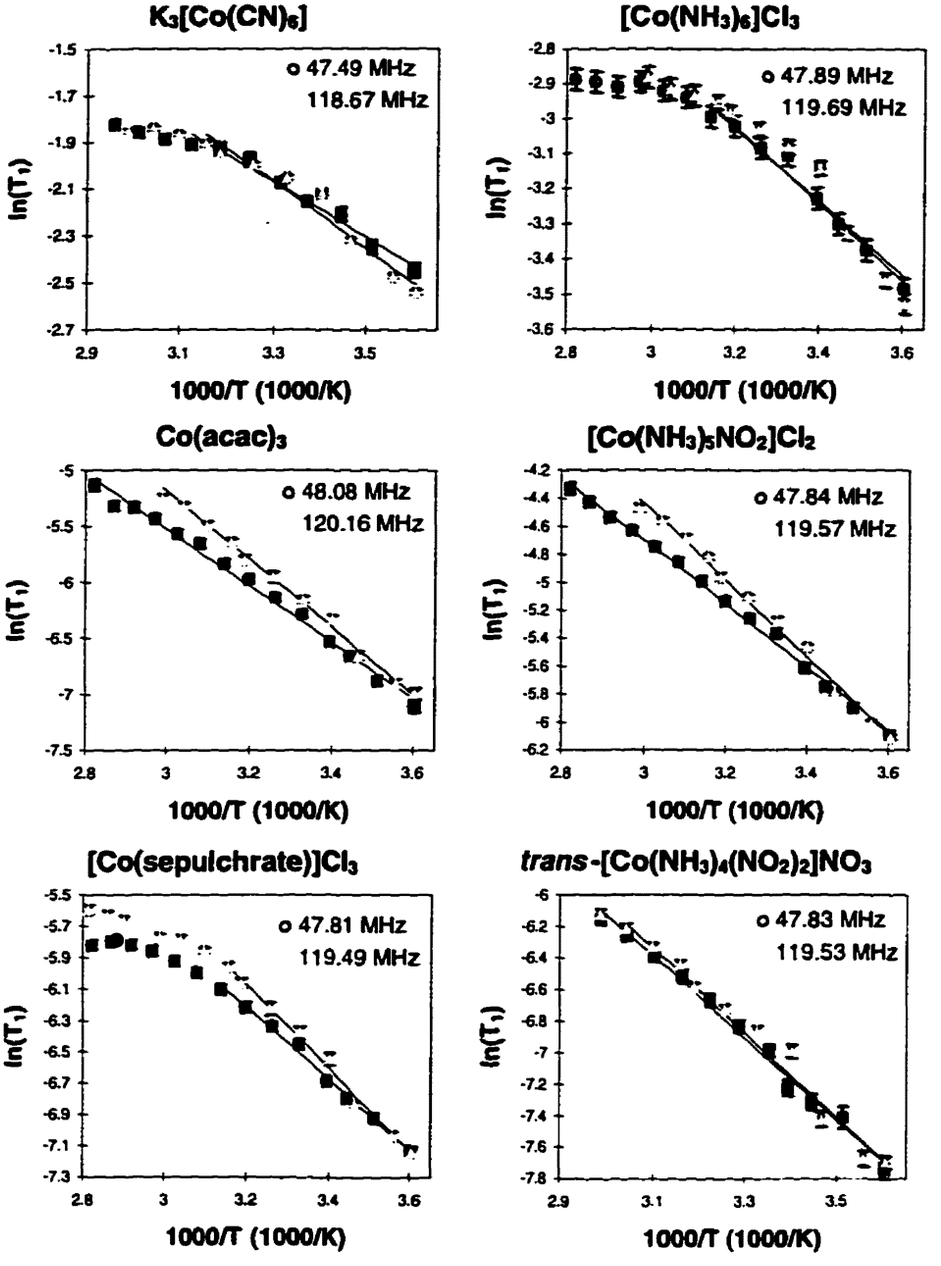


Figure 3.6: Plots of $\ln(T_1)$ *vs.* 1000/T for the 6 octahedral cobalt(III) complexes with longer room temperature T_1's studied at 4.7 and 11.7 T.

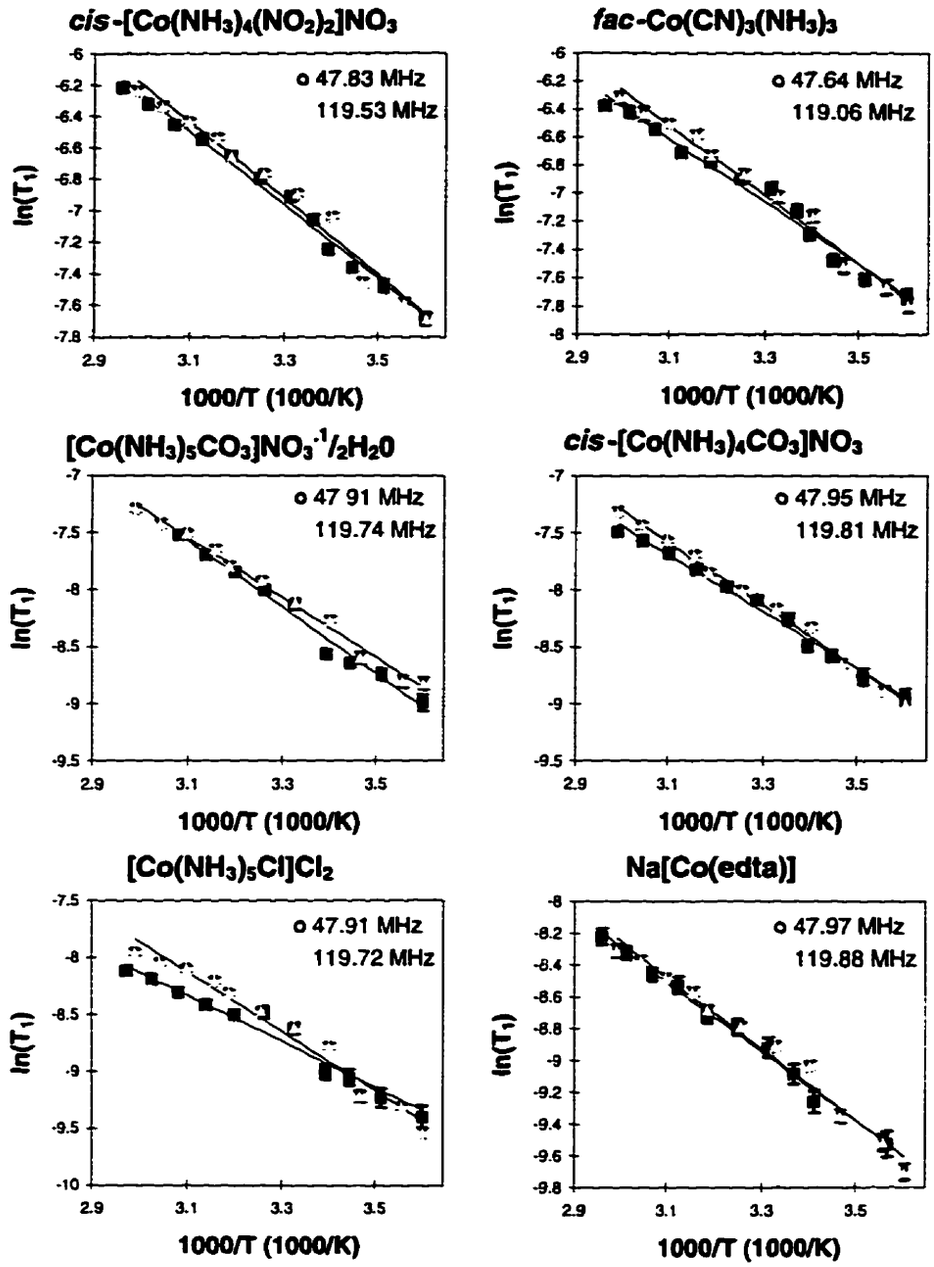


Figure 3.7: Plots of $\ln(T_1)$ *vs.* 1000/T for the 6 octahedral cobalt(III) complexes with the shorter room temperature T_1's studied at 4.7 and 11.7 T.

used to determine rotational correlation times, since the ^{13}C-^{1}H dipolar interaction is well defined for such carbon sites.[50] Under extreme narrowing conditions (relevant at room temperature for the complexes studied according to the cobalt data), the nuclear Overhauser enhancement (nOe) exhibited by ^{13}C nuclei provides a direct measure of the importance of heteronuclear ^{13}C-^{1}H dipolar relaxation to the total relaxation of ^{13}C. The ^{13}C longitudinal relaxation times of $^{13}CH_2$ groups in the [Co(sepulchrate)]Cl_3 (0.650 s) and Na[Co(edta)] (0.593 s) complexes were determined at room temperature; the ^{13}C peaks due to the methylene carbons in both complexes exhibited full (200%) nOe's, consistent with exclusive relaxation *via* the ^{13}C-^{1}H dipolar interaction. Using C-H bond lengths of 110 to 112 pm (typical of the values provided by T_1 minima of protonated ^{13}C nuclei)[50] to estimate the strength of the dipolar interaction, rotational correlation times ranging from 151 to 185 ps are predicted from the ^{13}C measurements. The correlation times for all of the complexes studied here were assumed to fall within this range at room temperature.

Using this estimate for τ_2, analysis of the ^{59}Co longitudinal relaxation data provides values for the ^{59}Co quadrupolar coupling constants (assuming pure quadrupolar relaxation) given in Table 3.2. It should be noted that the rotational activation energies (also quoted in Table 3.2) are independent of this assumption, as they are determined solely by the temperature dependence of the relaxation. Quadrupolar coupling constants were determined under the assumption of complete axial symmetry ($\eta_Q = 0$). The maximum error introduced by this assumption is a reduction in the quoted value of the quadrupolar coupling constant by 25%, as the $1 + \eta_Q^2/3$

Table 3.2: Rotational activation energies and quadrupolar coupling constants determined from analysis of ^{59}Co relaxation data.

Compound	E_a (kJ/mol)	Quadrupolar coupling constant (MHz)
$K_3[Co(CN)_6]$	12.0 ± 2.0	0.351 ± 0.019
$[Co(NH_3)_6]Cl_3$	13.0 ± 0.8	0.585 ± 0.032
$[Co(NH_3)_5(NO_2)]Cl_2$	18.9 ± 2.9	1.87 ± 0.10
$Co(acac)_3$	23.4 ± 1.7	2.88 ± 0.16
[Co(sepulchrate)]Cl_3	18.8 ± 3.2	3.21 ± 0.18
trans-$[Co(NH_3)_4(NO_2)_2]NO_3$	21.6 ± 0.7	4.01 ± 0.21
cis-$[Co(NH_3)_4(NO_2)_2]NO_3$	19.3 ± 0.8	4.10 ± 0.22
fac-$Co(CN)_3(NH_3)_3$	18.4 ± 2.0	4.46 ± 0.24
$[Co(NH_3)_5(CO_3)]NO_3 \cdot \frac{1}{2}H_2O$	24.1 ± 2.3	7.57 ± 0.42
cis-$[Co(NH_3)_4(CO_3)]NO_3$	20.7 ± 2.3	7.81 ± 0.43
$[Co(NH_3)_5Cl]Cl_2$	16.9 ± 4.7	9.79 ± 0.53
Na[Co(edta)]	18.0 ± 0.5	11.1 ± 0.6

term in equation 3.7 will fall in a range from 1 to 4/3. The T_1 minima anticipated, using the estimated τ_2, should occur within a temperature range of 215 ± 15 K (varying with applied magnetic field strength), well below that accessible in aqueous solution.

The relaxation behavior of the twelve compounds studied can be classified into four categories depending on the ligands surrounding the cobalt center: 1) CoX_6, 2) six of the same nuclei (*e.g.*, six O or six N) but not six of the same ligand, 3) *fac*-CoX_3Y_3, and 4) low symmetry cobalt complexes. For all complexes studied, there was no indication of field-dependent relaxation, in spite of the ratio of 6.25 in the square of the magnetic field strengths at which the experiments were performed (4.7 T and 11.7 T). Contributions from the anisotropic chemical shielding

relaxation mechanism will increase with the square of the applied magnetic field strength. The field-independent T_1 values we have determined rule out any significant contributions by the chemical shielding anisotropy mechanism to the overall relaxation rate.

Analysis of a T_1 curve provided details concerning relaxation mechanism(s) of a complex. The T_1 curves for $K_3[Co(CN)_6]$ and $[Co(NH_3)_6]Cl_3$ both display linear and non-linear regions. In the linear region, relaxation must be either through Q, D, or J because there is no field dependence (therefore no CSA). Since 98.9% of carbon nuclei are spin 0, there would not be any dipolar or scalar relaxation through carbon in $K_3[Co(CN)_6]$. The dipolar coupling constant (R_{DD} from equation 2.15) is only 75 Hz for Co-N in $K_3[Co(CN)_6]$ (using a value of 3.05 Å for r_{CoN})[51] and 268 Hz in $[Co(NH_3)_6]Cl_3$ (using a value of 1.97 Å for r_{CoN}).[52] The maximum relaxation rate is observed at the T_1 minimum where the following expression for dipolar relaxation applies,[6]

$$T_{1D_{IS}}^{-1} = \frac{4\pi^2}{5} R_{DD}^2 S(S+1)\tau_2 \qquad (3.17)$$

At the T_1 minimum, the value of τ_2 is defined *via* the condition $\omega_o\tau_2 = 1$, which is 1.33×10^{-9} s for $[Co(NH_3)_6]Cl_3$ (using a Larmor frequency of 119.69 MHz). This yields a relaxation rate of 0.00151 s^{-1} for a single ^{14}N dipolar coupled to the ^{59}Co centre. The rate would be six times faster for the six ^{14}N in $[Co(NH_3)_6]Cl_3$. Therefore a minimum T_1 of 110 s is expected for six ^{14}N dipolar coupled to ^{59}Co. In extreme narrowing (the region of the T_1 curve sampled in these compounds), the contribution from the dipolar relaxation mechanism would be even less than the

value given here. Therefore dipolar relaxation from ^{14}N to ^{59}Co does not contribute to the relaxation of this compound or any of the other compounds in the study because the dipolar coupling from ^{14}N to ^{59}Co would be strongest in $[Co(NH_3)_6]Cl_3$. Dipolar relaxation *via* the protons of the amino groups could also contribute. The dipolar contribution due to the 18 ^1H's have been measured by acquiring a ^1H decoupled ^{59}Co spectrum in H_2O (*i.e.*, an nOe experiment) and the dipolar contribution to relaxation has been measured to be 0.3%. In ^2H_2O all of the amino H's would be exchanged for ^2H's as previously demonstrated,[53] and the dipolar coupling through ^2H's would be less than through ^1H's by a factor of the square of the magnetogyric ratios (the contribution of dipolar relaxation through the ^2H's would be 0.05% at room temperature). All of the other compounds in this study would have a lesser contribution *via* the dipolar mechanism because there are less protons (or ^2H) around cobalt in the other compounds with respect to $[Co(NH_3)_6]Cl_3$. Scalar relaxation has been observed to affect only T_2[54] and therefore can be discounted for T_1. Relaxation in the linear region of the T_1 curve must be through the quadrupolar mechanism of relaxation. In the non-linear region, SR must contribute to the relaxation because of the observed behavior.

In the following set of compounds, there are either six N ($[Co(NH_3)_5(NO_2)]Cl_2$, [Co(sepulchrate)]Cl_3 [sepulchrate = 1,3,6,8,10,13,16,19-octazabicyclo[6.6.6]eicosane], *cis*- and *trans*-$[Co(NH_3)_4(NO_2)_2]NO_3$), or six O ($Co(acac)_3$ [acac = acetylacetonate]) around the cobalt(III) center. Therefore, there is high local symmetry but the overall symmetry is not as high as having six equivalent ligands as in the compounds previously discussed. As symmetry decreases, the efg at the cobalt centre

increases and therefore relaxation through the quadrupolar mechanism is more efficient (the T_1's of these compounds are about an order of magnitude faster than $[Co(NH_3)_6]Cl_3$). All of these compounds relax through Q because D and J would be inefficient (as described above) but [Co(sepulchrate)]Cl_3 is also observed to have a non-linear region and therefore SR must contribute to its relaxation at higher temperatures.

fac-$Co(CN)_3(NH_3)_3$ has a T_1 on the same order of magnitude as for the compounds with six N or six O around the cobalt(III) centre even though the symmetry of this compound is lower. At first inspection, it might be expected that the T_1 would be shorter than that observed, but if it is remembered that the efg is the Laplacian of the potential, it is obvious that the efg would not be very large for *fac*-$Co(CN)_3(NH_3)_3$ (indeed, for complete *fac* symmetry, the efg would be zero). Because of the relative relaxation rate (*i.e*, D and J would give a T_1 with a longer relaxation time), there must be an efg for Q to be the dominant mechanism of relaxation.

The symmetries of the remaining four compounds ($[Co(NH_3)_5CO_3]NO_3 \cdot \frac{1}{2}H_2O$, *cis*-$[Co(NH_3)_4CO_3]NO_3$, $[Co(NH_3)_5Cl]Cl_2$, and Na[Co(edta)]) are low and therefore large efg's are expected. This is observed because the T_1's of these compounds are much shorter than any of the previously described compounds and therefore Q is the dominant relaxation mechanism in these compounds. If we compare the symmetry of compounds in this set with those previously discussed, a trend is observed. The symmetry of the $Co(NH_3)_5CO_3^+$ and $Co(NH_3)_5NO_2^{2+}$ are the same (if the H's and O's are ignored), but the T_1 for $Co(NH_3)_5CO_3^+$ is an order of magnitude faster

than $Co(NH_3)_5NO_2^{2+}$. This change of an N for an O is similar to the change of NH_3 to NO_2 for $Co(NH_3)_6^{3+}$ to $Co(NH_3)_5NO_2^{2+}$ which also have T_1's that differ by an order of magnitude. This trend shows that local molecular symmetry (*i.e.*, CoN_6 to CoN_5N') and the ligands around the cobalt(III) centre (*i.e.*, change of CoN_5N' to CoN_5O) have a similar effect on the efg.

Figure 3.8 demonstrates the dependence of the ^{59}Co NMR transverse relaxation times (inverse linewidths) on temperature. For most of the complexes, the transverse relaxation times mimic the behavior of the longitudinal relaxation times, increasing with temperature, satisfying the extreme-narrowing condition $T_{1Q} = T_{2Q}$. Two notable exceptions are the slowest-relaxing complexes, $Co(CN)_6^{3-}$ and $Co(NH_3)_6^{3+}$. Since these complexes possess small quadrupolar coupling constants, their relaxation behavior is more susceptible to influences from competing mechanisms. The increase in transverse relaxation times with decreasing temperature suggests that scalar relaxation of the second kind from the surrounding quadrupolar ^{14}N nuclei is a contributor to T_2, as previously suggested by Bryant.[31, 32] This mechanism might also be expected to contribute to the ^{59}Co longitudinal relaxation in these complexes; however the difference in the resonance frequencies of the ^{59}Co-^{14}N spin-pair makes this unlikely[6] and, indeed, such contributions were not evident.

Three of the complexes demonstrate relaxation behaviour that does not conform to the temperature dependence anticipated for exclusive contributions from the quadrupolar relaxation mechanism. For these complexes, namely $K_3[Co(CN)_6]$, $[Co(NH_3)_6]Cl_3$, and [Co(sepulchrate)]Cl_3, a bifunctional relaxation time *vs.* inverse

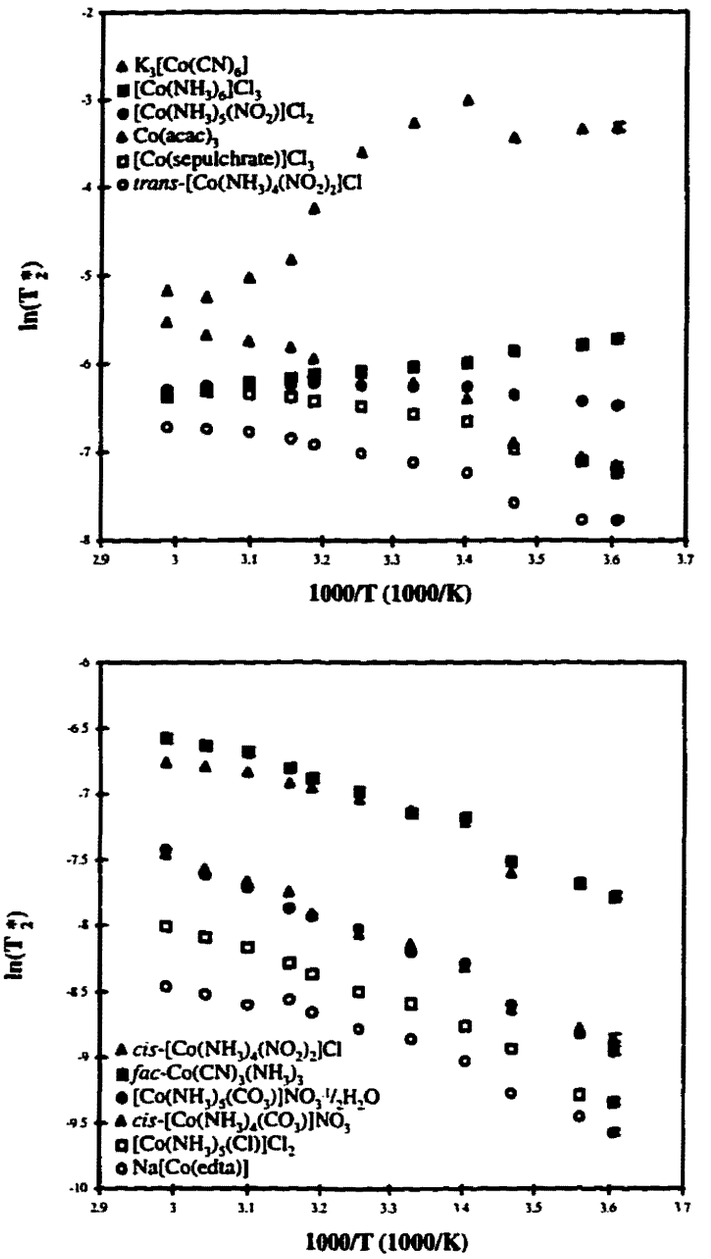


Figure 3.8: Plots of $\ln(T_2^*)$ *vs.* 1000/T for the twelve complexes studied at 11.7 T.

Table 3.3: Isotropic ^{59}Co chemical shifts, moments of inertia, and spin-rotation constants (derived from analyses of relaxation data) for three cobalt complexes displaying spin-rotation relaxation.

Compound	δ_{iso} (ppm)	Moment of inertia (10^{45} kg m^2)	Spin-rotation constant (kHz)
$K_3[Co(CN)_6]$	-1	11.5	217
$[Co(NH_3)_6]Cl_3$	8076	6.36 (a)	676
[Co(sepulchrate)]Cl_3	6931	21.9	671

(a) perdeuterated form in ^2H_2O solution

temperature fitting was performed, allowing the total relaxation rate (equation 3.14) due to contributions from both the quadrupolar mechanism (*via* 3.7) and spin-rotation mechanism (*via* 3.12) to be quantified. The Hubbard relation[55] (equation 3.13) was used to provide τ_J from τ_2, which should be a reasonable model for the rotational diffusion of these complexes in the presence of the aqueous solvent,[56] based on the high viscosity and small relative molecular size of water. Insertion of 3.13 into 3.12 provides an equation that depends on τ_2 and $c^2\mathcal{I}^2$, the former of which has been estimated from the carbon longitudinal relaxation time measurements. The spin-rotation constants, $(c^2)^{1/2}$, have been derived from the fitted interaction constant $c^2\mathcal{I}^2$ by assuming the moment of inertia, $\mathcal{I}$, of the complex in solution is identical to that of the isolated molecule (for Co(sepulchrate)$^{3+}$, a symmetric top, an isotropic average of the moment of inertia tensor was used). The results of the bifunctional fitting for these three complexes is presented in Table 3.3.

3.5.2 Variable Concentration

Great care was taken to ensure that dilute solutions were used for all relaxation measurements. Evidence supporting this approach was provided by the concentration-dependent study of Na[Co(edta)], as well the previous results in the ^{59}Co relaxation studies of $Co(acac)_3$ in acetonitrile.[42]

In the variable concentration study of Na[Co(edta)], four nuclei were studied - ^{1}H, ^{13}C, ^{23}Na, and ^{59}Co. The ^{23}Na and ^{59}Co spectra each contain only one peak over all concentrations while the ^{1}H and ^{13}C spectra contain multiple peaks due to magnetic inequivalence.

A linear relationship between T_1^{-1} and concentration is observed for concentrations up to 140 mM for the single ^{59}Co signal in Na[Co(edta)], as expected according to the Debye expression. At concentrations greater than 140 mM, the linear relationship no longer holds and the ^{59}Co relaxation times appear to reach a plateau at these concentrations. Figure 3.9 shows the plot of T_1^{-1} (^{59}Co) *vs.* concentration. These results are significant because it brings into question the ^{59}Co relaxation studies previous to those described here. In these earlier studies, arguments based on isolated molecules undergoing rotational diffusion, which are questionable based on these results, were used.

Sodium-23 is a quadrupolar nucleus like ^{59}Co and therefore relaxes purely through the quadrupolar mechanism of relaxation. The T_1's observed were short (on the order of 20 ms) as expected for a quadrupolar nucleus. A plot of T_1^{-1} (^{23}Na) *vs.* concentration for Na[Co(edta)] is shown in Figure 3.10. This plot shows that the one sodium site has a linear relationship between T_1^{-1} and concentration over all the

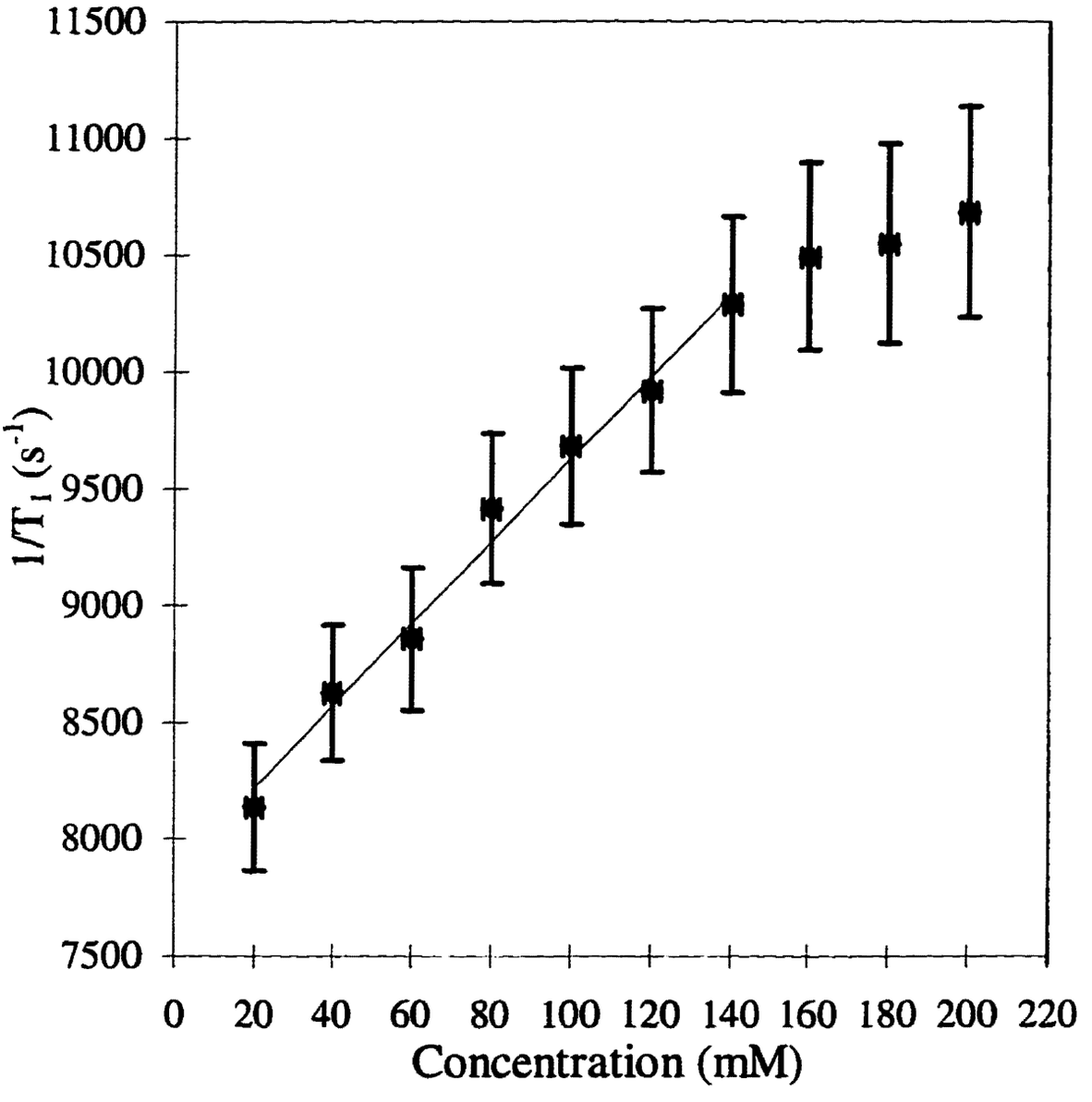


Figure 3.9: Plot of T_1^{-1} (^{59}Co) *vs.* concentration for Na[Co(edta)].

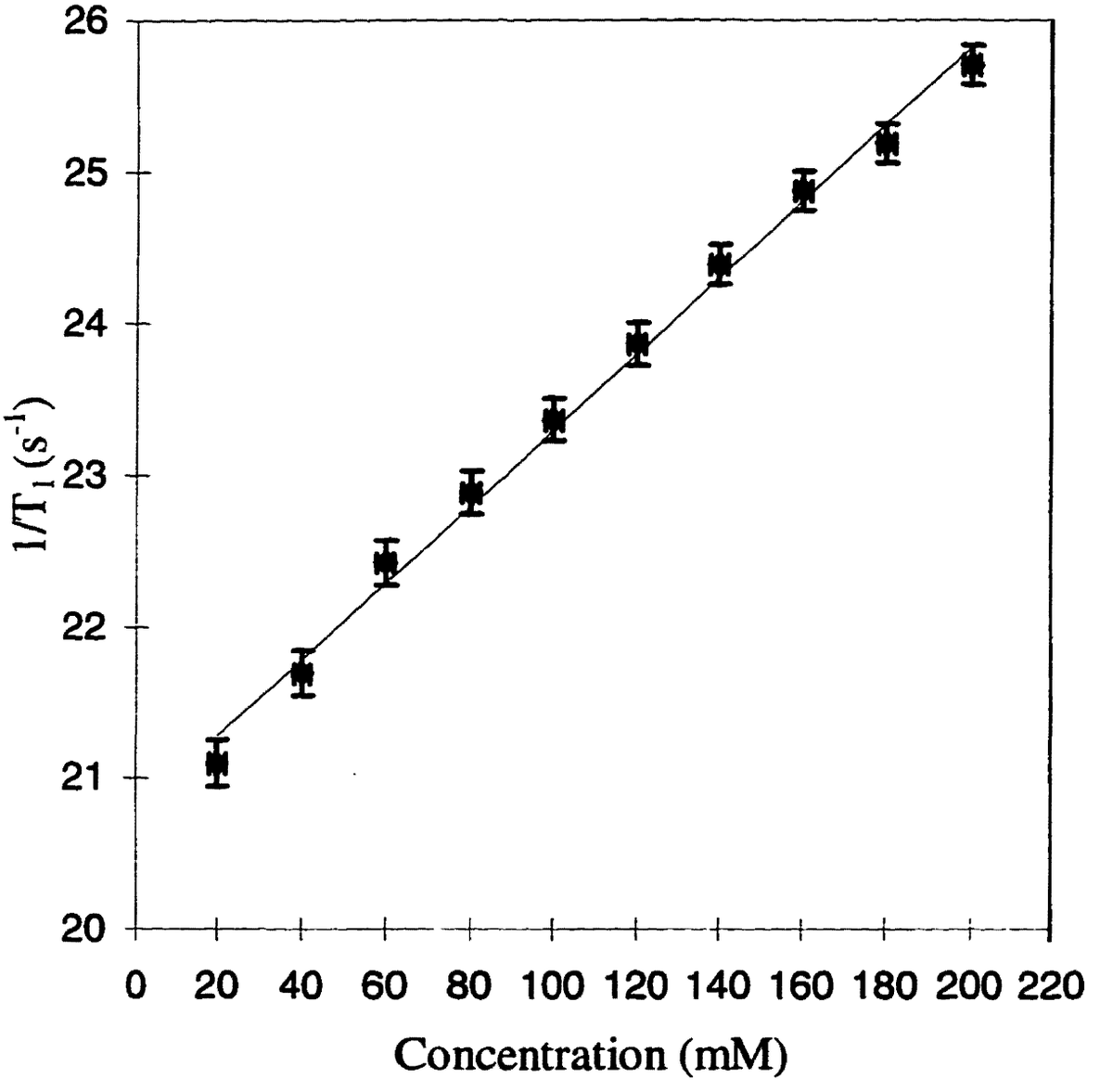


Figure 3.10: Plot of T_1^{-1} (^{23}Na) *vs.* concentration for Na[Co(edta)].

Table 3.4: pH measurements of Na[Co(edta)] solutions

Concentration of Na[Co(edta)] (mM)	p^1H (measured)	p^2H (corrected)*
20	5.68	6.08
40	5.72	6.12
60	6.10	6.50
80	5.62	6.02
100	6.15	6.55
120	6.10	6.50
140	5.58	5.98
160	6.55	6.95
180	6.45	6.85
200	6.76	7.16

* Conversion from p^1H to p^2H taken from reference [57].

concentrations in this study. Therefore the process occurring at the cobalt nucleus does not have any effect on the sodium counterion.

Unlike the previous two nuclei, there are multiple signals in both the proton and carbon spectra of Na[Co(edta)]. This can be understood by looking at a model of the complex in Figure 3.11. In this representation, one observes that the $Co(edta)^-$ anion has a two-fold rotation axis. Therefore, there are six unique protons and five carbons. The methylene region of the proton and the $^{13}C\{^1H\}$ spectra show three distinct types of spectra. These three types of spectra can be understood by looking at the p^2H's of the solutions given in Table 3.4. The $^{13}C\{^1H\}$ and proton spectra are given for the ten concentrations as a function of p^2H in Figures 3.12 - 3.14. The carbonyl region of the spectra are not shown because signals for the two carbonyl carbons were found to be consistent (at 182.7 $\pm$ 0.1 ppm and 182.0 $\pm$ 0.1 ppm) over all concentrations.

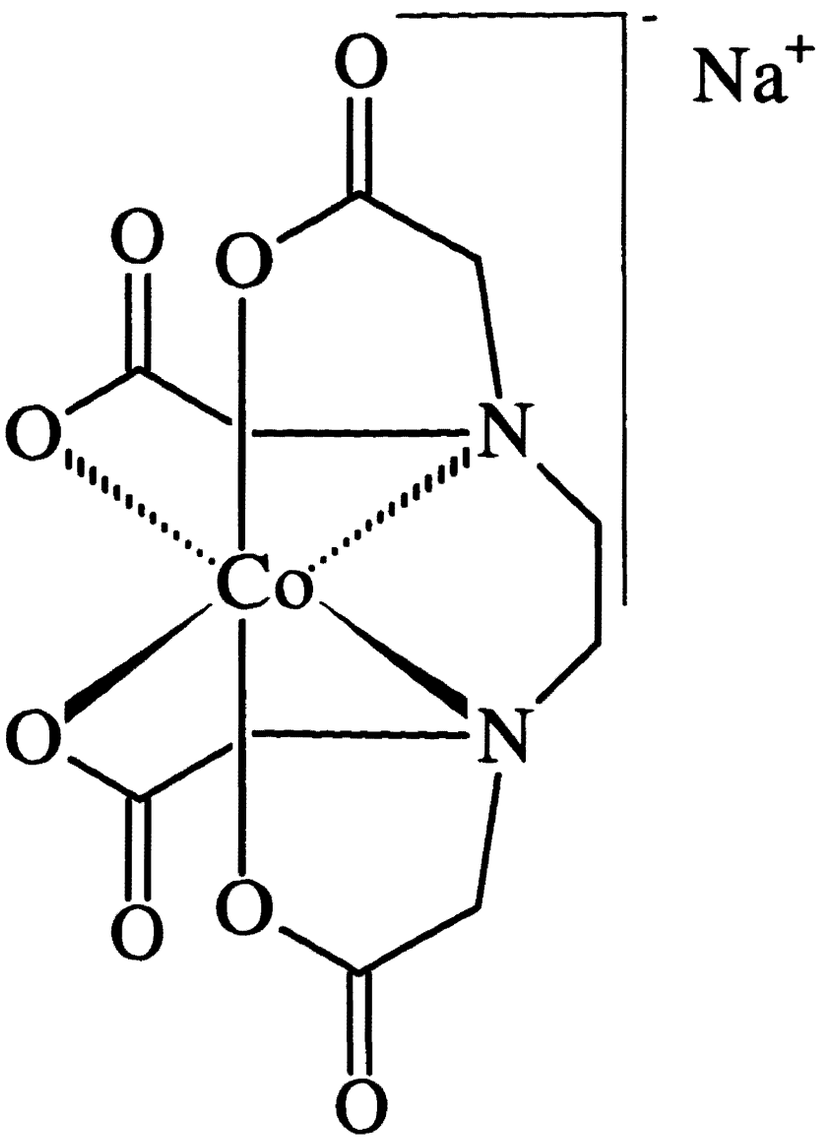


Figure 3.11: Pictorial representation of Na[Co(edta)].

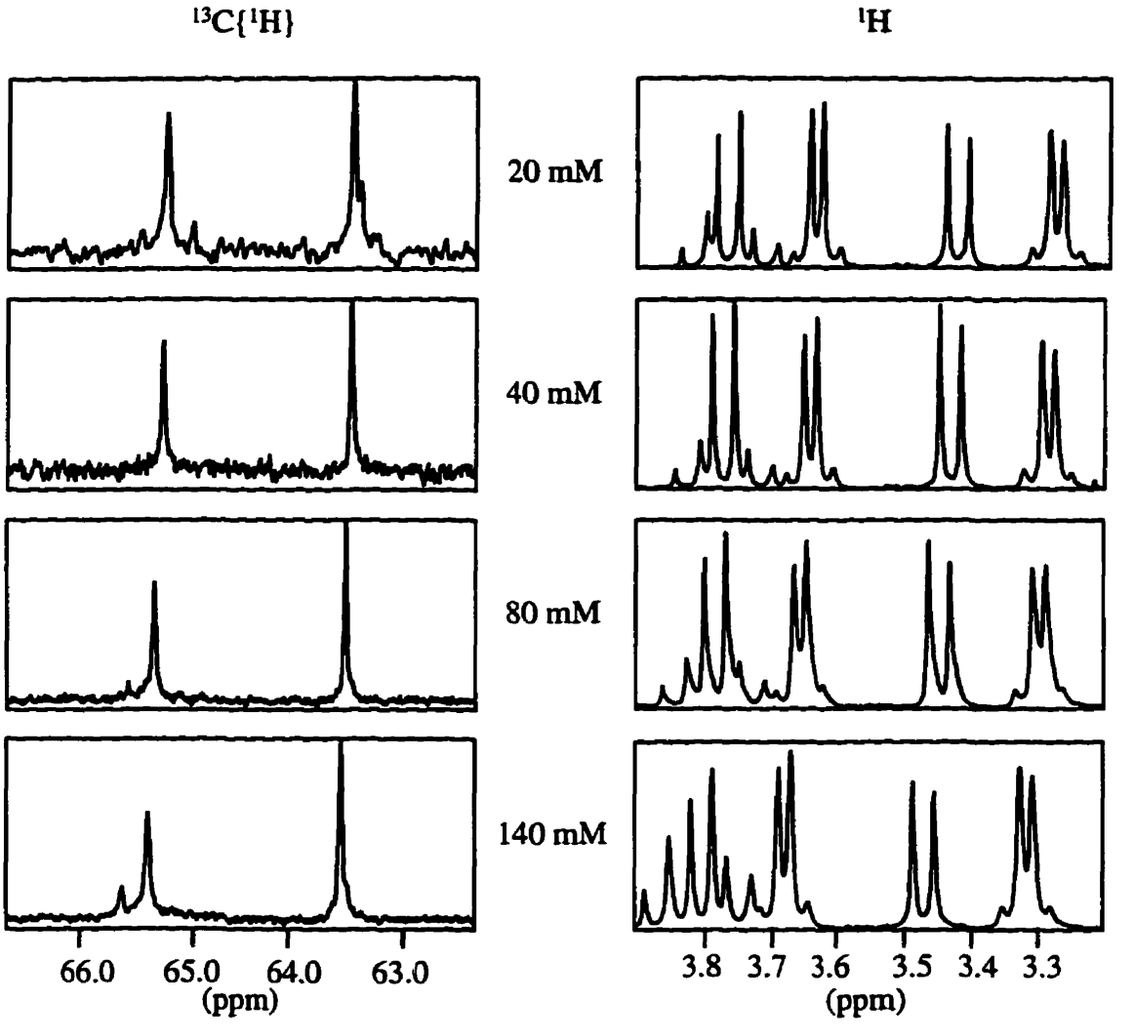


Figure 3.12: Plots of the $^{13}C\{^1H\}$ and ^1H spectra of Na[Co(edta)] in the p^{2}H range of 5.98 - 6.12 at 11.7 T.

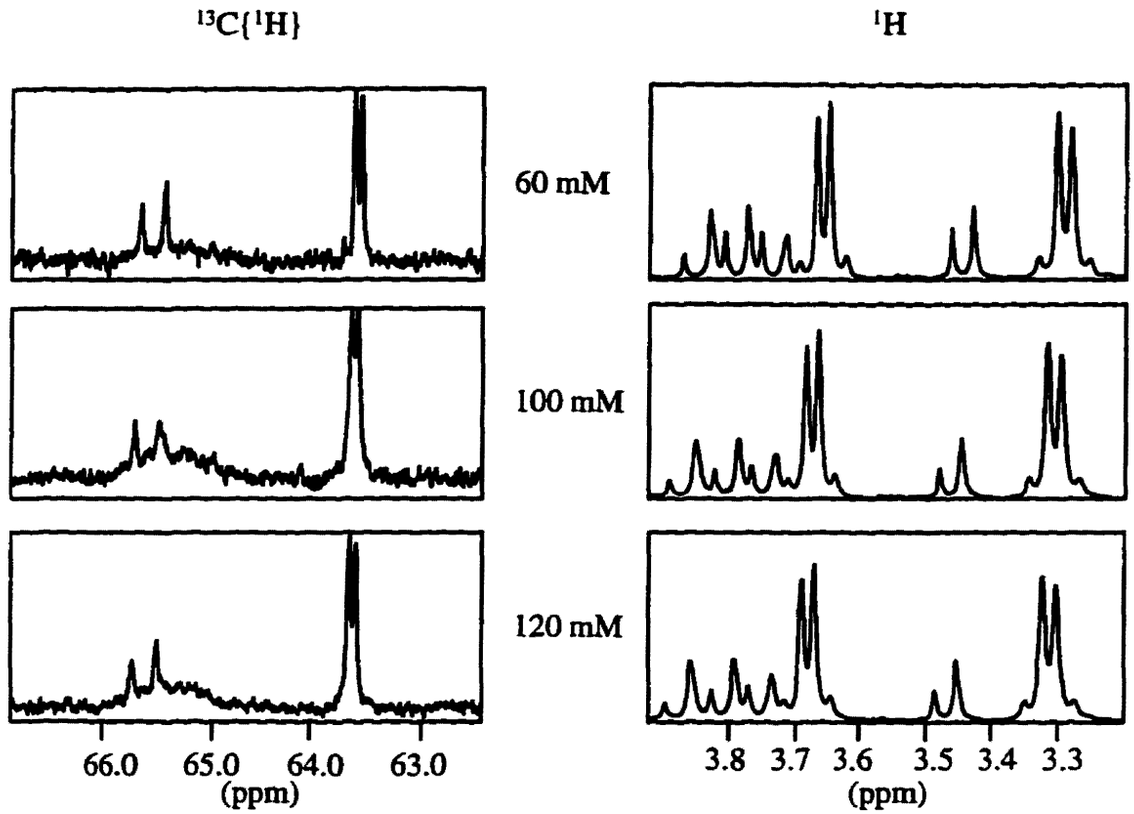


Figure 3.13: Plots of the $^{13}C\{^1H\}$ and ^1H spectra of Na[Co(edta)] in the p^{2}H range of 6.50 - 6.55 at 11.7 T.

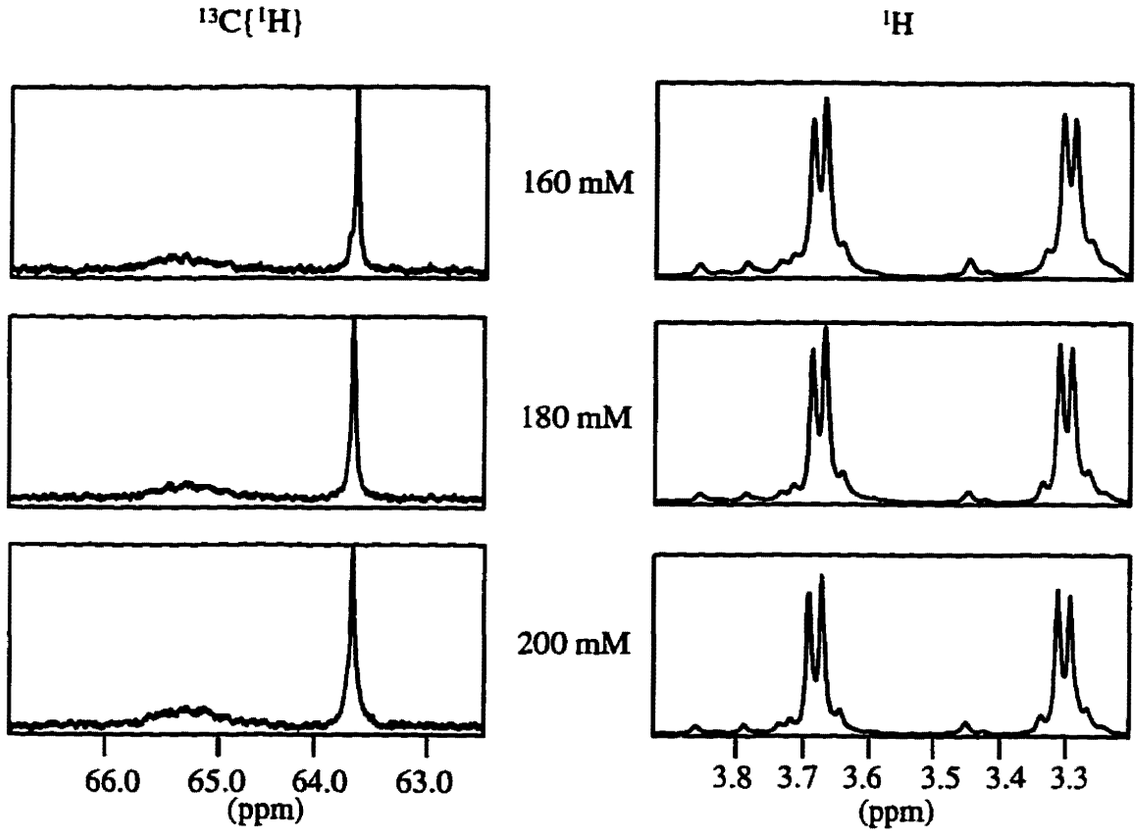


Figure 3.14: Plots of the $^{13}C\{^1H\}$ and ^1H spectra of Na[Co(edta)] in the p^{2}H range of 6.85 - 7.16 at 11.7 T.

From the model in Figure 3.11, six magnetically distinct proton signals are expected by symmetry which should be constant over all concentrations. The experimental proton spectra, however, only have two signals which are consistent over all concentrations. The signals at 3.63 ppm and 3.28 ppm form an AA'BB' pattern and, therefore, can be identified as the ethylene bridge protons. All of the other proton signals observed are not consistent as concentration increases, but the spectra (both $^{13}C\{^1H\}$ and ^1H) are observed to be consistent within a given p^2H range (as shown in Figures 3.12 - 3.14). Therefore the determining factor for the changes in the spectra is p^2H and not concentration. A possible reason for the different p^2H values could be due to the glass of the NMR tubes (all of the solutions were prepared from the same stock solution so this cannot be a factor). The tubes were washed, rinsed with methanol, and dried before use, but the tubes themselves can have acidic sites causing the observed fluctuations of p^2H. The observed p^2H dependent behaviour must arise from a proton exchange involving one of the oxygens of the acetate groups. It is, however, interesting that the highest three concentrations give the same spectra and at these concentrations the cobalt relaxation measurements no longer follow the behavior expected from the Debye expression.

3.6 Discussion

The dominant mechanism of relaxation at room temperature for all the cobalt nuclei in this study has been determined to be the quadrupolar mechanism. The values of the quadrupolar coupling constants determined for these complexes closely follow the expectations based on local symmetry arguments. Highly symmetric complexes,

such as $Co(CN)_6^{3-}$ and $Co(NH_3)_6^{3+}$, exhibit very small values, while more asymmetric complexes have significantly larger values. There is no relationship between the observed ^{59}Co chemical shifts and the quadrupolar coupling constants derived from the relaxation data for a given complex. At temperatures above 323 K, $Co(CN)_6^{3-}$, $Co(NH_3)_6^{3+}$, and Co(sepulchrate)$^{3+}$ show a non-linear dependence of T_1 *vs.* 1000/T, consistent with an increasing contribution of the spin-rotation mechanism. This behavior has been suggested previously by Osten and Jameson[29] for tetrahedral complexes with a quadrupolar nucleus at the centre. If spin-rotation is contributing to only these three compounds, they must possess characteristics unique from the other complexes. Spin-rotation is able to contribute to the relaxation of the two compounds with high symmetry because they have small χ's and therefore inefficient quadrupolar relaxation allowing SR to contribute to the longitudinal relaxation and scalar relaxation of the second kind to contribute to the transverse relaxation. [Co(sepulchrate)]Cl_3 is different from the other compounds in this study in that it is a bulky complex which has a large moment of inertia. This increases the susceptibility to SR relaxation. In Figure 3.15, T_1 curves showing competition between Q and SR mechanisms of relaxation are displayed. As this figure shows, if Q relaxation is inefficient, SR relaxation can occur at lower temperatures than if Q relaxation is efficient, and molecules which have large moments of inertia are observed to have SR relaxation contribute at lower temperatures than molecules with small moments of inertia.

Previous studies have proposed that the chemical shielding anisotropy relaxation mechanism contributes to the ^{59}Co relaxation in octahedral cobalt(III) complexes.[37,

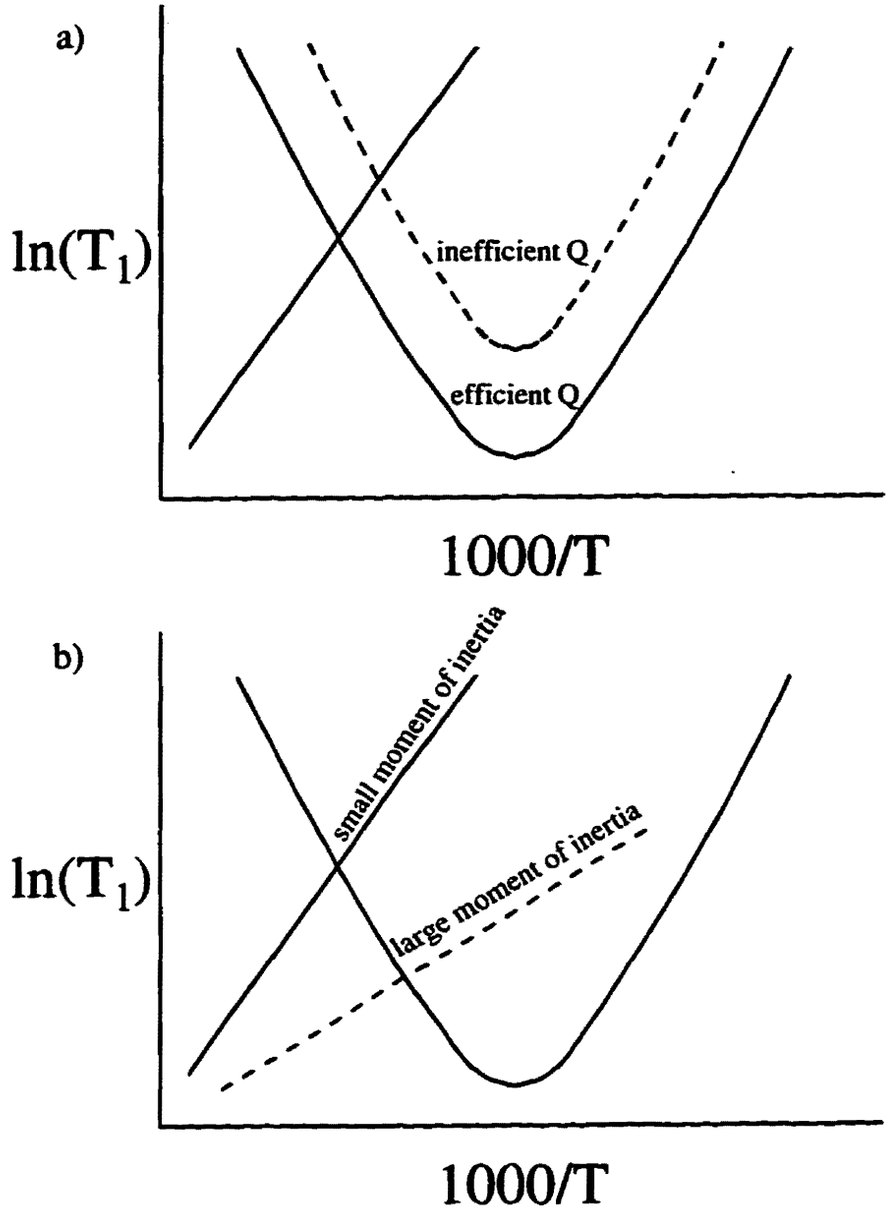


Figure 3.15: T_1 curves show the competition between Q and SR mechanisms of relaxation for (a) efficient *vs.* Q relaxation and (b) two different moments of inertia for SR relaxation.

38, 39, 40] Evidence presented here shows that this conclusion is incorrect. As described in Section 3.2, CSA was believed to participate because the linewidths were observed to vary with increasing field strength and the longitudinal relaxation times were observed to be less than transverse relaxation times. One possible explanation of the previous observations could be the use of saturated solutions in those studies. The variable-concentration studies on Na[Co(edta)] as well as the recent results of $Co(acac)_3$ in acetonitrile[42] show behavior which deviates from the Debye model for ^{59}Co relaxation in solutions with high concentrations.

Osten and Jameson[29] have suggested a model for intermolecular effects causing transient distortions of the efg, thereby modulating the quadrupolar local field necessary for relaxation. In this model, the temperature dependence is not limited to the spectral density *via* the rotational correlation time, but also includes a temperature (T) and density (ρ) dependent quadrupolar interaction, χ. This $\chi(T,\rho)$ given here is analogous to the $\sigma(T,\rho)$ given by Osten and Jameson for chemical shielding.

$$\chi(T,\rho) = \chi_o(T) + \chi_1(T)\rho + ... \tag{3.18}$$

The first term in this expansion is the temperature dependence of the quadrupolar interaction for an isolated molecule, *i.e.*, the intramolecular χ; the intermolecular effects (also temperature-dependent) are contained in $\chi_1(T)$. The anharmonic vibrational distortions of the equilibrium (r_e) structure of a molecule account for the temperature-dependence of $\chi_o(T)$ term and these can be determined as the density-invariant component of a gas-phase ρ-dependent study. At high densities, such as those encountered in condensed phases (including aqueous solutions), the

intermolecular term, $\chi_1(T)$, is believed to dominate any temperature-dependence of $\chi(T,\rho)$.

Much has been made of the influence of intermolecular interactions on, in particular, ^{59}Co relaxation, most notably in the extensive literature relating ^{59}Co T_1's and T_2's to ion-pairing effects.[24, 30, 34, 35] It is believed that $\chi_{static}(^{59}Co)$ is insensitive to ion-pairing effects,[30] such effects being limited to changes in $J(\omega_o)$ or the rotational correlation time of the ion. However, there have also been several suggestions that the rotational correlation time of the ion is not relevant to cobalt relaxation, particularly when saturated solutions are studied.[26, 37, 38, 39, 40] These observations are probably the result of $\chi_1(T)$, where the extra temperature-dependence of the interaction as well as that of the spectral density result in more efficient relaxation and "apparent" correlation times orders of magnitude longer than anticipated from the T_1's of other nuclei (*e.g.*, ^{13}C and ^{14}N). This agrees with our observations of more efficient relaxation as concentration is increased.

Characterization of the spin-rotation constants for the three complexes described above provides an opportunity to estimate the degree of paramagnetic shielding exhibited in each complex. Ramsey,[11] Flygare[18] and Deverell[19] each have demonstrated the connection between paramagnetic shielding and spin-rotation constants, and, where both are available, absolute chemical shielding scales, relative to the bare nucleus at 0 ppm, have been determined for several nuclei.[12] No such scale has been reported for cobalt. A plot of the ^{59}Co spin-rotation constants *vs.* chemical shift determined for the three complexes in this study, seen in Figure 3.16, extrapolated to a spin-rotation constant of zero, provides a value

of -3578 ± 1137 ppm, relative to 1.0 M $K_3[Co(CN)_6]$ (aq) for the diamagnetic contribution to the ^{59}Co chemical shielding. The spin-rotation constants determined from the relaxation data are absolute values, since only the square of these constants is available from relaxation data. A positive sign has been assumed, although all that is significant in this assumption is that all three complexes possess SR constants of the same sign. This should be a good approximation for these complexes as all possess the same geometry. Also, the effects of any anisotropy in the spin-rotation constant have been neglected, which will also affect the values determined from relaxation data.[19] In this regard, only the spin-rotation constant derived for $Co(sepulchrate)^{3+}$ may be significantly in error due to this simplification, as the octahedral symmetry of the other two complexes ensures minimal (if any) anisotropy. Using calculated values of σ_d provided by Hartree-Fock calculations of the atomic wave function of cobalt of 2166 ppm (non-relativistic)[13] or 1892 ppm (relativistic),[14] an approximate value of the chemical shift of the bare cobalt nucleus can be obtained. The absolute chemical shielding scale (with respect to the bare nucleus) (non-relativistic) and the chemical shift scale (with respect to 1.0 M $K_3[Co(CN)_6]$) are plotted together in Figure 3.17. This figure shows that the chemical shift of the bare cobalt nucleus is -1412 ppm (non-relativistic) with a significant error from the above extrapolation. If relativistic effects are also considered, the chemical shift of the bare nucleus is -1686 ppm. Further determinations of spin-rotation constants for cobalt nuclei with diverse values of chemical shifts clearly would be beneficial in improving these estimates of the absolute chemical shielding relative to the experimentally-measured chemical shift.

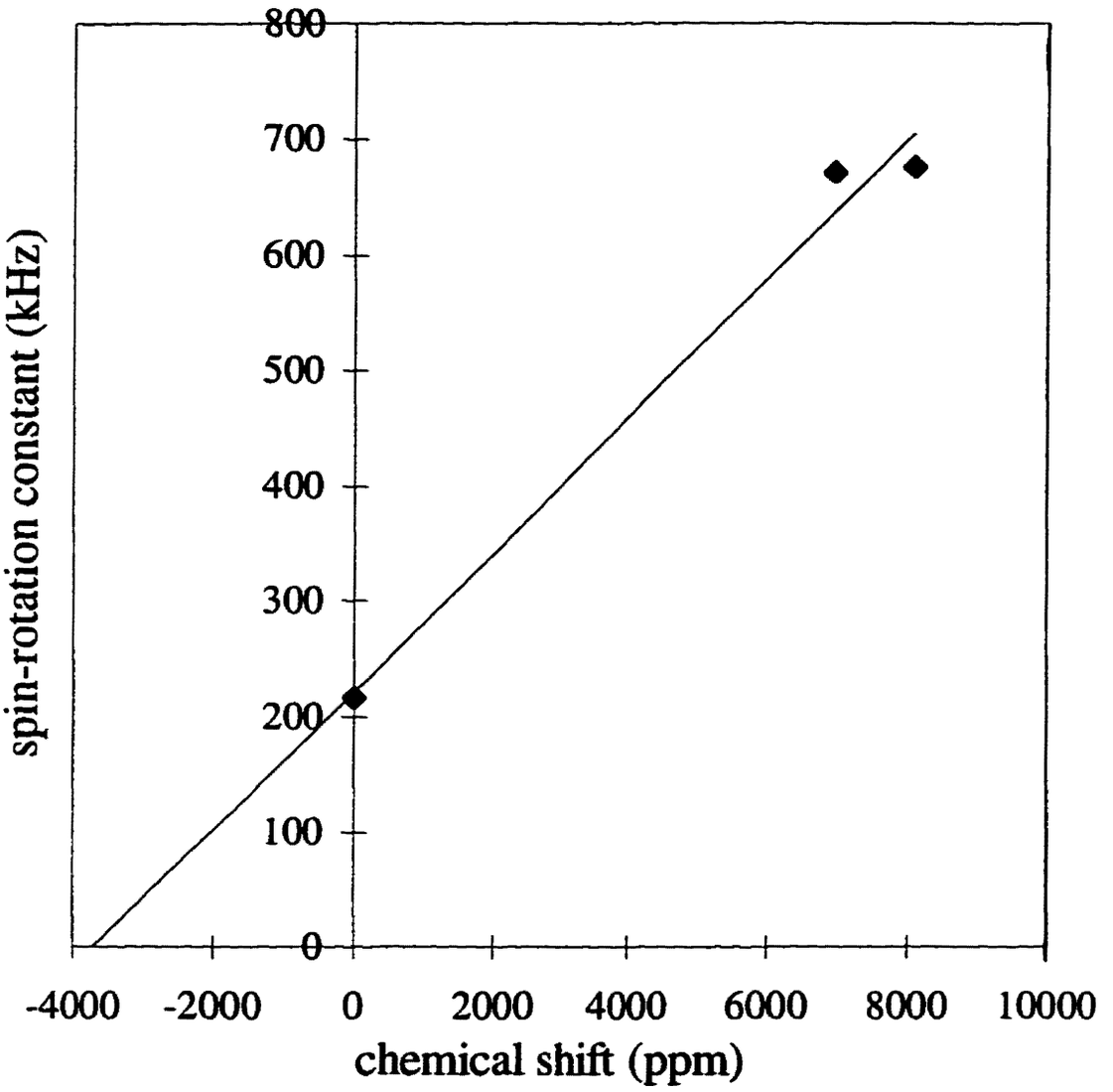


Figure 3.16: Plot of spin-rotation constant (c) *vs.* chemical shift (δ_{iso}) for the three complexes. The line intercepts the x-axis at -3578 ppm.

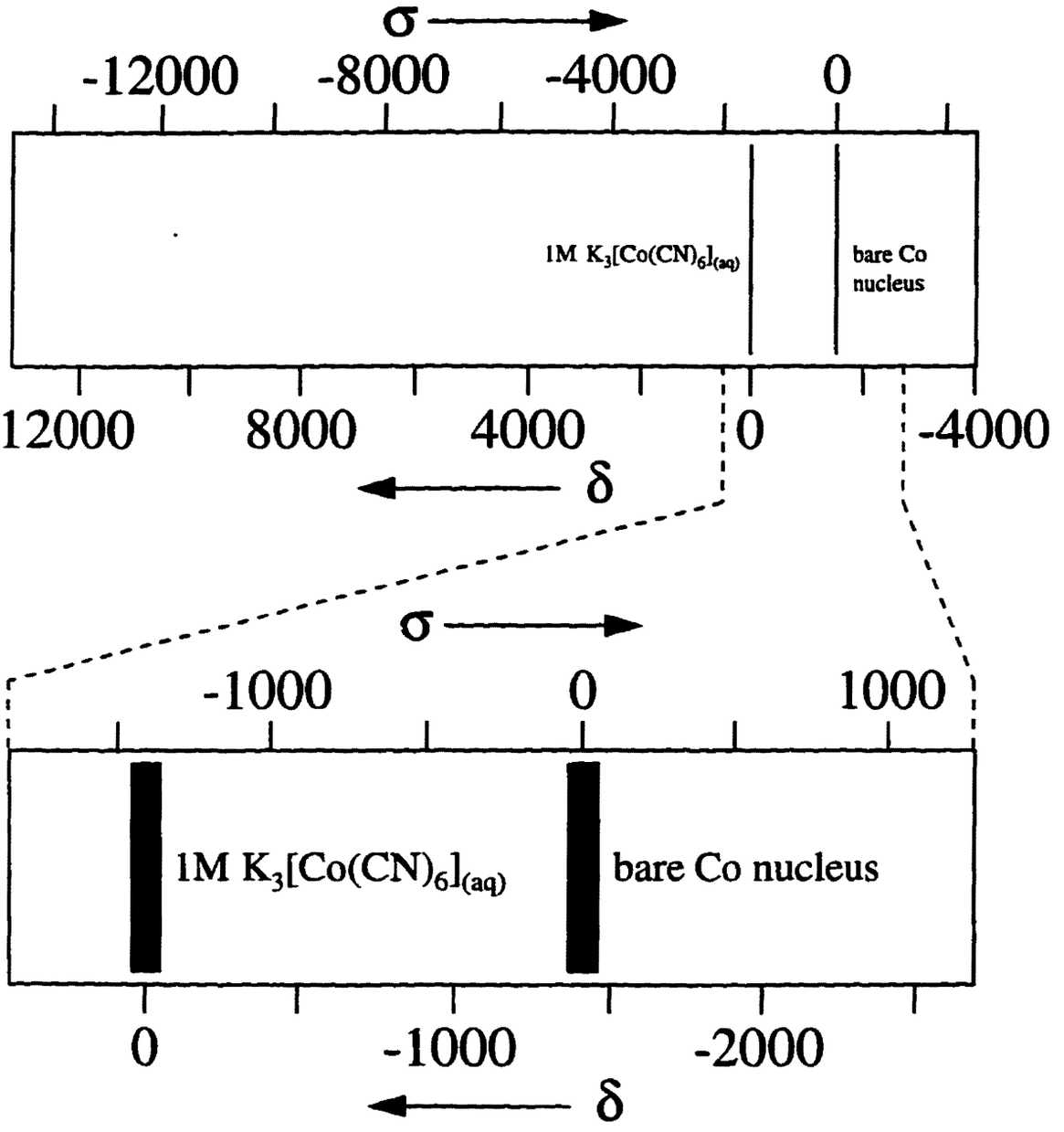


Figure 3.17: The chemical shift and absolute chemical shielding scales for cobalt. The chemical shift for the bare cobalt nucleus is determined to be -1412 (non-relativistic).

3.7 Conclusions

Variable-temperature measurements at two magnetic fields of the longitudinal and transverse ^{59}Co relaxation times of twelve different octahedral cobalt(III) complexes demonstrate that the quadrupolar mechanism dominates the relaxation behavior of cobalt nuclei, with a few notable exceptions. Two complexes with high symmetry and concomitant small quadrupolar coupling constants at the cobalt nuclei exhibit quadrupolar relaxation that is also influenced by the spin-rotation mechanism at high temperatures in the longitudinal relaxation and by scalar relaxation of the second kind in the transverse relaxation. The sepulchrate complex of cobalt exhibits contributions from the spin-rotation mechanism of ^{59}Co longitudinal relaxation at high temperatures owing to the large moment of inertia possessed by this complex. In none of the complexes was behavior observed that was indicative of contributions due to CSA relaxation. An estimate of the absolute cobalt chemical shielding scale has been provided by comparison of the spin-rotation constants determined from the relaxation data and the isotropic chemical shifts, as well as previously reported calculations of the diamagnetic shielding of atomic cobalt.

The variable-concentration multinuclear NMR study of Na[Co(edta)] demonstrates the need for the use of dilute solutions for ^{59}Co relaxation measurements. The pH's of solutions of Na[Co(edta)] are observed to determine the ^{1}H and ^{13}C NMR spectra while the ^{23}Na and ^{59}Co spectra are not affected by pH. At concentrations of 160 mM or greater, evidence is provided that intermolecular effects are important in solution.

Chapter 4

Solid-State Cobalt-59 NMR

4.1 Introduction

4.1.1 Previous Solid-State Cobalt-59 NMR Studies

In contrast to the number of solution ^{59}Co NMR studies, there is little data concerning ^{59}Co in the solid-state. In fact, there are only 17 chemical shift anisotropies reported for cobalt in the literature.

The first single-crystal ^{59}Co NMR study was reported in 1969 by Spiess, Hass, and Hartmann.[58] In this study, the chemical shift (CS) and electric field gradient (efg) tensors of five cobalt(III) complexes were reported. The quadrupolar coupling constants (obtained from the efg tensors) ranged from 13.217 MHz to 165.609 MHz. Sheline and co-workers[59, 60, 61] produced the next three reports of solid-state ^{59}Co NMR studies which were also performed using single-crystal NMR. The compounds of these studies were all cobalt-carbonyl complexes with

large quadrupolar coupling constants (from 89.3 MHz to 159.88 MHz) and the CS tensors were also reported in these studies. In reality, these first studies were not true NMR studies but Zeeman perturbed NQR (nuclear quadrupolar resonance) because the χ's measured were greater than the Larmor frequencies (*vide infra*).

Reynhardt published two papers in 1974 in which he described single-crystal ^{59}Co NMR studies of $[Co(NH_3)_6]Cl_3$[62] and $Co(acac)_3$.[63] In the $[Co(NH_3)_6]Cl_3$ study, the CS and efg tensors of five individual cobalt sites (though two were taken together) were determined and the quadrupolar coupling constants at the different sites were found to vary significantly from site to site. These two studies were also done at a low magnetic field (1.6 T) and, therefore, the precision of the experiments is low.

After their efforts in solution ^{59}Co NMR studies, Eaton and co-workers published a paper showing powder spectra of six high symmetry cobalt(III) complexes at 11.7 T.[64] From the spectra of $Co(CN)_6^{3-}$, $Co(NO_2)_6^{3-}$, and $Co(en)_3^{3+}$ the chemical shift anisotropies were estimated. For $Co(acac)_3$ and $Co(C_2O_4)_3^{3-}$ the chemical shift anisotropies were not measured due to a mixture of quadrupolar and chemical shift anisotropy effects and $Co(NH_3)_6^{3+}$ was "quite complicated" and analysis was not attempted. The spectra presented in this paper are reasonably good but no axes are given making comparison or confirmation of their results impossible.

The most recent solid-state ^{59}Co NMR studies have been performed on cobalt clusters. The cobalt powder spectra of $A[MCo_3(CO)_{12}]$ (where M = Fe or Ru and A = N(ethyl)$_4$ or H) were obtained at two magnetic fields (4.7 T and 7.1 T) allowing for the determination of the CS and efg tensors of these four compounds.[65]

The chemical shift anisotropies changed very little when Fe was replaced with Ru (less than 4 %), but there are large changes in the anisotropy in the change from $N(ethyl)_4$ to H. A second paper by the same group has been published earlier this year on $HFeCo_3(CO)_9[P(OCH_3)_3]_3$,[66] but the efg and CS tensors were not determined for ^{59}Co because of multiple sites in the unit cell.

4.1.2 NMR Lineshapes

As described in Chapter 2, NMR interactions can be anisotropic and one can measure these anisotropic interactions in the solid-state. The two interactions that are important for cobalt, as a quadrupolar nucleus in the solid-state, are the chemical shielding (CS) anisotropy and the quadrupolar (Q) interactions. These two interactions give rise to lineshapes which depend on both the magnitudes and relative orientations of the two tensors. The site symmetry of the nucleus in the crystal lattice may put constraints on the orientation of the two tensors.

Jones *et al.*[67] were the first to describe the nature of the lineshape that contained both Q and CS but under the constraint that the tensors had to be axially symmetric and had the same orientation. This occurs only for nuclei at 3-fold or higher symmetry point group sites in the crystal. Baugher *et al.*[68] provided a more general treatment than that proposed by Jones and co-workers. In their paper, a description of non-axially symmetric tensors was given but the tensors were still constrained to have the same orientation dependence. Any powder lineshapes of quadrupolar nuclei described in the literature from 1969 until 1990 used this assumption that the two tensors were coincident. This assumption is valid for nu-

clei which are at sites of orthorhombic or higher point symmetry but excludes any nuclei that occur in monoclinic (point symmetry C_{2h}, C_s, or C_2) or triclinic (C_i or C_1) crystal sites. In 1990, Power *et al.*[69] published the first analysis of powder lineshapes of half-integer spin quadrupolar nuclei (I = n/2 where n = 3, 5, 7, or 9) which have chemical shielding and quadrupolar tensors that were both non-axially symmetric and non-coincident. This allows for the analysis of all quadrupolar lineshapes.

4.2 Theory

For quadrupolar nuclei, we must first consider the difference between NMR and NQR. Figure 4.1 shows E/h for different nuclear spin energy levels and the effect the cobalt Larmor frequency has on the levels using a fixed quadrupolar coupling constant of 33 MHz. The following equation is used to obtain the frequencies in Figure 4.1.[70]

$$E_m/h = -\frac{\gamma B_o m}{2\pi} + \frac{\chi}{4I(2I-1)}[3m^2 - I(I+1)] \qquad (4.1)$$

At a magnetic field of zero, one can do pure NQR and obtain quadrupolar coupling constants and the asymmetry of the efg tensor. When a small magnetic field is applied (corresponding to a small Larmor frequency), a perturbation of NQR occurs. This is known as Zeeman perturbed NQR. The experimental conditions relevant to NMR do not occur until the nuclear spin energy levels are in the correct order, from 7/2 to 5/2 to 3/2, etc. up to -7/2. In Figure 4.1 this occurs at approximately

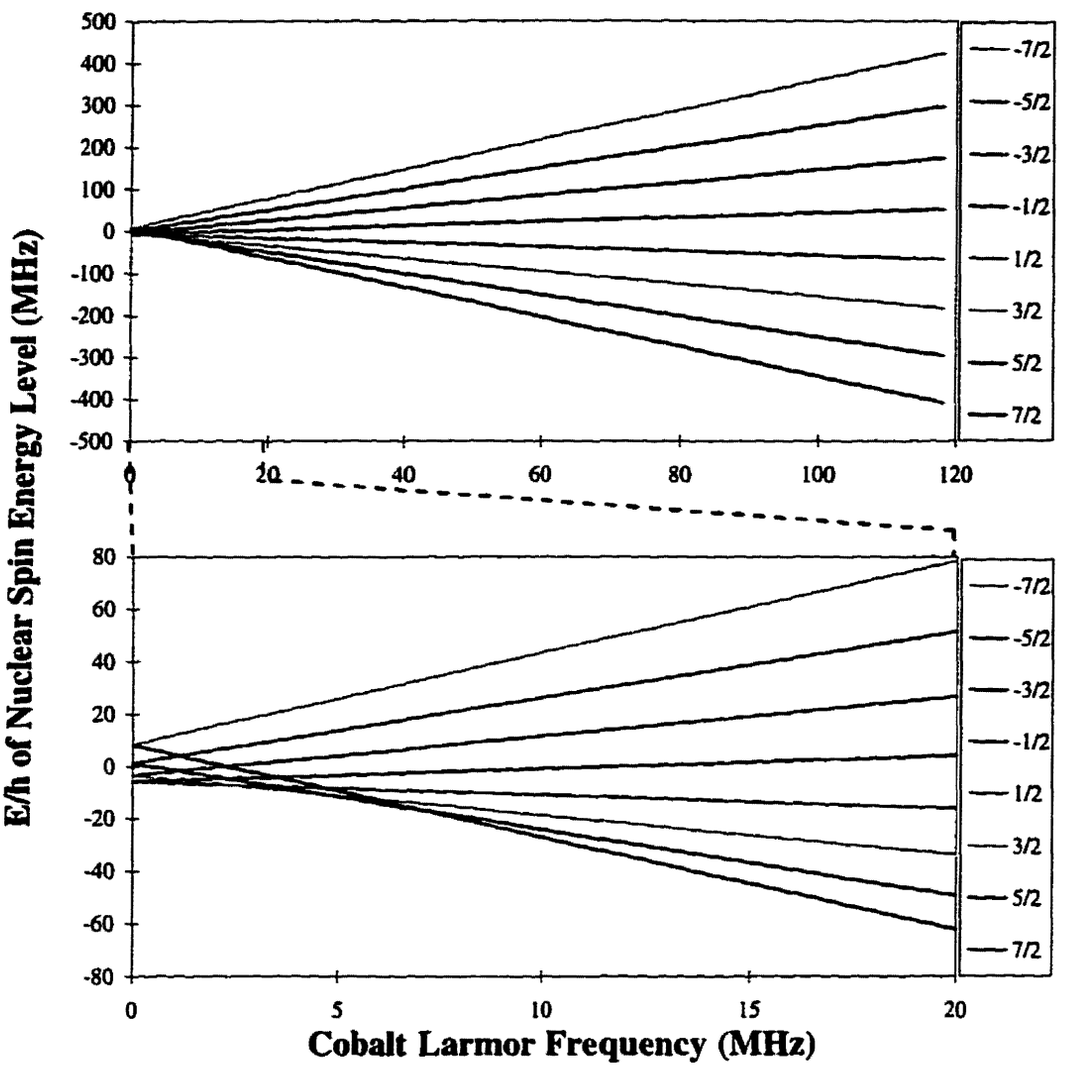


Figure 4.1: Plots of E/h of nuclear spin energy level *vs.* ^{59}Co Larmor frequency using a constant quadrupolar coupling constant of 33 MHz.

$\nu_o = 8$ MHz for a quadrupolar coupling constant of 33 MHz.

Once the magnetic field strength is sufficient to ensure NMR conditions for a quadrupolar nucleus, only the Zeeman, quadrupolar, and chemical shielding interactions need to be considered and the nuclear spin Hamiltonian simplifies to

$$\hat{\mathcal{H}}_T = \hat{\mathcal{H}}_Z + \hat{\mathcal{H}}_Q + \hat{\mathcal{H}}_{CS}. \tag{4.2}$$

Even though the Zeeman term now dominates, there are two situations that arise depending on the strength of the efg with respect to the Zeeman interaction. These situations are known as first- and second-order quadrupolar effects. The two situations can be defined in terms of the following expression,

$$\frac{\nu_Q^2[I(I+1) - \frac{3}{4}]}{144\nu_o} \tag{4.3}$$

where

$$\nu_Q = \frac{3\chi}{2I(2I-1)}. \tag{4.4}$$

First-order quadrupolar effects are sufficient to describe the response of the quadrupolar nucleus when expression 4.3 is less than 10; *i.e.*, the quadrupolar interaction is only a first order perturbation of the Zeeman interaction (similar to all other NMR interactions which are only first-order perturbations). If the value of equation 4.3 is greater than 10, second-order quadrupolar effects need to be considered. Using this as a guide, a χ of 1.5 MHz or greater is required before second-order effects need to be considered for cobalt at 11.7 T; a χ of 950 kHz necessitates consideration of second-order effects at 4.7 T. Using the estimates of χ from Table 3.2, we observe

that the majority of the cobalt complexes fall into the second-order domain if the solution and solid-state χ's are equivalent.

In the general case where the CS and efg tensors are neither coincident nor symmetric, the general expression for a powder lineshape, I(ν), is given as

$$I(\nu) = \sum_{m=-I+1}^{+I} \rho(m) g(\nu - \nu_m) \tag{4.5}$$

where ρ(m) is the probability of a m $\leftrightarrow$ m-1 transition, g(ν) is a line-broadening function, and $\nu_m = \nu_\sigma$ - $\mathcal{Q}$. $\mathcal{Q}$ is dependent on the value of equation 4.3 (*i.e.*, first- or second-order quadrupolar effects). If only first-order perturbations need to be considered, $\mathcal{Q}$ is given by

$$\mathcal{Q} = \frac{\nu_Q}{2}[(3\cos^2\theta - 1) - \eta_Q \sin^2\theta \cos^2 2\phi](m - \frac{1}{2}). \tag{4.6}$$

If second-order perturbations need to be considered, the central m = 1/2 $\leftrightarrow$ -1/2 transition usually dominates the spectrum. In this case, $\mathcal{Q}$ is given by

$$\mathcal{Q} = \frac{\nu_Q^2[I(I+1) - \frac{3}{4}]}{6\nu_o}[A(\phi)\cos^4\theta + B(\phi)\cos\theta + C(\phi)] \tag{4.7}$$

where

$$A(\phi) = -\frac{27}{8} - \frac{9}{4}\eta_Q \cos 2\phi - \frac{3}{8}\eta_Q^2 \cos^2 2\phi, \tag{4.8}$$

$$B(\phi) = \frac{30}{8} - \frac{1}{2}\eta_Q^2 + 2\eta_Q \cos 2\phi + \frac{3}{4}\eta_Q^2 \cos^2 2\phi, \tag{4.9}$$

and

$$C(\phi) = -\frac{3}{8} + \frac{1}{3}\eta_Q^2 + \frac{1}{4}\eta_Q \cos 2\phi - \frac{3}{8}\eta_Q^2 \cos^2 2\phi. \tag{4.10}$$

If the satellite transitions are observed, they would also be shifted by the second-order quadrupolar effects but the splitting between any pair of satellite transitions remains constant.

For a quadrupolar nucleus it is difficult, if not impossible, to obtain the orientation of the CS or efg tensor with respect to the molecular geometry without performing a single-crystal NMR experiment. To simplify the simulation of quadrupolar spectra, the Euler angles (α, β, and γ) can be used to obtain the orientation of the CS tensor with respect to the efg tensor (as seen in Figure 4.2) using the following expressions,

$$\begin{aligned}
\sin\vartheta\cos\varphi &= \cos\gamma\cos\beta\cos(\phi-\alpha) + \sin\gamma\sin\theta\sin(\phi-\alpha) - \cos\gamma\sin\beta\cos\theta, \\
\sin\vartheta\sin\varphi &= -\sin\gamma\cos\beta\sin\theta\cos(\phi-\alpha) + \cos\gamma\sin\theta\sin(\phi-\alpha) + \sin\gamma\sin\beta\cos\theta. \\
cos\vartheta &= \sin\beta\sin\theta\cos(\phi-\alpha) + \cos\beta\cos\theta
\end{aligned} \tag{4.11}$$

The expressions in 4.11 were determined using a rotational transformation matrix. $R(\alpha\beta\gamma) = R_{z'}(\gamma)R_{y'}(\beta)R_z(\alpha)$.[9] This matrix rotates the CS tensor in the reference frame of the efg tensor.

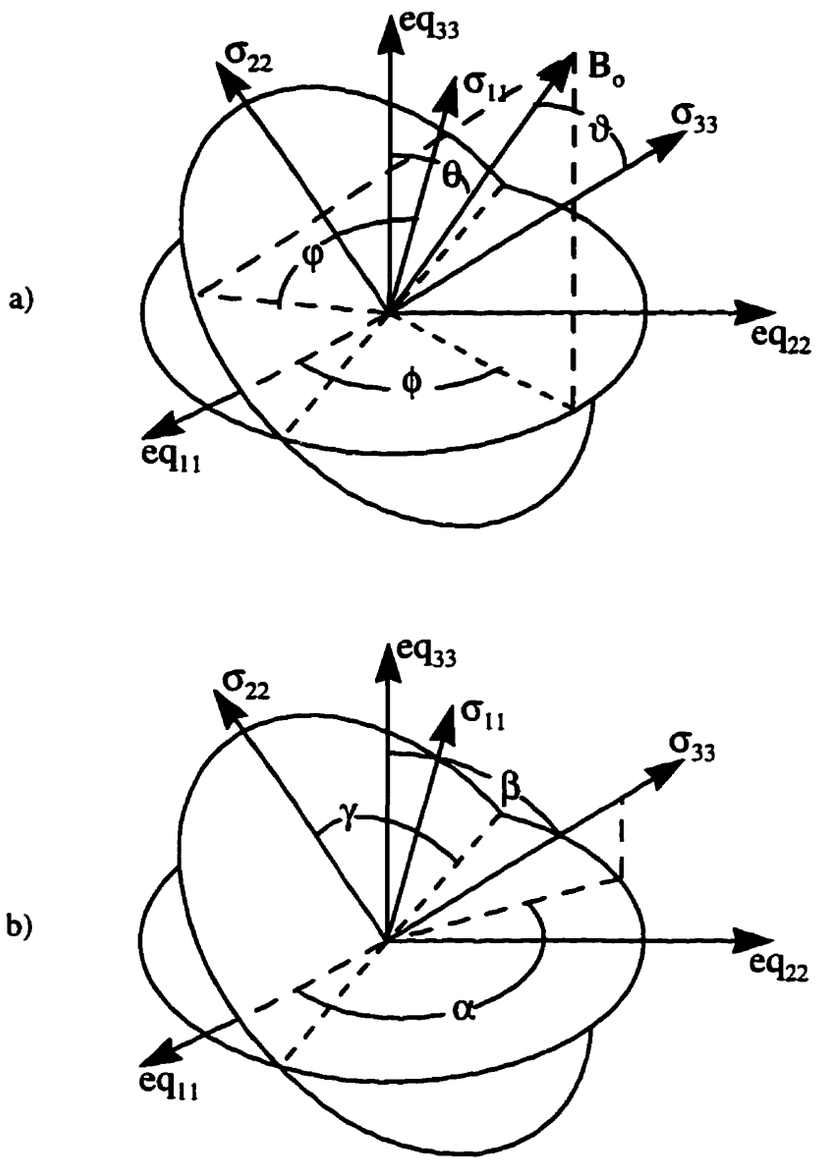


Figure 4.2: a) The magnetic field vector, B_o, is oriented in PAS of the chemical shielding tensor by (ϑ, φ) and in the PAS of the efg tensor by (θ, ϕ). b) The Euler angles (α, β, γ) orient the chemical shielding tensor in the PAS of the efg tensor.

4.3 Experimental

The cobalt(III) complexes were made by standard literature procedures or were commercially available, as given previously in Table 3.1. Compounds studied in the solid-state not present in Table 3.1 were made/obtained as follows: $[Co(en)_3]Cl_3$, see reference [71], $[Co(NH_3)_5CH_3](NO_3)_2$, see reference [72], and $Na_3[Co(NO_2)_6]$, obtained from Aldrich. All samples were referenced to 1.0 M $K_3[Co(CN)_6]$ (aq). Solid-state ^{59}Co NMR spectra were acquired at 11.7 T on a Bruker AMX-500 spectrometer and at 4.7 T on a Bruker ASX-200 spectrometer where possible (*vide infra*). Samples were prepared by crushing the sample with a mortar and pestle and packing them into 5 mm NMR tubes cut to a length of 28 mm. At 4.7 T, a spin-echo pulse sequence was used due to large dead times associated with the probe. At 11.7 T, a simple one pulse experiment was attempted to obtain all spectra except for compounds with quadrupolar coupling constants greater than 30 MHz for which a spin-echo pulse sequence was required to obtain useful spectra due to a large amount of uncorrectable baseline roll (*vide infra*).

A solid-state ^{13}C magic angle spinning NMR spectrum of $[Co(NH_3)_5CH_3](NO_3)_2$ was obtained at 50.3 MHz on a Bruker ASX-200 spectrometer (B_o = 4.7 T). The sample was packed into a 7 mm outer-diameter zirconium oxide rotor. Cross polarization under the Hartmann-Hahn matching condition was used to increase the sensitivity of the spectrum using a contact time of 3 ms. The proton 90° pulse width was 4.2 μs and high power ^1H decoupling was used during the acquisition of the spectrum. During the acquisition the sample was spun at a rate of 2.8 kHz. Carbon chemical shifts were referenced to TMS by setting the high-frequency carbon signal

of adamantane to 38.56 ppm.

Calculations of the ^{59}Co NMR powder lineshapes were performed on a Silicon Graphics Indigo^2 XL workstation with a FORTRAN-77 program that incorporates the POWDER routine[73] with additions for quadrupolar nuclei.[69] The values for the three principal components of the chemical shift tensor, the quadrupolar coupling constant, the asymmetry of the efg tensor, and the Euler angles were optimized to maximize the agreement between the experimental and calculated lineshapes of the central transition. Crystal structures were used to determine if any constraints on the CS or efg tensors had to be present due to site symmetry.

The orientations of the efg tensors were either estimated using local symmetry arguments, obtained computationally using Gaussian 94,[74] or *via* residual quadrupolar effects on the dipolar coupling with an adjacent spin-$\frac{1}{2}$ nuclei. The structures used for the Gaussian 94 calculations were obtained from solid-state crystal structures with the hydrogens optimized using the same program.

4.4 Results

Simulations of the ^{59}Co NMR spectra were performed for all of the spectra at 11.7 T as well as for the complexes for which spectra were obtained at 4.7 T. The results of the simulations are summarized in Table 4.1. Any values in Table 4.1 without a "$\pm$" are parameters which are exactly zero or 90 by symmetry. All of the spectra and the simulations are given in Appendix A.

For most compounds, only the central transition (m = $\frac{1}{2} \leftrightarrow -\frac{1}{2}$ transition) is observed. One example where the satellites as well as the central transition are

Table 4.1: Summary of the solid-state ^{59}Co NMR data.

Compound	δ_{11} (ppm)	δ_{22} (ppm)	δ_{33} (ppm)	χ (MHz)	η_Q	$\beta[\alpha,\gamma]$* (°)
$[Co(NH_3)_5CH_3](NO_3)_2$	6865 ± 25	6362 ± 20	5160 ± 45	33 ± 1	0 ± 0.05	16 ± 1
$[Co(en)_3]Cl_3$	7116 ± 5	7116 ± 5	6891 ± 5	2.99 ± 0.01	0	0
trans-$[Co(NH_3)_4(NO_2)_2]NO_3$	7175 ± 25	7050 ± 10	6755 ± 25	13.5 ± 1	0.15 ± 0.05	85 ± 3
						[50 ± 10, 63 ± 3]
cis-$[Co(NH_3)_4(NO_2)_2]NO_3$	7400 ± 30	6990 ± 10	6970 ± 25	12 ± 1	0.7 ± 0.1	22 ± 2
$[Co(NH_3)_5(NO_2)]Cl_2$	7470 ± 15	7400 ± 10	7350 ± 15	9 ± 2	0.4 ± 0.1	90 ± 2
$Na_3[Co(NO_2)_6]$	7690 ± 5	7510 ± 5	7510 ± 5	8.35 ± 0.05	0	90
$[Co(NH_3)_5Cl]Cl_2$	9385 ± 35	9385 ± 35	7800 ± 60	27 ± 2	0 ± 0.1	0 ± 2
$[Co(NH_3)_5(CO_3)]NO_3 \cdot \frac{1}{2}H_2O$	9750 ± 30	9260 ± 10	7720 ± 20	20.5 ± 0.5	0.1 ± 0.05	6 ± 1
cis-$[Co(NH_3)_4(CO_3)]NO_3$						
site 1	10035 ± 15	9870 ± 10	8840 ± 20	18 ± 1	0 ± 0.1	9 ± 1
site 2	10035 ± 15	9820 ± 10	8840 ± 20	18 ± 1	0 ± 0.1	9 ± 1
Na[Co(edta)]	11750 ± 40	9900 ± 25	9025 ± 25	35 ± 2	0.4 ± 0.1	18 ± 2
$Co(acac)_3$	13015 ± 15	12115 ± 5	11890 ± 10	6.73 ± 0.01	0.23 ± 0.01	90 ± 2
						[90 ± 2, 90 ± 2]

*Unless values are given in brackets, α and γ are 0°.

observed is $[Co(en)_3]Cl_3$. From the crystal structure of $[Co(en)_3]Cl_3$[75], one discovers that the compound crystallizes in the trigonal space group $P\bar{3}c1$. Therefore the cobalt CS and efg tensors must be both axially symmetric and coincident, thus putting constraints on the analysis of the spectra of this complex. As seen in Table 4.1, the CS tensor is axially symmetric with $\delta_{11} = \delta_{22}$ and the 11, 22, and 33 components of the CS and efg tensors are aligned (*i.e.*, $\beta = 0$). Figure 4.3 shows the calculated spectra of this compound at 11.7 T if only the chemical shift tensor was present, if only the efg tensor was present, the effect of both tensors interacting, and the experimental spectrum. There are uncorrectable distortions in the experimental spectrum due the loss of the first few points of the FID which is associated with the dead time of the probe (*vide infra*), but there is an excellent match between the frequencies of the experimental and calculated spectra. As χ increases and/or the tensors are not aligned, the central transition dominates the spectrum and the satellites are usually not observed.

The only other complex that has constraints placed upon it by the crystal structure is $Na_3[Co(NO_2)_6]$ which crystallizes in the rhombohedral space group $R\bar{3}m$[76] and the cobalt nuclei sit on sites of three-fold symmetry. All of the other complexes do not have any constraints placed on them by the crystal structures and therefore all eight parameters were used to try to obtain good simulations of the spectra. However, variation of α and γ did not help to give good simulations for many of the compounds so these angles are zero for all of the complexes unless otherwise given in brackets in Table 4.1. Therefore, in general, only six parameters needed to be fit and these values are given in Table 4.1.

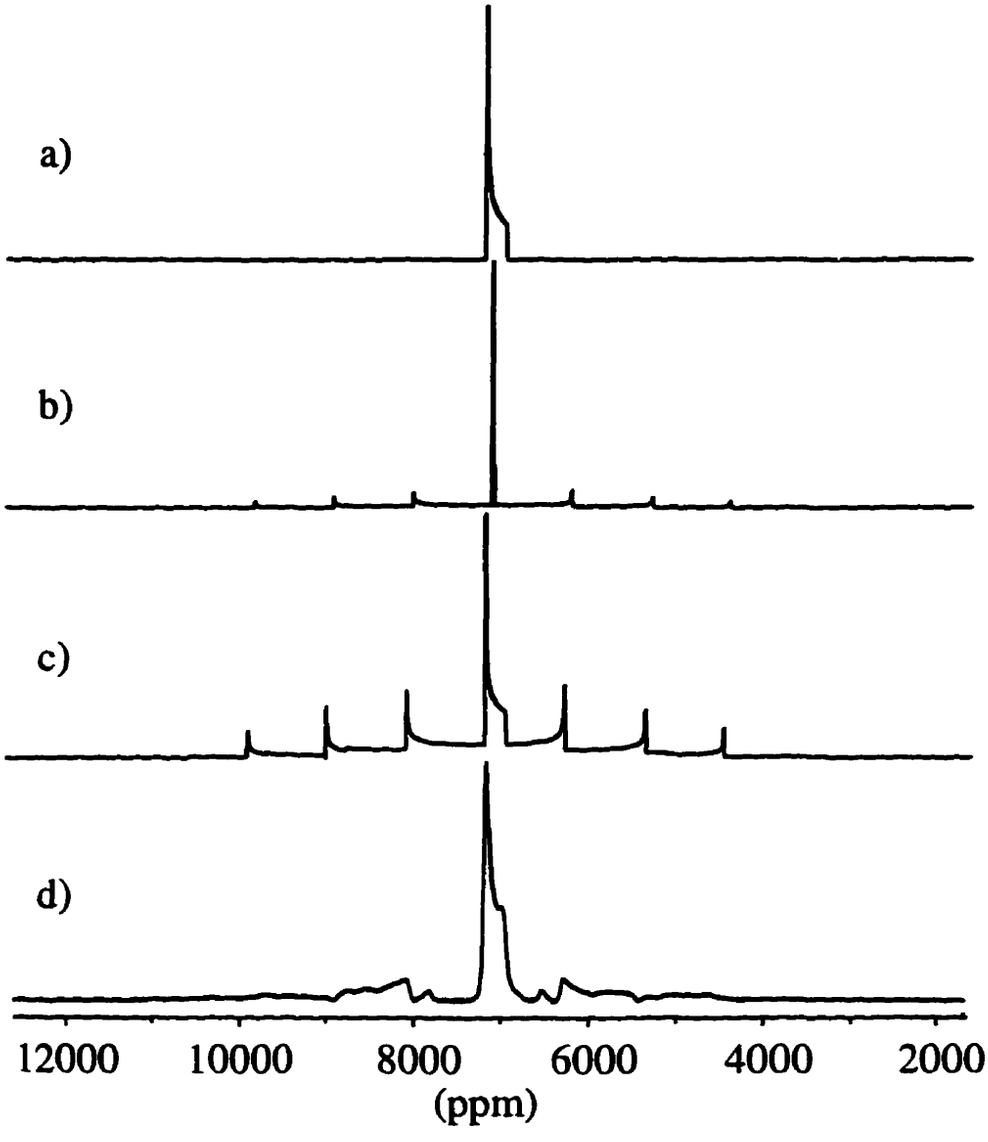


Figure 4.3: Simulations of $[Co(en)_3]Cl_3$ at 11.7 T if a) only chemical shift anisotropy is present, b) only the quadrupolar interaction is present, c) both tensors are present. d) The experimental spectrum.

At the lower magnetic field, the spectra of $[Co(NH_3)_5Cl]Cl_2$, Na[Co(edta)], and $[Co(NH_3)_5CH_3](NO_2)_2$ were difficult to obtain due to the large χ's associated with these complexes and therefore useful spectra were not obtained. A spectrum of *cis*-$[Co(NH_3)_4(NO_2)_2]NO_3$ was not obtained at the lower magnetic field due to the small amount of compound (approximately 5 mg) which was insufficient for sensitivity reasons.

One interesting observation from the spectra obtained at both fields is a problem with baseline roll. This problem is associated with the dead times of the probes. A probe's dead time is the time it takes for all of the electronics of the spectrometer to dissipate the energy that the RF pulse added to the system; the greatest of these is usually the ringdown of the probe. The dead time makes it impossible to start to collect data immediately after the pulse. Therefore, one loses the first few points of the FID. This loss of points can give spectra with large amounts of baseline roll. The baseline roll can be corrected by baseline correction, but when there are extremely large amounts of distortion it is sometimes difficult to tell what the real spectrum should look like. One method to correct for dead times is the use of a spin-echo pulse sequence.[77] When using such a sequence, one refocuses the magnetization at a time that is greater than the dead time of the probe, at which point acquisition is initiated, hence removing this problem. Cobalt-59 spectra of $[Co(NH_3)_5Cl]Cl_2$ are given in Figure 4.4 showing the baseline roll problem, a spectrum after the baseline has been corrected, and the results using a spin-echo pulse sequence. All of the spectra collected on the ASX-200 spectrometer had to be collected with a spin-echo pulse sequence because the dead time was extremely long (over 14 μs). Spin-echo

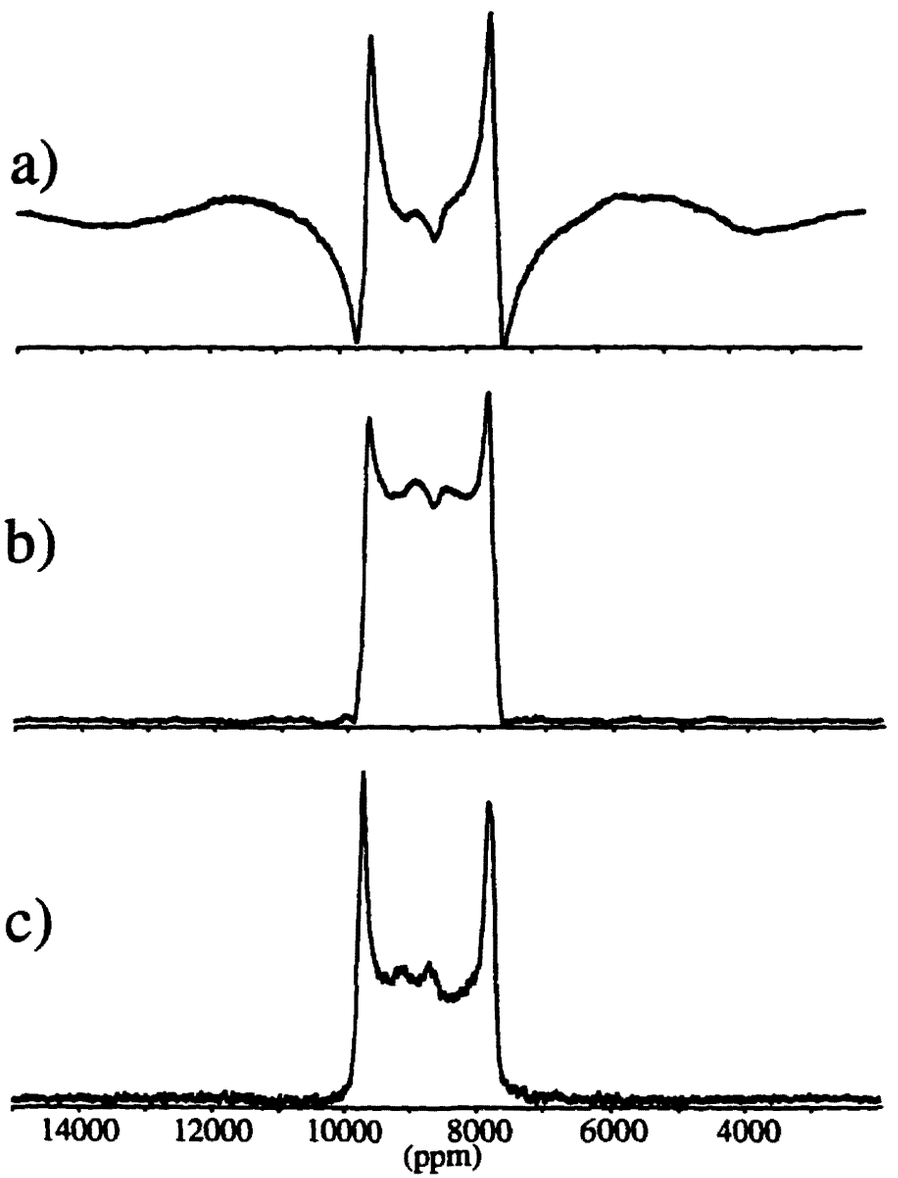


Figure 4.4: Cobalt-59 spectra of $[Co(NH_3)_5Cl]Cl_2$ after phasing using a) a single pulse experiment b) a single pulse experiment and baseline correcting c) a spin-echo experiment.

Table 4.2: Comparison of solution and solid-state ^{59}Co NMR results.

Compound	δ_{iso} solution (ppm)	δ_{iso} solid (ppm)	χ solution (MHz)	χ solid (MHz)	Ω solid (ppm)
$[Co(NH_3)_5(NO_2)]Cl_2$	7565	7407	1.87	9	120
$Co(acac)_3$	12570	12340	2.88	6.73	1125
trans-$[Co(NH_3)_4(NO_2)_2]NO_3$	7157	6993	4.01	13.5	420
cis-$[Co(NH_3)_4(NO_2)_2]NO_3$	7227	7120	4.10	12	430
$[Co(NH_3)_5(CO_3)]NO_3 \cdot \frac{1}{2}H_2O$	9053	8910	7.57	20.5	2030
cis-$[Co(NH_3)_4(CO_3)]NO_3$	9662	9581/9565	7.81	18	1195
$[Co(NH_3)_5Cl]Cl_2$	8793	8857	9.79	27	1585
Na[Co(edta)]	10237	10225	11.1	35	2725

spectra were collected for complexes with χ's greater than 10 MHz on the AMX-500 spectrometer but only the spectra of Na[Co(edta)] and $[Co(NH_3)_5CH_3](NO_3)_2$ (the compounds with the largest χ's) were simulated using the spin-echo spectra.

4.5 Discussion

The chemical shift and efg tensors were acquired for all of the compounds in Table 4.1. A comparison between the solution and solid-state NMR results can now be undertaken. The solid-state isotropic chemical shifts (δ_{iso}) can be obtained from the average of the principal components of the chemical shift tensors. Table 4.2 shows the solution and solid-state NMR δ_{iso}'s, χ's, and Ω's. From Table 4.2 one can see that the isotropic chemical shifts in solution and in the solid state are all within approximately 200 ppm which is close considering the large chemical shift range for cobalt. There is no trend observed between the isotropic shifts and the

χ's, but Ω, in general, increases with increasing χ. The solid-state χ's are much larger than those measured in solution. This could be due to several reasons. First, all of the other values in Table 4.2 are measured directly from a spectrum while the $\chi_{solution}$ is measured indirectly from the relaxation studies. Therefore, $\chi_{solution}$ is only as good as the correlation time measured, which, in the relaxation studies, was from the carbon T_1's of two complexes. Recalling $\chi(T,\rho)$ from equation 3.18, intermolecular *vs.* intramolecular χ's can be discussed. Since the isotropic shifts are consistent between solution and the solid-state, the intramolecular term should be constant between phases. Intermolecular effects could arise from interactions between two (or more) solute molecules or between a solute and a solvent. Since $\chi_{solution}$ is less than χ_{solid}, one might take this as evidence that the intermolecular χ has a negative sign, but if one uses the arguments of Osten and Jameson,[29] one would expect that intermolecular effects would increase as concentration increases as observed in the ^{59}Co relaxation of Na[Co(edta)]. At maximum concentration (a solid) the largest χ is observed and therefore, the intermolecular χ is positive between solute molecules. Thus, if there is an influence from the solvent on χ, it must be negative.

When studying chemical shift tensors, it is of great interest to determine any trends that are present from similar compounds. Plots of the chemical shift/shielding tensors only (*i.e.*, no quadrupolar interaction) of the complexes in this study are shown on the chemical shielding scale (determined from the relaxation measurements) at the top and the chemical shift scale (with respect to 1.0 M $K_3[Co(CN)_6]$) at the bottom of Figure 4.5.

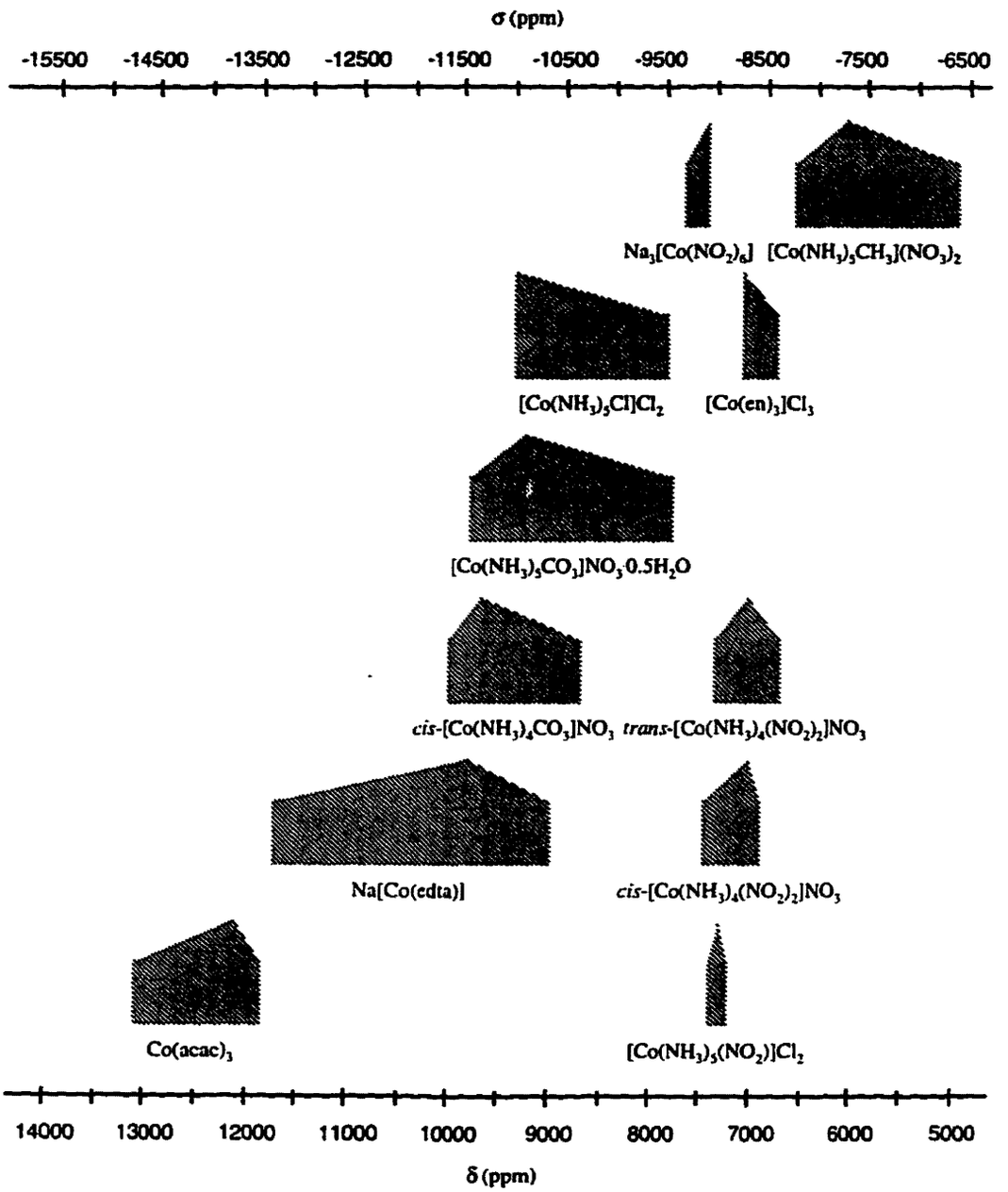


Figure 4.5: Chemical shift/shielding tensors for the complexes in this study.

When considering trends, it is also important to consider the orientation of the tensors. Using basic symmetry arguments, as well as results from Gaussian 94, one can predict the orientation of the efg tensor. This, in turn, can give the orientation of the CS tensor using the Euler angles. Two definitions are needed before continuing the discussion of trends: the principal component of the efg is eq_{33} and the principal director of the chemical shift tensor is the principal component of this tensor which is furthest from δ_{22}. The complexes will be discussed in four basic frameworks: CoX_6, CoX_5Y, *trans*-CoX_4Y_2, and *cis*-CoX_4Y_2.

Considering the CoX_6 complexes first, there are three complexes: $[Co(en)_3]Cl_3$, $Na_3[Co(NO_2)_6]$, $Co(acac)_3$. $Na_3[Co(NO_2)_6]$ crystallizes in the rhombohedral space group $R\bar{3}m$[76] with the cobalt nucleus at the origin of the rhombohedral cell. The principal component of the efg tensor must lie along the three-fold axis and, since β is 90°, it lies along δ_{11} (the principal director). $Co(acac)_3$ is similar to $Na_3[Co(NO_2)_6]$ in that the principal component of the efg lies along the normal to one face of the octahedron which is closest to a three-fold axis ($Co(acac)_3$ does not have a true 3-fold axis since in crystallizes in the space group $P2_1/c$).[52] A β value of 90° was found for this complex which would put the principal component of the efg along δ_{11}. The chemical shift tensor for this complex indicates that δ_{11} is the principal director which agrees with the β value of 90°. For $[Co(en)_3]Cl_3$, β is 0° and the δ_{33} lies along the principal component of the efg tensor. The principal component of the efg would lie along the three-fold axis of this molecule which crystallizes in a trigonal space group.[75]

Within the CoX_5Y group, there are four complexes: $[Co(NH_3)_5CH_3](NO_3)_2$,

$[Co(NH_3)_5Cl]Cl_2$, $[Co(NH_3)_5CO_3]NO_3 \cdot \frac{1}{2}H_2O$, and $[Co(NH_3)_5NO_2]Cl_2$. For the first three of these complexes, β is small (16° or less). Therefore, the unique component of the efg should lie close to δ_{33} in these cases. If eq_{33} is along δ_{33}, δ_{33} would have to be the principal director of the chemical shift tensor. This is observed for all of these complexes even though the spans (Ω) vary from complex to complex. In $[Co(NH_3)_5NO_2]Cl_2$, β is 90° and thus, eq_{33} should lie close to δ_{11}. The principal director in $[Co(NH_3)_5NO_2]Cl_2$ is observed to be δ_{11} in agreement with the β observed.

The orientation of the efg tensor can be obtained directly (not based on symmetry arguments) *via* the residual quadrupolar effects upon the dipolar interaction between cobalt and a second nucleus.[78] In $[Co(NH_3)_5CH_3](NO_3)_2$, ^{59}Co will dipolar couple to ^{13}C. Dipolar coupling is usually averaged to zero in solid-state NMR using magic angle spinning (MAS), but, since ^{59}Co is a quadrupolar nucleus, the Zeeman levels of ^{59}Co are perturbed and the dipolar interaction is not completely removed by MAS. This results in a ^{13}C MAS spectrum that exhibits residual dipolar coupling. The spectral lineshape obtained in such a system depends on several factors including χ, η_Q, ν_Q (the Larmor frequency of the quadrupolar nucleus), S (the nuclear spin of the quadrupolar nucleus), R_{DD}, and the Euler angles, α_{DD} and β_{DD} (γ_{DD} is not needed because the dipolar tensor is axially symmetric), which define the orientation of the efg tensor with respect to the dipolar tensor. Also, if the two nuclei J-couple, J_{iso} and ΔJ also influence the spectrum. The ^{13}C MAS NMR spectrum of $[Co(NH_3)_5CH_3](NO_3)_2$ acquired at 4.7 T is given in Figure 4.6. In the simulation of the experimental spectrum, seven parameters had to be opti-

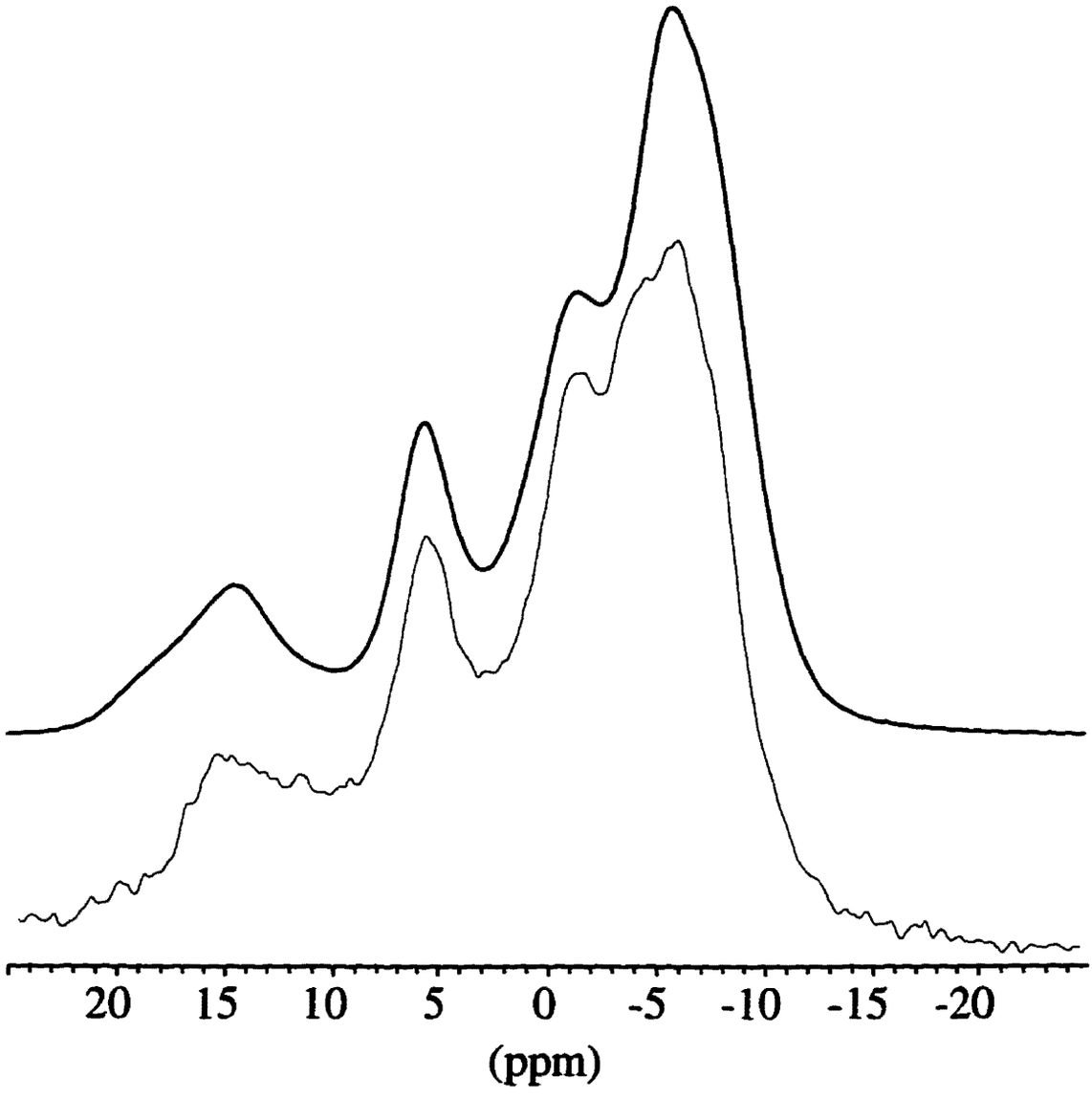


Figure 4.6: ^{13}C MAS spectrum of $[Co(NH_3)_5CH_3](NO_3)_2$ acquired at 4.7 T. The simulation was done using the following parameters: χ = 33 MHz, η_Q = 0, R_{DD} = 925 Hz, J_{iso} = 110 Hz, ΔJ = -4275 Hz, α_{DD} = 0°, and β_{DD} (the orientation of the eq_{33} with respect to the Co-C bond) = 90°.

mized. However, χ and η_Q were known from the simulation of the solid-state ^{59}Co spectrum (χ = 33 MHz and $\eta_Q = 0$), α_{DD} had to be zero because η_Q was zero, and R_{DD} was obtained from the Co-C bond length of 1.972 Å[79] in this complex (R_{DD} = 925 ± 25 Hz). Therefore, only three parameters remained to be optimized. The best-fit simulation indicates that J_{iso} is 110 Hz ± 5 Hz, ΔJ is either -4275 Hz ± 250 Hz or 9825 Hz ± 250 Hz (it is not possible to determine which is correct from this spectrum), and β_{DD} is 90° (the angle between eq_{33} and the dipolar tensor). Thus, the local symmetry argument for determination of the orientation of the efg tensor was incorrect for this complex because the dipolar tensor has to lie along the Co-C bond. Therefore, eq_{33} for $[Co(NH_3)_5CH_3](NO_3)_2$ is in the plane containing 4 ammine groups.

trans-$[Co(NH_3)_4(NO_2)_2]NO_3$ is in a category by itself because it is the only one in this series with this arrangement of ligands. The principal component of the efg tensor lies along a Co-NO_2 bond. Since the Euler angles for this complex are all non-zero and non-90°, the efg and the chemical shift tensors do not have any components which lie along each other. The principal director of the chemical shift tensor is observed to be δ_{33}, but η_{CS} (as defined in equations 2.12 and 2.13) of this complex is quite large at 0.53. Therefore, there is not a true principal director in this complex since the chemical shift tensor is far from axial symmetry.

The last three complexes, Na[Co(edta)], *cis*-$[Co(NH_3)_4(NO_2)_2]NO_3$, and *cis*-$[Co(NH_3)_4CO_3]NO_3$ all have a *cis*-CoX_4Y_2 arrangement of ligands. From a Gaussian 94 calculation of the efg tensor of *cis*-$[Co(NH_3)_4(NO_2)_2]NO_3$, the principal component of the efg tensor is observed to lie close to a Co-NH_3 bond which is

perpendicular to the ligand plane containing the two nitro groups, and is then slightly tilted away from the nitro groups. A similar orientation is assumed for the other two complexes in that the efg lies close to one of the Co-X bonds and perpendicular to the ligand plane containing the two Y groups. The principal director of the chemical shift tensors of Na[Co(edta)] and *cis*-$[Co(NH_3)_4(NO_2)_2]NO_3$ is δ_{11} while it is δ_{33} for *cis*-$[Co(NH_3)_4CO_3]NO_3$. With a β value of 6° for *cis*-$[Co(NH_3)_4CO_3]NO_3$, the principal component of the efg lies close to the principal director of the chemical shift tensor. In the other two complexes, the principal director of the chemical shift tensor does not lie along the principal component of the efg tensor. For Na[Co(edta)] a similar case to that of *trans*-$[Co(NH_3)_4(NO_2)_2]NO_3$ is observed in that η_{CS} is large (0.57) and there is not a true principal director in the complex. For *cis*-$[Co(NH_3)_4(NO_2)_2]NO_3$ the principal component of the efg is not very different from eq_{11} since η_Q is 0.7. Therefore, the principal component of the efg and the principal director of the chemical shift tensor are not relevant to these two complexes.

When studying chemical shift tensors, it is beneficial to determine planes that are responsible for specific components of the chemical shift tensors. Using the data from this study, the following ligand planes have been determined to give rise to specific components of chemical shift tensors: A) a 3N 1C plane gives rise to shifts between 5190 and 6362 ppm (as observed from $[Co(NH_3)_5CH_3](NO_3)_2$), B) a 4N plane gives rise to shifts between 6860 and 7800 ppm (as observed from numerous complexes), C) a 3N 1O or 1Cl plane gives rise to shifts between 9385 and 9868 ppm (as observed from $[Co(NH_3)_5Cl]Cl_2$ and $[Co(NH_3)_5CO_3]NO_3$), and D) a 4O plane

Table 4.3: T_{1CSA} from solid-state ^{59}Co NMR data.

Compound	η_{CS}	$\Delta\sigma^e$	$T_{1CSA}{}^a$	$T_1{}^b$ (solution)
$[Co(NH_3)_5(NO_2)]Cl_2$	0.79	95 ppm	7.5 s	4.23 ms
$Co(acac)_3$	0.33	1013 ppm	76.9 ms	1.78 ms
trans-$[Co(NH_3)_4(NO_2)_2]NO_3$	0.53	358 ppm	583 ms	921 μs
cis-$[Co(NH_3)_4(NO_2)_2]NO_3$	0.07	420 ppm	463 ms	879 μs
$[Co(NH_3)_5Cl]Cl_2$	0	1585 ppm	32.5 ms	154 μs
$[Co(NH_3)_5(CO_3)]NO_3 \cdot \frac{1}{2}H_2O$	0.41	1785 ppm	25.6 ms	258 μs
cis-$[Co(NH_3)_4(CO_3)]NO_3$	0.32	1084 ppm	67.3 ms	242 μs
Na[Co(edta)]	0.57	2286 ppm	14.1 ms	119 μs

Room temperature measurements using a τ_2 of 168 ps. (a) Calculated. (b) Experimentally measured (see Chapter 3).

gives rise to shifts between 11890 and 13015 ppm (as observed from $Co(acac)_3$). The two other planes that are possible, but not really clear due to the orientation of the efg and chemical shift tensors in the *cis*-CoX_4Y_2 type of complexes, are E) 2N and 2O planes giving rise to shifts between 9025 and 10040 ppm, and F) 3O and 1N planes giving rise to shifts between 9900 and 11750 ppm.

As discussed in the previous chapter, chemical shielding anisotropies were claimed to be contributors to ^{59}Co relaxation in solution. Values of T_{1CSA} can be calculated for complexes for which the chemical shift tensors are available assuming there are no gross changes between solution and solid states. This data is summarized in Table 4.3. The T_1's calculated using the anisotropies measured in the solid-state give T_1's that are two to three orders of magnitude longer than those measured in solution. This provides further evidence that the suggestion that CSA contributes to ^{59}Co relaxation in solution was incorrect.

4.6 Conclusions

Solid-state ^{59}Co NMR spectra have been obtained at 11.7 and 4.7 T. From the spectra, the CS and efg tensors have been obtained for eleven complexes. The isotropic chemical shifts in the solid-state are close to those found in solution considering the large chemical shift range for cobalt. The quadrupolar coupling constants determined from the solid-state spectra were all larger than those determined from the ^{59}Co relaxation studies but the spans were, in general, found to increase with increasing quadrupolar coupling constants. Several ligand planes responsible for specific chemical shifts have been determined namely A) 3N 1C planes gives rise to shifts between 5190 and 6362 ppm, B) 4N planes gives rise to shifts between 6860 and 7800 ppm, C) 3N 1O or 1Cl planes gives rise to shifts between 9385 and 9868 ppm, and D) 4O planes gives rise to shifts between 11890 and 13015 ppm. Using the anisotropy of the CS tensors, T_{1CSA} has been calculated for several complexes showing that the earlier ^{59}Co relaxation studies, which state that the CSA mechanism of relaxation is a contributor to cobalt-59 relaxation in solution, were incorrect.

Chapter 5

Concluding Remarks

Several goals have been achieved through this research. In Chapter 3, the spin-lattice relaxation mechanism of ^{59}Co in aqueous cobalt(III) complexes was unambiguously determined to be the quadrupolar mechanism at room temperature. Also in Chapter 3, the first determination of the absolute chemical shielding scale for cobalt was presented from the characterization of spin-rotation constants of three cobalt complexes. The chemical shift and electric field gradient tensors of eleven cobalt complexes have been elucidated and are presented in Chapter 4. These results have furthered our interest in using cobalt-59 NMR as a site-specific probe of molecular structure, but further work needs to be completed on simple cobalt(III) complexes to gain a better understanding of their solution and solid-state structure before attempting to apply this work to more complicated systems. An improvement of the chemical shielding scale would be beneficial allowing a better comparison of experimental chemical shift tensors with calculated chemical shielding tensors. A larger variety of ligands, especially those containing a spin-$\frac{1}{2}$ nucleus

and/or those which can be used as biochemical binding site models, should be studied in both solution and the solid state. To aid in the analysis of solid-state ^{59}Co NMR spectra, multiple-quantum NMR experiments should be developed. Calculation of chemical shielding tensors of complexes in which the chemical shift tensors have been experimentally determined should also be performed.

Improvement of the quality of the chemical shielding scale would be obtained by determining the ^{59}Co relaxation of the cobalt(III) complex of 2,2,2-cryptand. This complex should have a large moment of inertia, being larger than the sepulchrate, and would have an isotropic chemical shift in the range of 12000 to 13000 ppm allowing for a complex with a chemical shift larger than the others used in the chemical shielding scale thus far. This will aid in the comparison of calculated chemical shielding tensors with experimentally measured chemical shift tensors.

Other complexes for which the ^{59}Co relaxation should be studied, as they could be used as models for biochemical binding sites, are $Co(NH_3)_4PO_3$, DNA intercalators ($Co(phenanthroline)_3^{3+}$ and $Co(bipyridine)_3^{3+}$),[3] cobalt(III)-ATP and ADP complexes,[80] and several small peptide complexes of cobalt(III).[2, 81] The ^{59}Co CS and efg tensors of these complexes should also be determined *via* solid-state ^{59}Co NMR.

As shown in Chapter 4, symmetry arguments are not necessarily correct as in the case of $Co(NH_3)_5CH_3^{2+}$ where simulation of the ^{13}C MAS NMR spectrum gave an orientation different from that expected based on symmetry arguments. Therefore, the solid-state NMR spectra of spin-$\frac{1}{2}$ nuclei in complexes (where available) should be done. Four examples are ^{31}P NMR of $Co(NH_3)_4PO_4$, ^{15}N NMR of

$Co(NH_3)_5^{15}NO_2^{2+}$, and ^{13}C NMR of $Co(NH_3)_5^{13}CO_3^+$ and *cis*-$Co(NH_3)_4^{13}CO_3^+$. This would involve labeling the ^{13}C or ^{15}N in the last three complexes.

As described in Chapter 4, there are eight variables that must be considered in the simulation of quadrupolar NMR spectra which creates errors in simulation of spectra obtained at a single magnetic field. Even with spectra acquired at two fields, simulations can still be difficult if not impossible. To allow for the simulation of such compounds, development of static multiple-quantum NMR experiments would be beneficial. In these two dimensional techniques, either the quadrupolar or chemical shift interaction could be refocused, thereby removing one of the interactions from one of the axes. Multiple-quantum NMR experiments[82, 83] have been developed for spin-$\frac{3}{2}$[82, 83, 84, 85] and $\frac{5}{2}$[86] nuclei but not for $\frac{7}{2}$ nuclei. Also, the experiments developed thus far have all been MAS experiments and it would be beneficial to develop such experiments for powder samples.

With modern computational resources, it is now possible to attempt the calculation of first row transition metal chemical shielding tensors. The chemical shielding tensors presented in this thesis as well as those suggested here should be calculated with *ab initio* methods for comparison between theory and experiment. This may allow for the determination of structures of complexes for which the chemical shift tensors can be obtained but crystal structures cannot.

Finally, once a better understanding of cobalt complexes in both solution and the solid state is obtained, examination of binding interactions between cobalt(III) and chromium(III) complexes with nucleic acids[3] and polymers[5] can be attempted. The reason for looking at both the cobalt(III) and chromium(III) complexes stems

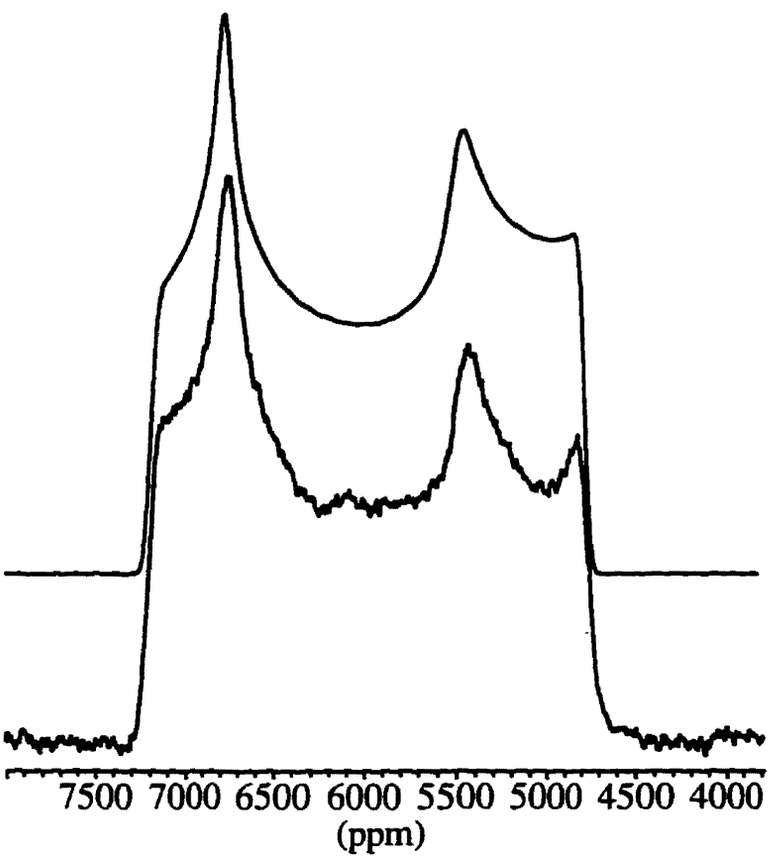
from the fact that these two cations are the same size and cobalt(III) is diamagnetic while chromium(III) is paramagnetic. The environment of the metal in a binding site(s) can be studied using ^{59}Co NMR. The environment surrounding the binding site(s) can also be elucidated *via* the changes in the NMR spectral properties of nuclei of the nucleic acid or polymer (^{1}H, ^{13}C, or ^{31}P) by replacing cobalt with chromium(III) causing paramagnetic relaxation of the spin-$\frac{1}{2}$ nuclei. In this way, the metal centres can be used in parallel for the determination of molecular structure.

Appendix A

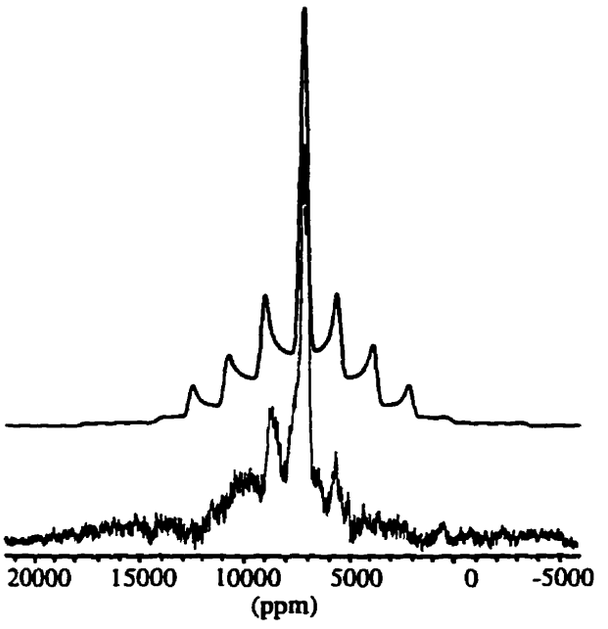
Solid-State ^{59}Co NMR Spectra

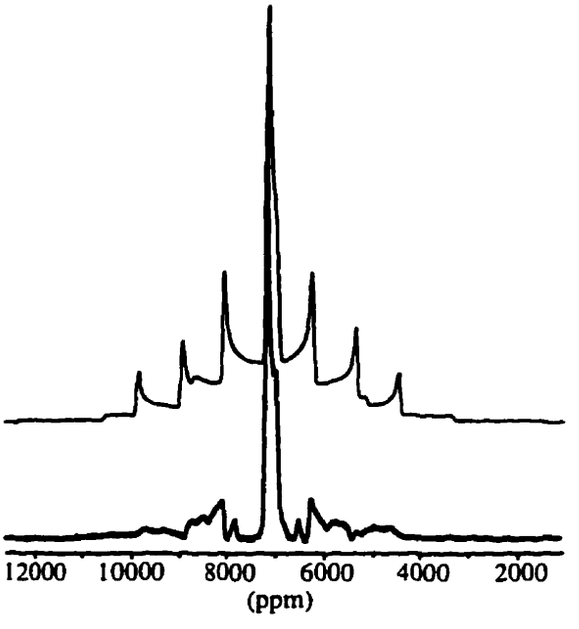
Throughout this appendix, the solid-state ^{59}Co NMR are presented for all of the complexes discussed in chapter 4. For each complex, both the simulation (upper) and experimental (lower) spectra are given as well as spectra acquired at both 4.7 T (top) and 11.7 T (bottom) fields. If only one spectrum and simulation are shown. the spectrum was recorded at 11.7 T.

$[Co(NH_3)_5CH_3](NO_3)_2$

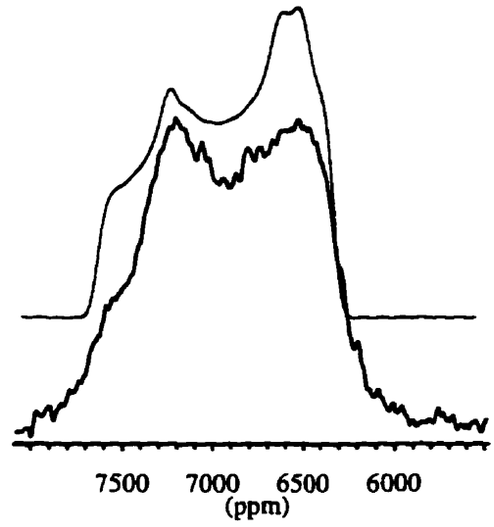


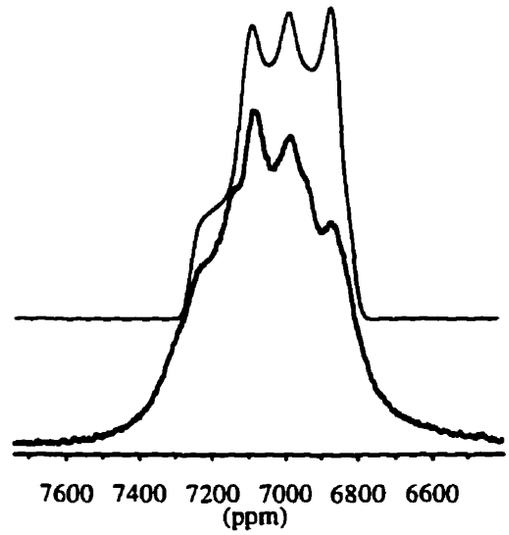
$[Co(en)_3]Cl_3$


20000
15000
10000
5000
0
-5000
(ppm)

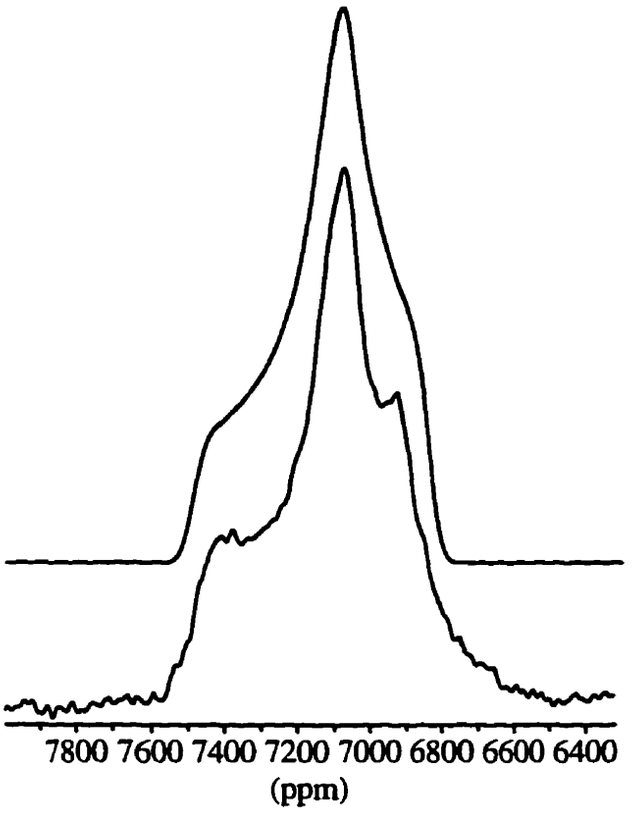

12000
10000
8000
6000
4000
2000
(ppm)

trans-$[Co(NH_3)_4(NO_2)_2]NO_3$

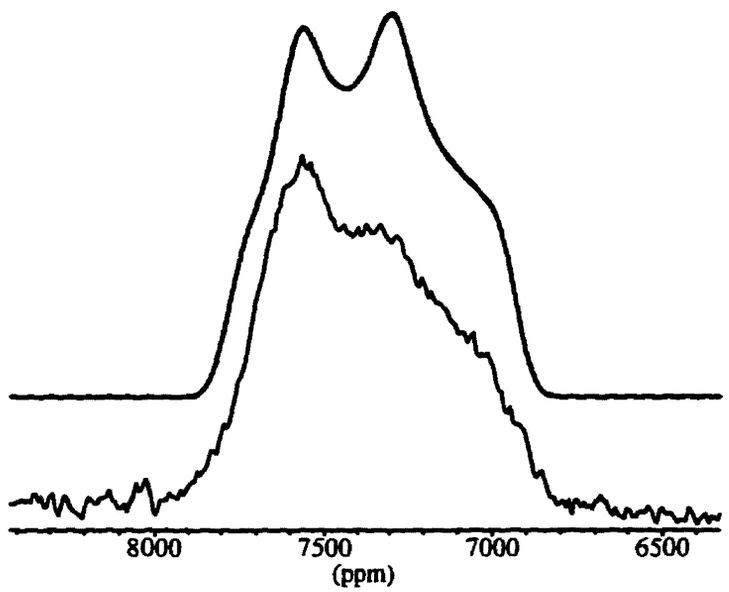


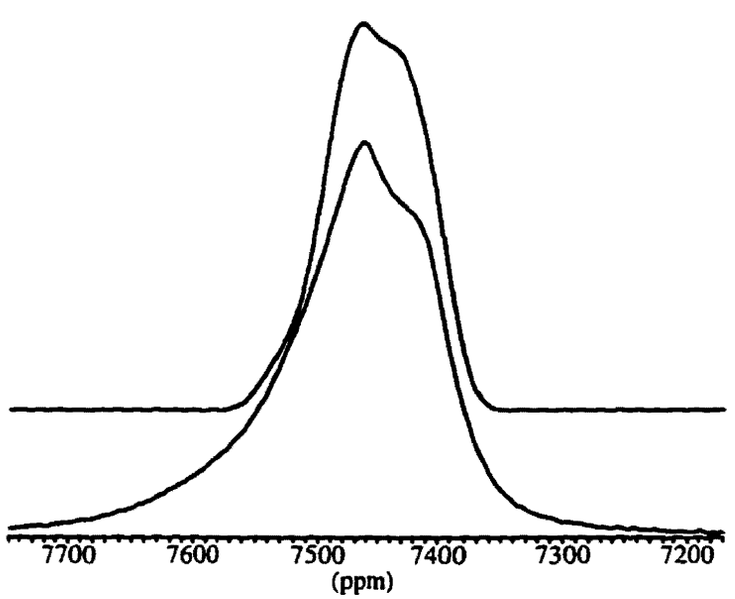


cis-$[Co(NH_3)_4(NO_2)_2]NO_3$

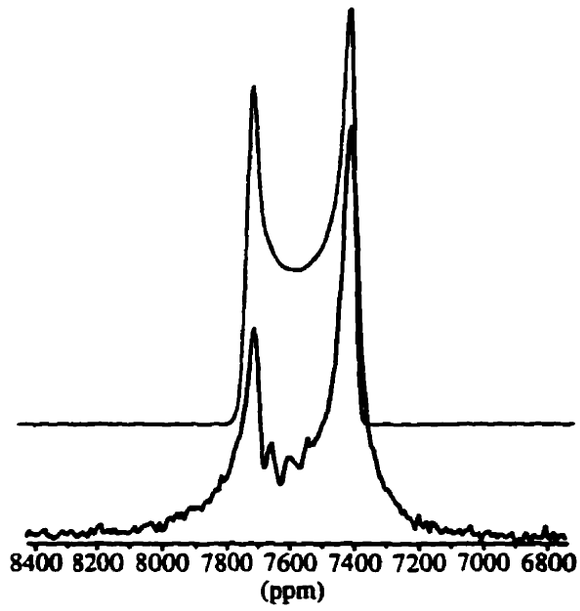


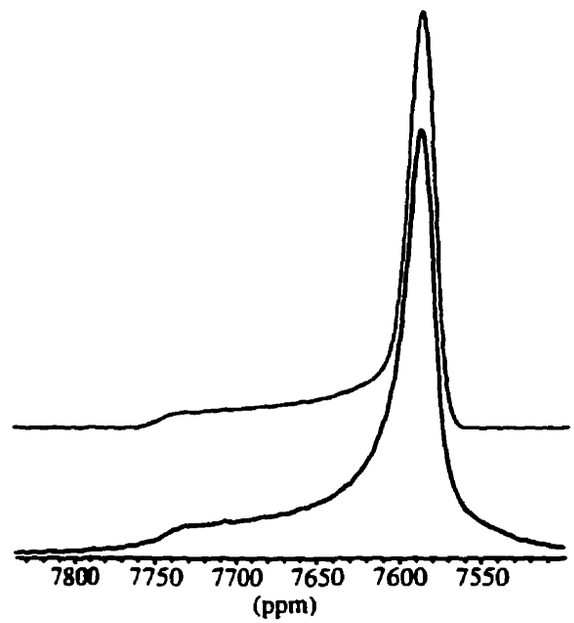
$[Co(NH_3)_5(NO_2)]Cl_2$



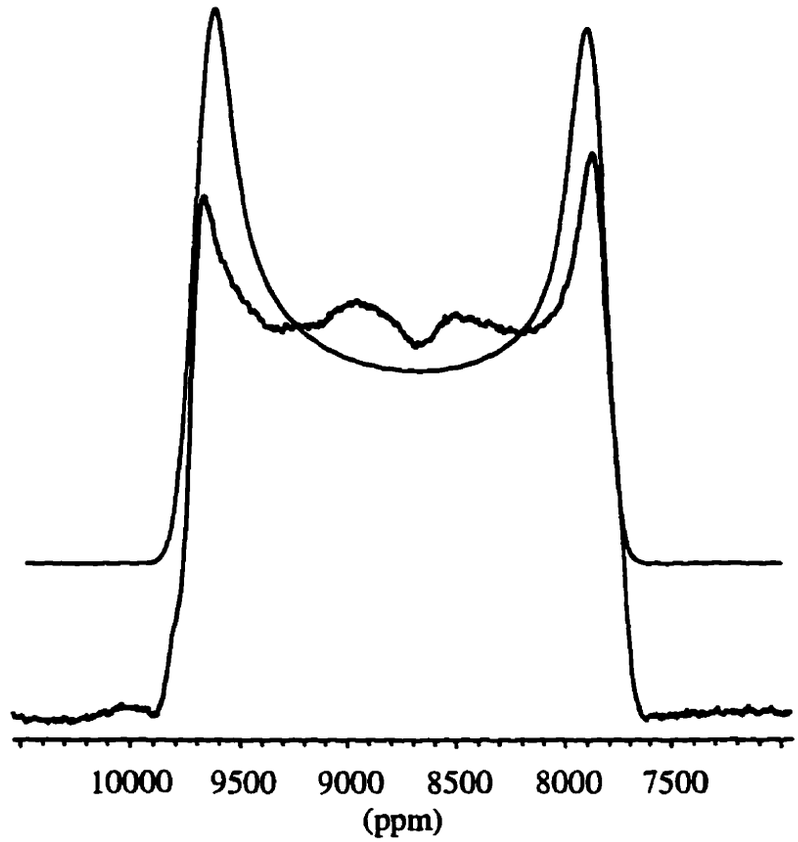


$Na_3[Co(NO_2)_6]$

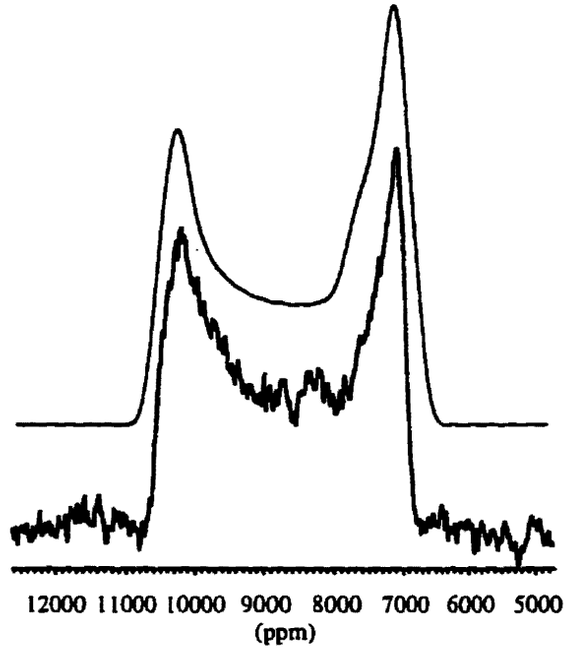

8400 8200 8000 7800 7600 7400 7200 7000 6800
(ppm)

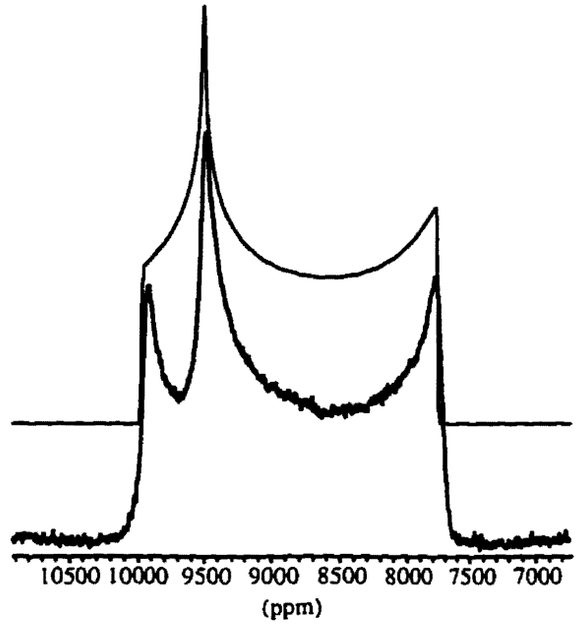

7800 7750 7700 7650 7600 7550
(ppm)

$[Co(NH_3)_5Cl]Cl_2$

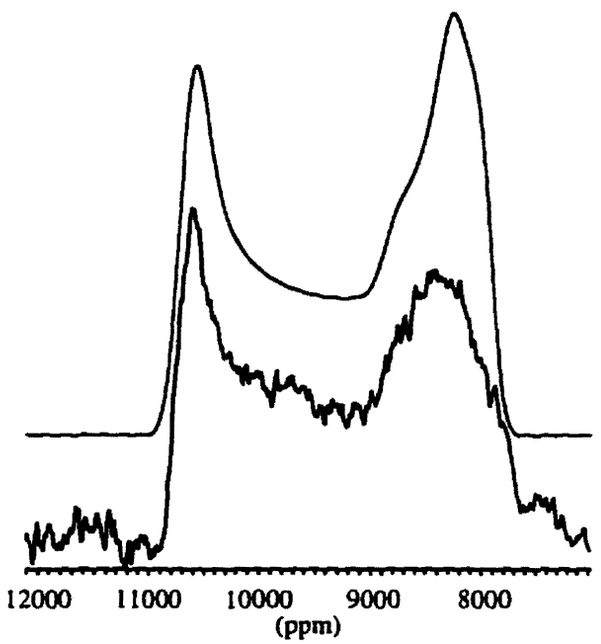


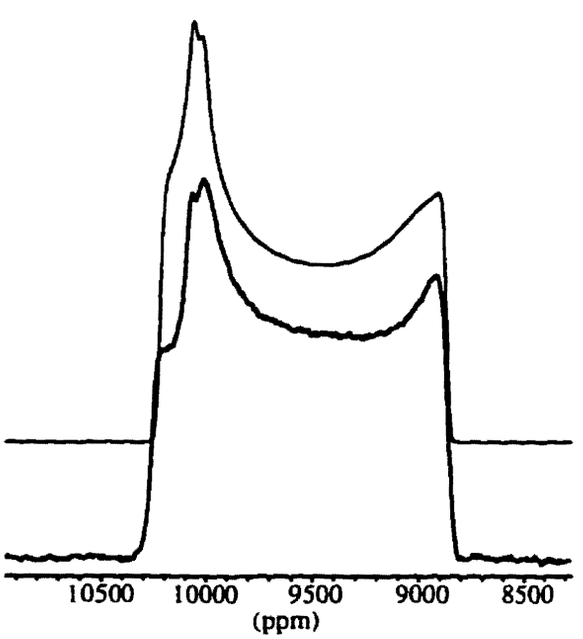
$[Co(NH_3)_5CO_3]NO_3 \cdot \frac{1}{2}H_2O$



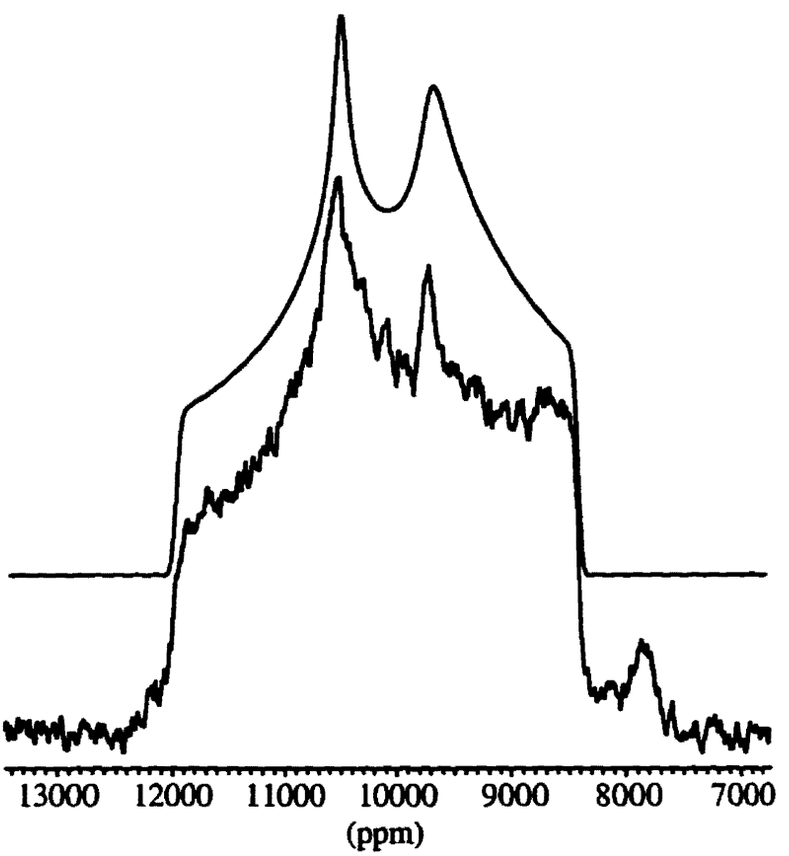


cis-$[Co(NH_3)_4CO_3]NO_3$

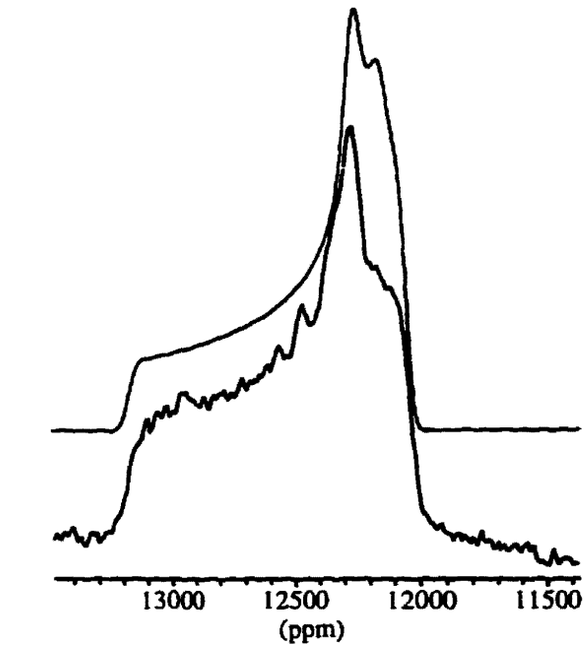


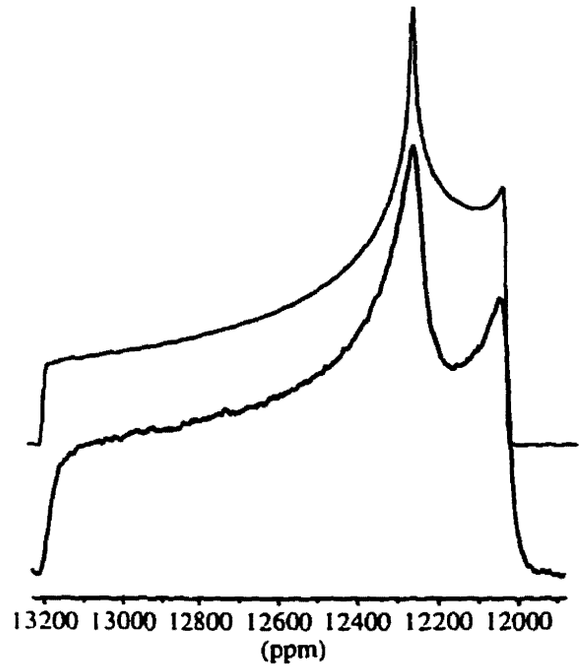


Na[Co(edta)]



$Co(acac)_3$


13000
12500
12000
11500
(ppm)


13200 13000 12800 12600 12400 12200 12000
(ppm)

Bibliography

[1] Krautler, B.; Kratky, C. *Angew. Chem., Int. Ed. Engl.* **1996,** *35,* 167.

[2] Sutton, P. A.; Buckingham, D. A. *Acc. Chem. Res.* **1987,** *20,* 357.

[3] Pyle, A. M.; Barton, J. K. *Prog. Inorg. Chem.* **1990,** *38,* 413.

[4] Adamson, A. W.; Fleischauer, P. D., Eds.; *Concepts of Inorganic Photochemistry;* Wiley-Interscience Publication: Toronto, 1975.

[5] Tsuchida, E.; Nishide, H. In *Advances in Polymer Science, Vol. 24;* Cantow, H.-J.; Dall'Asta, G.; Dušek, D.; Ferry, J. D.; Fugita, H.; Gordon, M.; Kern, W.; Natta, G.; Okamura, S.; Overberger, C. G.; Saegusa, T.; Schulz, G. V.; Slichter, W. P.; Stiller, J. K., Eds.; Springer-Verlag: New York, 1977; pp 1-88.

[6] Spiess, H. S. In *Dynamic NMR Spectroscopy;* Diehl, R., Fluch, E., Kosfeld, R., Eds.; Springer-Verlag: New York, 1978; pp 91-140.

[7] Haeberlen, U. In *Advances in Magnetic Resonance, Supplement 1;* Waugh, J. S., Ed.; Academic Press: New York, 1976; pp 5-15.

[8] Taylor, P. C.; Baugher, J. F.; Kriz, H. M. *Chem. Rev.* **1976,** *75,* 203.

[9] Arfken, G. *Mathematical Methods for Physicists, 3rd Ed.;* Academic Press: San Diego, 1985; pp 198-203.

[10] Mason, J. *Solid State Nucl. Magn. Reson.* **1993,** *2,* 285.

[11] Ramsey, N. F. *Phys. Rev.* **1950,** *78,* 699.

[12] Jameson, C. J.; Mason, J. In *Multinuclear NMR;* Mason, J., Ed.; Plenum Press: New York, 1987; pp 51-86.

[13] Malli, G.; Froese, C. *Int. J. Quantum Chem.* **1967,** *1S,* 95.

[14] Kolb, D.; Johnson, W. R.; Shorer, P. *Phys. Rev. A.* **1982,** *26,* 19.

[15] Derome, A. E. *Modern NMR Techniques for Chemistry Research;* Pergamon Press: New York, 1993; pp 97-127.

[16] Power, W. P.; Lumsden, M. D.; Wasylishen, R. E. *J. Am. Chem. Soc.* **1991,** *113,* 8257.

[17] Lumsden, M. D.; Eichele, K.; Wasylishen, R. E.; Cameron, T. S.; Britten, J. F. *J. Am. Chem. Soc.* **1994,** *116,* 11129.

[18] Flyfare, W. H. *Chem. Rev.* **1974,** *74,* 653.

[19] Deverell, C. *Molec. Phys.* **1970,** *18,* 319.

[20] Proctor, W, G.; Yu, F. C. *Phys. Rev.* **1951,** *81,* 20.

[21] Harris, R. K. *Nuclear Magnetic Resonance Spectroscopy;* Longman Scientific & Technical: Essex, England, 1989; p 238.

[22] Goodfellow, R. J. In *Multinuclear NMR;* Mason, J., Ed.; Plenum Press: New York, 1987; pp 521-562.

[23] Mason, J. *Chem. Rev.* **1987,** *87,* 1299.

[24] Ader, R.; Loewenstein, A. *J. Magn. Reson.* **1971,** *5,* 248.

[25] Jordan, R. B. *J. Magn. Reson.* **1980,** *38,* 267.

[26] Doddrell, D. M.; Bendall, M. R.; Healy, P. C.; Smith, B.; Kennard, C. H. L.; Raston, C. L.; While, A. H. *Aust. J. Chem.* **1979,** *32,* 1219.

[27] Valiev, K. A. *Sov. Phys. JEPT* **1960,** *37,* 77.

[28] Brown, R. J. C.; Colpa, J. P. *J. Chem. Phys.* **1982,** *77,* 1501.

[29] Osten, H. J.; Jameson, C. *J. Mol. Phys.* **1986,** *57,* 533.

[30] Craighead, K. L.; Bryant, R. G. *J. Phys. Chem.* **1975,** *79,* 1602.

[31] Rose, K. D.; Bryant, R. G. *Inorg. Chem.* **1979,** *18,* 1332.

[32] Rose, K. D.; Bryant, R. G. *Inorg. Chem.* **1979,** *18,* 2130.

[33] Chacko, V. P.; Bryant, R. G. *J. Magn. Reson.* **1984,** *57,* 79.

[34] Russell, J. G.; Bryant, R. G. *J. Phys. Chem.* **1984,** *88,* 4298.

[35] Iida, M.; Nakamori, T.; Mizuno, Y.; Masuda, Y. *J. Phys. Chem.* **1995,** *99,* 4347.

[36] Abragam, A. *The Principles of Nuclear Magnetism;* Clarendon Press: Oxford, England, 1961; pp 309-312.

[37] Au-Yeung, S. C. F.; Eaton, D. R. *Inorg. Chem.* **1983,** *L76,* 141.

[38] Au-Yeung, S. C. F.; Eaton, D. R. *J. Magn. Reson.* **1983,** *52,* 351.

[39] Au-Yeung, S. C. F.; Eaton, D. R. *J. Magn. Reson.* **1983,** *52,* 366.

[40] Au-Yeung, S. C. F.; Buist, R. J.; Eaton, D. R. *J. Magn. Reson.* **1983,** *55,* 24.

[41] Anet, F. A. L.; O'Leary, D. J. *Concepts Magn. Reson.* **1992,** *4,* 35.

[42] Kanakubo, M.; Ikeuchi, H.; Satô, G. P. *J. Magn. Reson. Ser. A.* **1995,** *52,* 366.

[43] Abragam, A. *The Principles of Nuclear Magnetism;* Clarendon Press: Oxford, England, 1961; p 297.

[44] Hollas, J. M. *Modern Spectroscopy;* John Wiley & Sons: New York, 1992, p. 68.

[45] Bjerrum, J.; McReynolds, J. P. *Inorg. Syn.* **1946,** *2,* 216.

[46] Kauffman, G. B.; Abbott, S. F.; Clark, S. E.; Gibson, J. M.; Meyers, R. D. *Inorg. Syn.* **1978,** *18,* 69.

[47] Siebert, V. J.; Siebert, C.; Wieghardt, K. Z. *Z. Anorg. Allg. Chem.* **1971,** *380,* 30.

[48] Schlessinger, G. *Inorg. Syn.* **1960,** *6,* 173.

[49] Kimura, M.; Miyamoto, I. *Bull. Chem. Soc. Jpn.* **1994,** *67,* 2136.

[50] Dill, K.; Allerhand, A. *J. Am. Chem. Soc.* **1979,** *101,* 4376.

[51] Reynhardt, E. C.; Boeyens, J. C. A. *Acta Cryst.* **1972,** *B28,* 524.

[52] Kruger, G. J.; Reynhardt, E. C. *Acta Cryst.* **1974,** *B30,* 822.

[53] Laszlo, P. In *NMR of Newly Accessible Nuclei, Vol. 2;* Laszlo, P., Ed.; Academic Press: New York, 1983; pp 253-274.

[54] Harris, R. K. *Nuclear Magnetic Resonance Spectroscopy;* Longman Scientific & Technical: Essex, England, 1989; pp 139-141.

[55] Hubbard, P. S. *Phys. Rev.* **1963,** *131,* 1155.

[56] Washylishen, R. E.; Pettitt, B. A. *Can. J. Chem.* **1977,** *55,* 2564.

[57] Primrose, W. U. In *NMR of Macromolecules;* Roberts, G. C. K., Ed.; IRL Press: New York, 1993; pp 22-23.

[58] Spiess, H. W.; Haas, H.; Hartmann, H. *J. Chem. Phys.* **1969,** *50,* 3057.

[59] Spiess, H. W.; Sheline, R. K. *J. Chem. Phys.* **1970,** *53,* 3036.

[60] Mooberry, E. S.; Pupp, M.; Slater, J. L.; Sheline, R. K. *J. Chem. Phys.* **1971,** *55,* 3655.

[61] Mooberry, E. S.; Sheline, R. K. *J. Chem. Phys.* **1972,** *56,* 1852.

[62] Reynhardt, E. C. *Can. J. Phys.* **1974,** *52,* 1398.

[63] Reynhardt, E. C. *J. Phys. C.* **1974,** *7,* 4135.

[64] Eaton, D. R.; Buist, R. J.; Sayer, B. G. *Can. J. Chem.* **1987,** *65,* 1332.

[65] Hirschinger, J.; Granger, P.; Rosé, J. *J. Phys. Chem.* **1992,** *96,* 4815.

[66] Kempgens, P.; Hirschinger, J.; Elbayed, K.; Raya, J.: Granger, P.; Rosé, J. *J. Phys. Chem.* **1996,** *100,* 2045.

[67] Jones, W. H.; Graham, T. P.; Barnes, R. G. *Phys. Rev.* **1963,** *132,* 1898.

[68] Baugher, J. F.; Taylor, P. C.; Oja, T.; Bray, P. J. *J. Chem. Phys.* **1969,** *50.* 4914.

[69] Power, W. P.; Wasylishen, R. E.; Mooibroek, S.; Pettitt, B. A.; Danchura, W. *J. Phys. Chem.* **1990,** *94,* 591.

[70] Slichter, C. P. *Principles of Magnetic Resonance;* Springer-Verlag: New York, 1990; pp 485-502.

[71] Work, J. B.; McReynolds, J. P. *Inorg. Syn.* **1946,** *2,* 221.

[72] Kofod, P. *Inorg. Chem.* **1995,** *34,* 2768.

[73] Alderman, D. W.; Solum, M. S.; Grant, D. M. *J. Chem. Phys.* **1986,** *84,* 3717.

[74] Frish, M. J.; Trucks, G. W.; Schlegel, H. B.; Gill, P. M. W.; Johnson, B. G.; Robb, M. A.; Cheeseman, J. R.; Keith, T.; Petersson, G. A.; Montgomery, J. A.; Raghavachari, K.; Al-Laham, M. A.; Zakrzewski, V. G.; Ortiz, J. V.; Foresman, J. B.; Cioslowski, J.; Stefanov, B. B.; Nanayakkara, A.; Challacombe, M.; Peng, C. Y.; Ayala, P. Y.; Chen, W.; Wong, M. W.; Andres, J. L.; Replogle, E. S.; Gomperts, R.; Martin, R. L.; Fox, D. J.; Binkley, J. S.; Defrees, D. J.; Baker, J.; Stewart, J. P.; Head-Gordon, M.; C., G.; Pople, J. A. *GAUSSIAN 94, Revision D.4;* GAUSSIAN, Inc.: Pittsburgh, PA, 1995.

[75] Whuler, P. A.; Brouty, C.; Spinat, P.; Herpin, P. *Acta Cryst.* **1975,** *B31,* 2069.

[76] Okaya, Y.; Pepinsky, R.; Takeuchi, Y.; Kiroya, H.; Shimada, A.; Gallitelli, P.; Stemple, N.; Beevers, A. *Acta Cryst.* **1957,** *10.* 798.

[77] Ronemus, A. D.; Vold, R. L.; Vold, R. R. *J. Magn. Reson.* **1986,** *70,* 416.

[78] Harris, R. K.; Olivieri, A. C. *Prog. Nucl. Magn. Reson. Spectrosc.* **1992,** *24.* 435.

[79] Kirby, C. W.; Power, W. P.; Taylor, N. J. Unpublished data.

[80] Cornelius, R. D.; Hart, P. A.; Cleland, W. W. *Inorg. Chem.* **1977,** *16,* 2799.

[81] Freeman, H. C. *Inorg. Biochem.* **1973,** *1,* 121.

[82] Frydman, L.; Harwood, J. S. *J. Am. Chem. Soc.* **1995,** *117,* 5367.

[83] Medek, A.; Harwood, J. S.; Frydman, L. *J. Am. Chem. Soc.* **1995,** *117,* 12779.

[84] Fernandez, C.; Amoureux, J. P. *Solid State Nucl. Magn. Reson.* **1995,** *5,* 315.

[85] Wu, G.; Rovnyak, D.; Griffin, R. G. *J. Am. Chem. Soc.* **1996,** *118,* 9326.

[86] Fernandez, C.; Amoureux, J. P. *Chem. Phys. Lett.* **1995,** *242,* 449.